Estimation of pollutant residence time and its integration into a Karst vulnerability methodology for the Yucatán karst system in México

Carolina Martínez Salvador

Thesis to obtain the Master of Science Degree in

Environmental Engineering

Supervisors:
Prof. Dr. Rudolf Liedl
Dr. Miguel Moreno
Prof. Luís Filipe Tavares Ribeiro

Examination Committee

Chairperson: Prof. Dr. José Manuel de Saldanha Gonçalves Matos
Supervisor: Prof. Dr. Luís Filipe Tavares Ribeiro
Members of the Committee: Prof. Dr. Christian Bernhofer

September 2018

Estimation of pollutant residence time and its integration into a Karst vulnerability methodology for the Yucatán karst system in México

Master of Science Thesis
by
Carolina Martínez Salvador

Supervisors
Prof. Dr. Rudolf Liedl

Dr. Miguel Moreno
Prof. Luís Filipe Tavares Ribeiro

Examination committee
Chairperson: Prof. Dr. José Manuel de Saldanha Gonçalves Matos
Supervisor: Prof. Dr. Luís Filipe Tavares Ribeiro
Members of the Committee: Prof. Dr. Christian Bernhofer

This thesis is submitted in partial fulfilment of the requirements for the academic degree of
Master of Science in Water Science and Engineering
UNESCO-IHE Institute for Water Education, Delft, the Netherlands
Master of Science in Environmental Engineering
Instituto Superior Técnico, Universidade de Lisboa, Portugal
Master of Science in Hydro Science and Engineering
Technische Universität Dresden, Germany

MSc research host institution
TUD, Dresden, Germany

September 2018

Acknowledgements

To my mom, dad and the strongest of us all, my sister Laura, whom I owe myself, my freedom and my happiness. Thanks for their love, because that is what allowed me to find myself. I am endlessly grateful for their support, comfort, and encouragement. I could not have done without them.

To my brother in law, who keeps them safe and happy.

To my family, for being there.

To all my friends and all the shared precious moments that constitute life itself. To long-life friends, who keep me grounded. To new friends, my Groundwatch family, for all the experiences, laughs, love, hugs, dances and friendship. I am a better person today thanks to all of you.

To the Erasmus Mundus programme and their financial support. I would not be here without it. Thanks to all the members of the MSc programme, specially Tibor, Teresa, Luis, Christian, Titia, Agata, Judith and many more that I had the pleasure to know and work with. Thanks for the effort and support. Many thanks for the opportunity. You have broadened my world.

To my mentor, Miguel Moreno, who worked side by side with me, guided me and trusted me over the last year.

To all the teachers that left a little bit of themselves in every classroom and lesson.

To Professor Rudolf Liedl and Professor Reimann for its valuable time and feedback along the way.

To the internet heroes that give us their time and effort in the pursuit of knowledge. They are also our teachers and we owe them tons.

To everyone that loved me along this journey. I am whole thanks to all.

Resumo

Os sistemas aquíferos cársicos estão amplamente distribuídos por todo o mundo e são uma importante fonte de água potável. No entanto, devido às suas características são recursos de água muito heterogéneos e vulneráveis a impactos tanto de origem natural como antrópica.

O sistema aquífero cársico do Yucatán é o principal recurso de água da região sendo partilhado entre o México, Belize e Guatemala. Localizado numa região tropical, possui um regime sazonal de precipitação, com chuvas intensas e eventos extremos como furacões. A área é composta principalmente por rochas calcárias, altamente fraturadas devido à dissolução de carbonatos e com uma elevada densidade de dolinas. Os solos são pouco espessos ou inexistentes, o que significa uma capacidade limitada de atenuação. Uma outra característica importante é tratar-se de uma área relativamente aplanada, com níveis freáticos pouco profundos. Estas características aumentam a vulnerabilidade do aquífero à poluição devido ao curto tempo de trânsito entre a superfície e os níveis freáticos.

O aquífero de Yucatán é a única fonte de água para a maior parte da península e atualmente subexplorada. Estudos recentes sugeriram que o aquífero enfrenta riscos de poluição. A falta de um sistema adequado de saneamento e estações de tratamento significa que as águas residuais são armazenadas em fossas sépticas artesanais que descarregam diretamente no aquífero.

Este trabalho faz parte de uma investigação mais alargada que visa criar uma ferramenta para determinar a vulnerabilidade e que seja capaz de integrar as particularidades de Yucatán. Desenvolvendo um modelo conceptual e numérico de fluxo para descrever o comportamento das águas subterrâneas no aquífero, e estimando o tempo de residência com o modelo de transporte, pretende-se incluir o tempo de residência como variável na determinação da vulnerabilidade do sistema aquífero.

Palavras Chave: aquíferos cársico, vulnerabilidade, tempo de residência, poluição, nitratos, Yucatán, México.

Abstract

Karst aquifers are widely spread all over the world and are a major source of drinking water. Their specific features make them highly heterogeneous and prompt to anthropogenic and natural impacts.

The Yucatán karst aquifer is a transboundary groundwater system shared by México, Belize, and Guatemala. Located in a tropical area, it has a seasonal precipitation regime, quite prompt to intense rainfalls and extreme events like hurricanes. The area is composed mainly of limestone, highly fractured due to carbonate dissolution with areas of high sinkhole density. Soils are mainly thick or nonexistent, which means limited buffer for attenuation. One of the most outstanding features is the relative flattened area, which also accounts for shallow water tables. These characteristics increase the aquifer vulnerability of pollution due to the short travel time from the surface to the water tables.

The Yucatan aquifer is the sole source of water for most of the peninsula and currently underexploited. Recent studies have suggested that the aquifer faces pollution risks. The lack of a proper sewage system and treatment plants means that wastewater is stored in artisanal septic tanks leaking directly into the aquifer.

This work is immersed within a broader research that aims to create an integrated vulnerability tool able to account for Yucatán particularities. Using modelling to estimate residence time, we aim to include time in such method, by setting up a conceptual and numerical model to depict the groundwater behaviour and estimate residence time with transport model.

Keywords: Karst aquifers, vulnerability, residence time, nitrate pollution, Yucatán, México.

Abbreviations

ADV: Advection Package, MODFLOW, MT3DMS

BTN: Basic Transport package, MODFLOW, MT3DMS

CFP: Conduit Flow Process

CONABIO (National Biodiversity Commission)

CONAGUA: Comisión Nacional del Agua (Mexican National Water Authority)

CONACYT: Consejo Nacional de Ciencia y Tecnología (Mexican Council for Science and Technology)

DEM: Digital Elevation Model

DSP: Dispersion package, MODFLOW, MT3DMS

GCG: Generalized Conjugated Gradient Solve Pane, MODFLOW, MT3DMS

ICR: Inner Cenote Ring

EPM: Equivalent Porous Medium

MMA: Mérida Metropolitan Area

RMSR: Root mean squared residuals or Root mean squared error

SSM: Sink/Source Mixing package, MODFLOW, MT3DMS

UNESCO: United Nations Educational, Scientific and Cultural Organization

Content

List of Figures

List of Tables

1 Introduction

1.1 Karst basic concepts

Karst aquifers are located all over the world. Nearly 25% of the global population water is being supplied with groundwater from karst aquifers (IGRAC, 2017) with the exploitation tendency on the rise. The resources are both important and highly vulnerable. One of the most common characteristics is the existence of sinkholes and dolines that may connect the surface with groundwater. The first ones can connect the surface with the shallow groundwater water table. Karst features reduce the time that any potential pollution coming from the surface will take to reach the aquifer, increasing vulnerability of the resources increases.

Karst stands for any system that contains caves and special features that develop in water-soluble rocks like limestone or gypsum (Ford and Williams, 2007). Defining characteristics of any karst system are the high rock solubility -solubility of the soil matrix- and the existence of a secondary or even tertiary porosity that is more related to the formation of conduits, caves, sinkholes, dolines and many other karstic specific features (Reimann, 2012).

Karst develops due to the dissolution of carbonate and evaporite rocks. Water drives dissolution processes given the constant water-rock interaction. The formation of karst obeys two main formation processes (Stevanović, 2015b):

1. Mechanical karstification: driven by the flow of water, especially through fissures or geological faults.
2. Chemical karstification: the erosion of the rock through the dissolution of calcite, dolomite, and gypsum and is highly dependent on temperature and pressure, and even salinity. The concentration of CO_2 in the water has also a huge impact on the karstification process.

Karst system is categorized using many criteria and are described in general having two-part zones: infiltration zone and flooded zone. The infiltration zone is vertically divided including a top feature called epikarst. Epikarst is the surface zone that may serve a dual purpose -mainly dependent on the recharge dynamics-: infiltrated water can be momentary store or delay as a discontinued saturated zone (or flooded zone), followed by a saturated area where water tables start. The epikarst can also play the role of a buffer area when recharge processes are high, the focal source of pollution that precedes drains and fracture media that ensures rapid vertical flow (Petelet-Giraud, Dörfliger, and Crochet, 2000). The epikarst, is a key factor in some vulnerability methodologies. Figure 1 depicts a conceptual understanding of a karst system. Groundwater can be connected with the surface by conduits, cave systems of preferential flow paths. In geological terms, karst systems develop rapidly, being among the most dynamics aquifers in the world, hence its inherent complexity. The flooded zone, on the other hand, may be formed by drains with fast flows (during wet seasons) and voids feed by the drains systems (Stevanović, 2015a).

Most karst aquifers experience a lack of natural attenuation of pollutants mainly because soils are poorly developed and the nature of infiltration processes- rapid in some areas given the existence of conduits and slow and delayed due to sediments, carbonate crust or the epikarst. Sinkholes and conduits in a karst system connect surface directly to the water table, preventing the pollutant to undergo degradation and sorption processes.

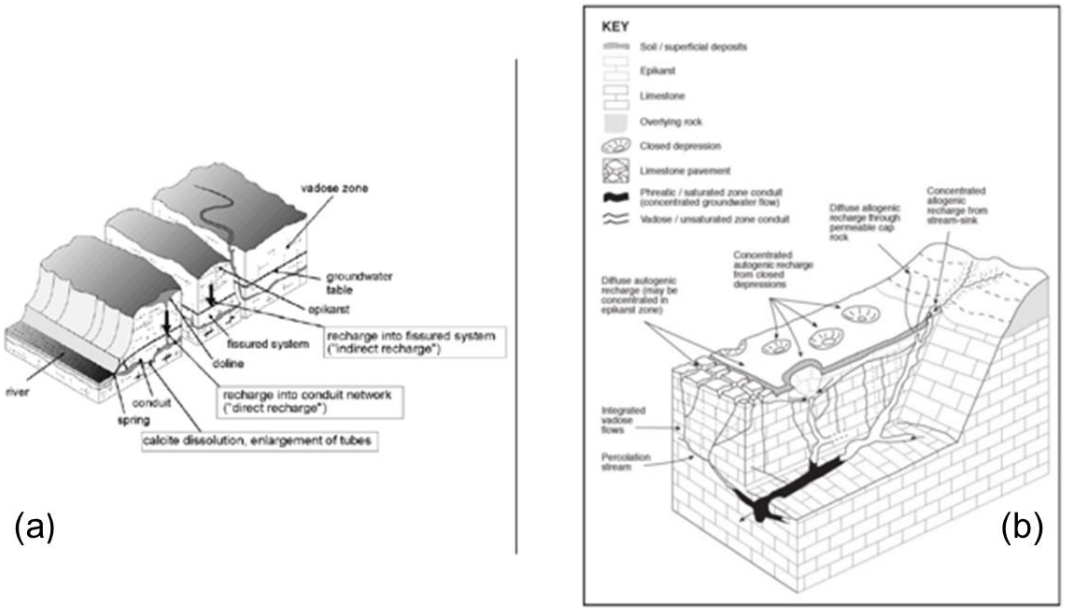

Figure 1: Karstic features Sources: (a) Zwahlen, 2003; b) Liedl, 2003)

1.2 Vulnerability

Groundwater vulnerability is a measure of the potential of a pollutant to percolate from the surface to the water reservoir under natural conditions (Petelet-Giraud, et.al., 2000). The trademarks of any vulnerability approach are some degree of subjectivity and expert judgment. The notion is based on the fact that physical properties inherent to any systems provide some degree of natural protection to groundwater resources against human -or even natural- impacts (Vrba and Zaporozec, 1994). Currently, two main approaches are being evaluated according to COST 620 report (Zwahlen, 2003):

1. Intrinsic vulnerability deals mainly with the sensitivity of the aquifer towards a pollution scenario, solely based on a geological, hydrological and hydrogeological point of view. It relies on the aquifer itself and does not consider the chemical nature of the pollutant. A small derivation is the concepts of resource and source vulnerability. When assessing resource vulnerability, we basically evaluate what happens between the surface and the water table, while source vulnerability will be a little bit more relative, because it estimates vulnerability towards from a drinking water supply point; it means that wells or springs are considered as the target of any possible pollution plume and the time it will take for a pollutant to reach those sources.

2. Specific vulnerability goes beyond that scope and considers the properties or the pollutant at hand.

Most developed vulnerability assessment methodologies assign rating values and scales to physical features of the aquifer and then sum them up to build a vulnerability index allowing a classification of a from very low to very high vulnerability (Figure 2). Such classification aims to provide important information for aquifer managers to take steps towards a better use and protection of the resources.

Figure 2: The general approach of vulnerability methodologies

Some problems arise when multiple tools are used and compared because most vulnerability methodologies come with a high degree of subjectivity and the results may not the be consistent among different methodologies. This means there would be as many classifications as methodologies are applying to any site (Moreno Gómez *et al.*, 2018).

1.3 The aim of the project

Our approach and the previous works this project is solely focused on intrinsic vulnerability. In fact, many GIS-based methodologies rely upon geological and hydrological information to build vulnerability indexes based on the sole characteristics of the study area to estimate travel time from surface to groundwater. The objective of any vulnerability approach is to identify in a map the different vulnerable zones of a catchment in order to provide tools for decision makers to act upon that goal (Marín and Andreo, 2015). Although many vulnerability assessments have been made, karstic particularities must be carefully understood and take into consideration. The COST Action 620 (Zwahlen, 2003) highlights this features and stressing the fact that karst is widely variable from one region to other, therefore the need to make regional studies.

So, according to the literature review and previous studies, we intended to answer inquiries regarding the behavior of an unspecific, conservative pollutant that travels from the surface to the water table in terms of time. Our current hypothesis follows most vulnerability approaches towards travel time in unsaturated conditions to be either higher or lower depending on the density of karst features and the nature of the epikarst. Moreover, some studies focus solely on the travel time of a pollutant through the unsaturated zone. So, moving forward to residence time, what are the factors that influence most of the traveling time of a certain pollutant? Time is a relative parameter that relates two major arbitrary spots: a source of pollution and an ending point. To know the behavior of a pollutant, we investigate and identify external parameters affecting the most the residence time of the pollutant? Our main hypothesis relies

on recharge playing an important role (Robins, 1998), but how does the recharge processes influence the residence time of a pollutant in the Yucatán karst system?

Once data has been estimated from the model, we aim to integrate results into vulnerability model. To sum up, four are our main driven questions:

1. How does the aquifer reacts, overall, to the recharge process in the study area?

2. What is the behavior of any conservative unspecific pollutant in the aquifer?

3. What are the factors that influence the most the travel time of unspecific pollutants in the aquifer?

1.4 The scope of the project

This study aims to contribute the uprising Yucatán studies on pollution and numerical modeling with the purpose of integrating residence time as a factor to estimate groundwater vulnerability. Few studies have been made available to public related with numerical modeling on the region, and even fewer have tried to couple transport models with groundwater solutions, especially using karstic codes. Based on previous studies already conducted with vulnerability indicators, we try to bring together preliminary results of this project with those vulnerability studies.

When it comes to vulnerability research, more studies have been conducted and several publications point out to increasingly high vulnerability zones. The IKAV project aims at the development of an integrated vulnerability. This is a Ph.D. part of the Researcher Group INOWAS at the TU Dresden.

IKAV project is currently funded by CONACYT, the Mexican Council for Science and Technology – in Spanish- and has already presented some results at international conferences especially focus on karst, like the one held in Zadar, Croatia, "Man and Karst 2017".

Another related vulnerability study was conducted at TU Dresden entitled *"Vulnerability assessment of karstic aquifer systems: Yucatán state case"*, which four existing vulnerability methodologies were applied for the karst aquifer at Yucatán. EPIK, Slovene approach based on COP, DRISTPi, and KARSTIC -based on DRASTIC method- are developed rating indexes that help to define vulnerable areas towards pollution, but are mainly based on intrinsic considerations and just COP considers vegetation cover that can be indirectly linked to land use and potential pollution sources (Marín, et.al. 2015; Moreno, 2017). Most methods came together when defining high and very high vulnerability zones, mainly because they would consider, in a way or another the karstic features specific to the areas. The question remains. How can we couple our estimated time with methodologies that were mainly modified to assess intrinsic resource vulnerability?

We postulate that when considering times, vulnerability becomes a relative parameter, because it will be dependent on two sites: a supply target, such a drinking well, a river, a field of pumping wells or even a city, and a release point, where pollution originates, so, any relevant time will relate those two points.

The original project aims to compute two main time parameters:

1. Residence time, defined as the time it takes to the particle to leave the system, using two tools: transport model and particle tracking.
2. Traveling time, understand as the time it takes for the pollutant to reach the water table and travel to the unsaturated zone.

To residence time, is necessary to evaluate possible impacts on source vulnerability, by considering times between a located pollution area and the closest source of drinking water in the system.

1. Using the constructed model, we were able to describe residence time in more detail and we are confident that it may shade light upon vulnerability analysis

We do not aim to design a new rating system for a vulnerability index, but to give some general notions as to how can it be done, and which elements may result useful for it.

2 Study Area

Yucatán peninsula is located south-east of México (Figure 3). Yucatán aquifer is one of the biggest transboundary aquifers in the world – around 165,000 km^2- and is shared by México, Guatemala, and Belize (IGRAC, 2017). In the Mexican area, it comprehends the states of Yucatán, Campeche, and Quintana Roo. Yucatán state (hereinafter Yucatan) has around 39 400 km^2, which represents 28% of the whole peninsula surface.

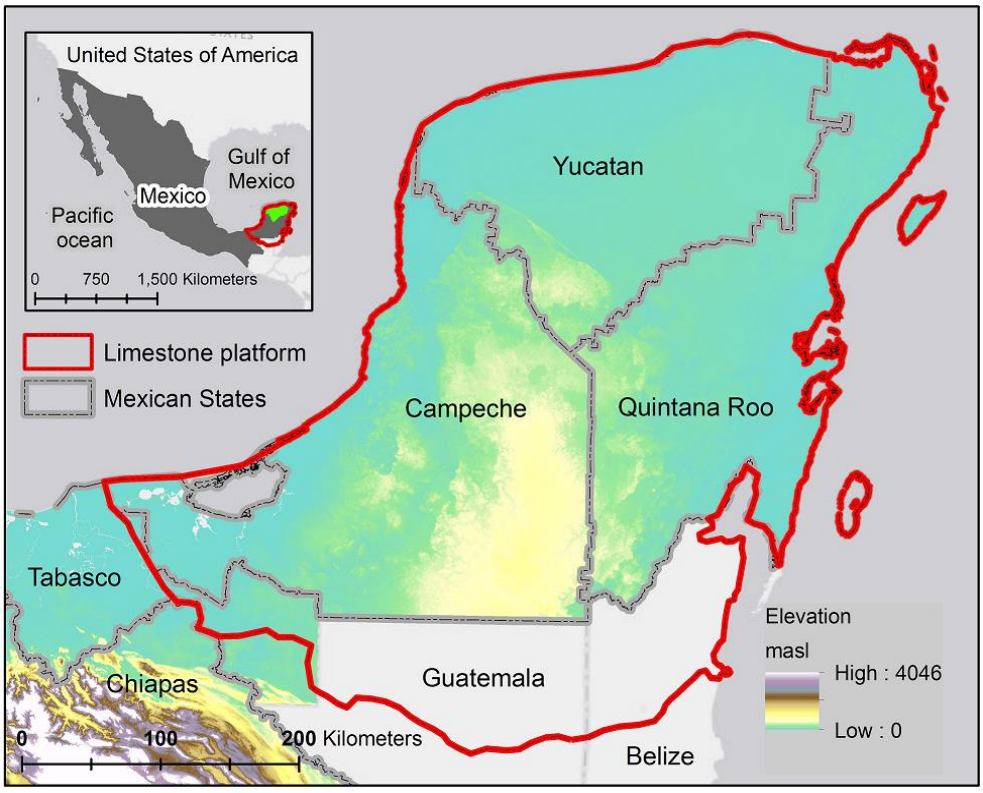

Figure 3: The Yucatán Peninsula as a transboundary aquifer. Source: Moreno, 2018. Aquifer limits as presented by (Bauer-Gottwein, *et al.*, 2011)

Yucatan is an arising developing area (Villasuso and Méndez, 2000), a situation which places groundwater resources under special stress and, therefore, calls for strong protection policies. In fact, Yucatán host one Ramsar UNESCO protected location by international laws – wetland directives- because of the ecological relevance of the ecosystems (Bauer-Gottwein, *et al.*, 2011).

2.1 Elevation, Slope, Lithology and Hydrogeological Areas

Flatness of the terrain is among the most characteristic features of the area, with an average slope of 1.5% and average altitude of 28 m above sea level, except for a small area of the southeast, where a hill area named “Sierrita of Ticul” is located; this the tallest point on the peninsula, formed by a fault system (Bauer-Gottwein, *et al.*, 2011). The flatness of the area and fissures do not allow the formation of superficial currents.

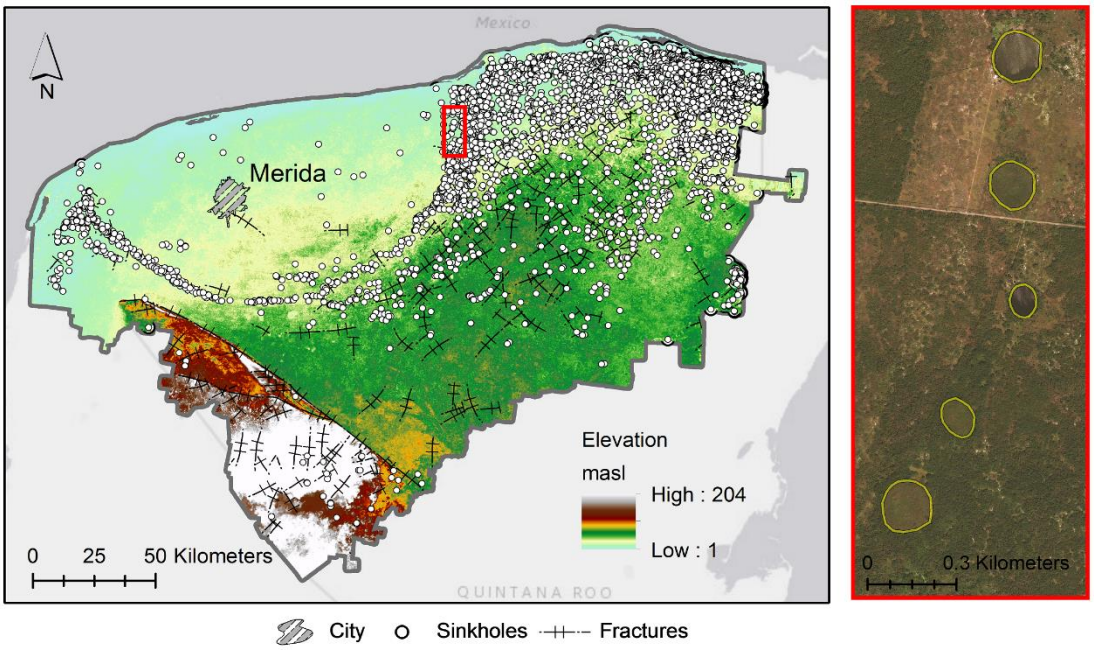

Figure 4: To the left, Yucatán Elevation, sinkhole density, and fissure distribution. To the right, a satellite imagines used to redefine by ArcGIS and LANDSAT tools sinkhole density in the area (work in progress by Moreno, 2017).

One of the many specific characteristics is the existence of sinkholes (locally called cenotes) and dolines- non-collapse sinkholes with not connection with groundwater currents-. The first ones are so deep that can connect the surface with the shallow groundwater water table directly, which then increases both recharge rates and risk of pollution while decreasing traveling times. In the study area, at least 454 km^2 are karstic depressions, with the majority of dolines.

Sinkholes are spatially distributed showing high sinkhole density areas. Due to the lack of available data regarding sinkholes location, a new map created using LANDSAT and GIS tools to redefine the sinkhole density of the area (see Appendix 2, figure 54). A total of 55555 sinkholes were located using combined tools (Moreno-Gomez, et. al. 2018, work in process).

Yucatán is administratively divided into four hydrogeological regions: cenote ring, coastal area, central plain and the fault and hilly area. The Inner Cenote area (ICR) is an area in the North-west Yucatan of 11,800 km^2, with approximately 208 km of the coast (Sanchez, 1999, 28pp). Coastal and inner ring area

account for 7% and 20% of the Yucatan total area but concentrate more than 57% of the state population (Bauer-Gottwein, *et al.*, 2011). Also, related with Yucatan terrain and low slopes, measured hydraulic gradients are low, with values between 7 and 10 mm/km (Marin *et al.*, 2000).

It is interesting to note that most of the inner cenote area seems to be younger than the rest of the emerged platform, mainly composed of limestone. Limestone can be found through the whole area and is covered by a highly permeable, yet hard crust known as caliche.

The Chixchulub ring is a fault formation that is believed was formed by a meteorite impact. This feature highly impacts groundwater flow and virtually isolates the inner circle area from the rest of the peninsula (Batllori, *et al.*, 2006). The cenote ring area has been classified as a slightly karstified area surrounded by a highly –although overestimated- karstified area.

Figure 5 shows the different limestone karstification levels adapted according to literature and sinkhole density maps and the hydrogeological regions, relevant characteristics for this project.

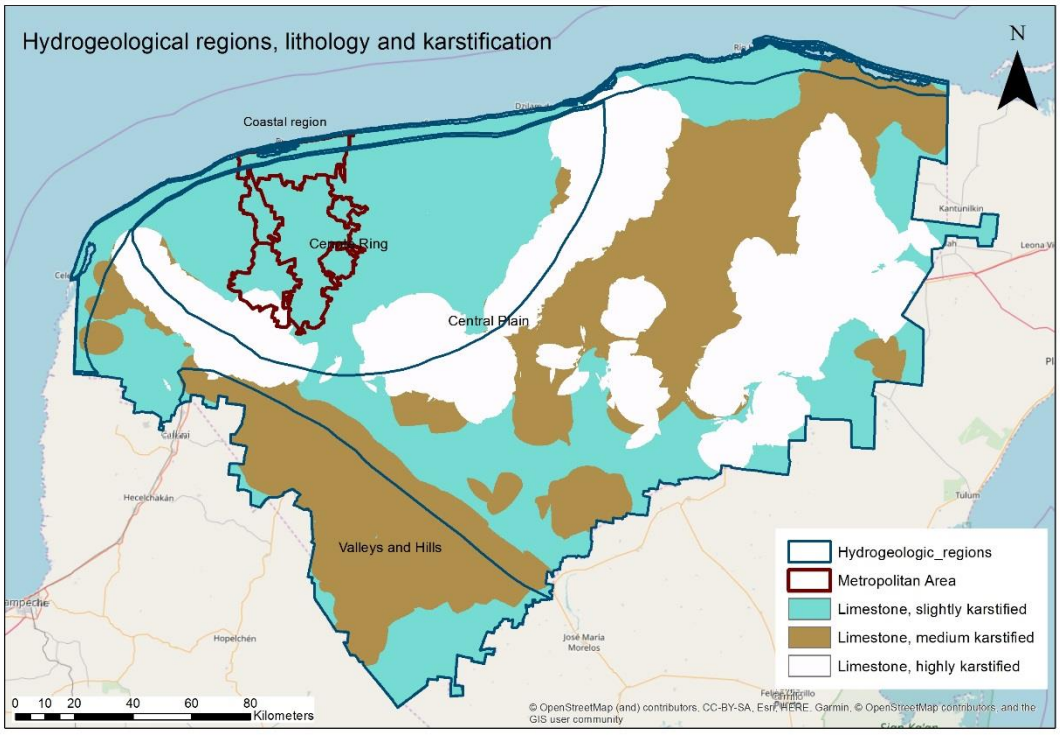

Figure 5: Hydrogeological areas and degree of karstification. The map was elaborated online available data and classified according literature to fit vulnerability classifications (Moreno-Gomez, et. al. 2018).

Most of the peninsula has limestone, dolomite, and anhydrite from the Mesozoic and Cenozoic period, where rocks have developed primary and secondary porosity, both in the rock matrix and due to cavernous fracture (Socki and Hughes, 2015). This different level of porosity also impacts the definition of hydraulic conductivities of the area.

Table 1 shows reported K values and their sources. Most data values are obtained from numerical modeling and calibration and are scale dependent. They are also related to the conceptualization of the flow paths and the type of aquifer (Bauer-Godwein, *et al.*, 2011).

Table 1: Hydraulic features reported in the literature for the study site

Value of some use or estimated Hydraulic conductivities	Source
1x10^0 1x10^-1 m/s North-western part of the region	Marín, 2000
1x10^-6 to 5x10^-3 m/s inflow channels in cores Along the highway to Progresso 0.55 m/s 6 m/s in the ring of cenotes 0.15m/s rest of the aquifer	González, 2002
1.115 m/s interior plain, coastal area and the cenote ring	(Pérez Ceballos, 2003)
$5.5x10^{-3}$ Valleys and hilly area	(Pérez Ceballos, 2003)
0.3 m/d to 1.2 m/d (value that is common for karst aquifers).	(Sanchez, 1999)

Topographical and lithological features account for the prevalence of diffuse infiltration pattern that dominates recharge processes. Most of the area would have diffuse infiltration instead of concentrated one, due to the lack of perennial streams and surface runoff. This also plays an important role when it comes to the dynamics of pollution because, as national reports have shown, the main problem is the quality of the water itself, not the amount that is being extracted (Bauer-Gottwein, et. al., 2011:518pp).

Although the existence of karstic features increases vulnerability, the study area is located within the relatively new sedimentary basin with low karstification development compared with the rest of the area. While the Chixchulub formation explains high density of sinkholes, it also explains why the degree of karstification and fracture in most inner ring area is quite low, comparatively speaking with the outer areas or the ones close to the cost.

2.2 Soils and vegetation

Another important feature in Yucatan is the soils distribution and its thickness. Besides the physicochemical properties of the soils, the thickness will play an important role both in recharge rates and pollution buffering. If the soil has a high clay content and is thicker will offer more protection than a thin sandy soil. Most of the area has almost no soil development, these characteristic increases karst vulnerability towards pollution.

The most common soil types are rendzina and lithosol, highly rocky soils related with tropical ecosystems with a superficial layer rich on organic matter. Soils layed over limestone and in average do not reach more than 25 cm depth (Instituto Nacional de Estadística y Geografía, 2004).

Figure 6 shows the most common types of soils reported by CONABIO. Most of the area has almost no soil development, which on average increases karst vulnerability towards pollution.

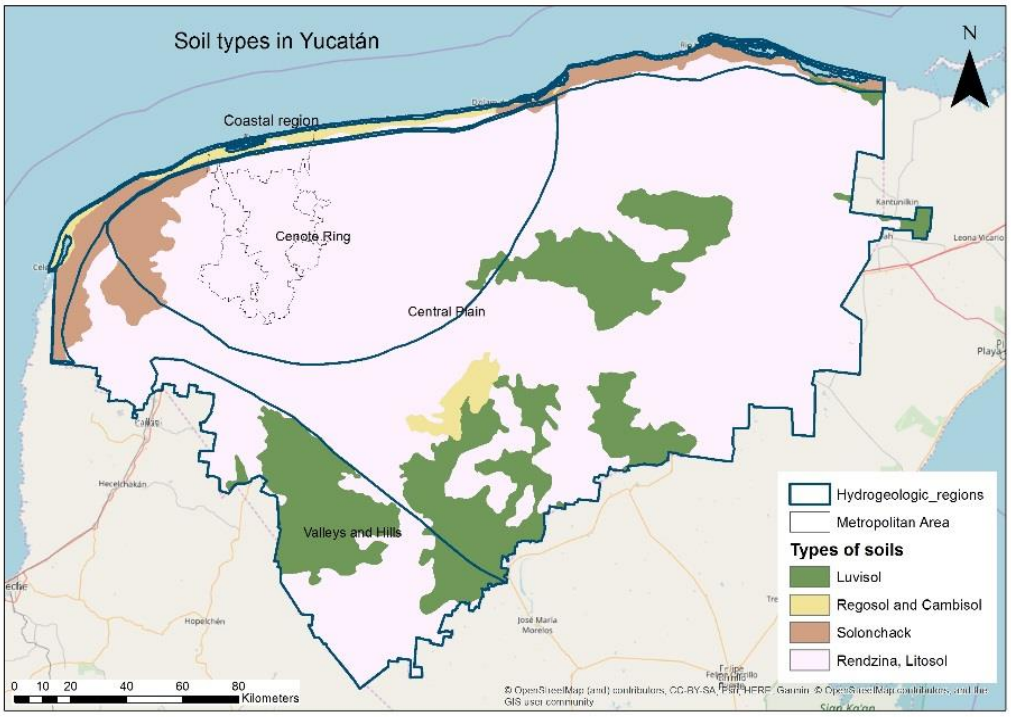

Figure 6: Soils in the Yucatán Peninsula, from available in at CONABIO (2001)

As any tropical ecosystem, most of the coastal area is characterized by mangrove while the most northern area of the central plains and a huge area of the cenote basin is already being used as agricultural land. This will become relevant when assessing nitrate pollution, mainly because agriculture is so far the most important source of nitrate diffuse pollution recognized today (FAO, 2002). Figure 7 shows average soil depths within the study site and the vegetation cover.

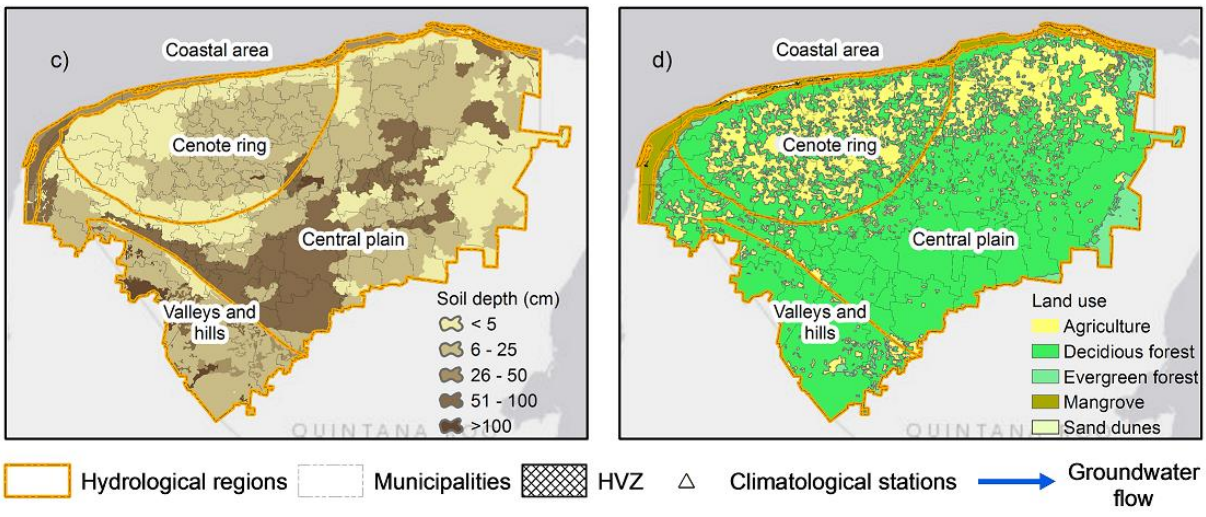

Figure 7: Soil depth (c) and land use (vegetation cover) (d) in the Yucatán area. Source: Moreno, 2017. Maps developed with public data from CONABIO

2.3 Water tables, Precipitation and Recharge

As most coastal aquifers, the system is deeply linked to the saline interface. In the Yucatán karst, the saline interface goes inland reaching from 40 to 110 km according to different sources. The depth of the seawater interface increases as it gets away from the coast southward, influencing most costal heads and reducing its impact zone inland (Fransson, 2015).

The shallow water tables are also a main feature in the area and maybe one that has been overlooked for some time when it comes to vulnerability assessment. Figure 8a shows the average annual water tables for the focus area, computed using a direct relationship between the surface topography and data from 105 different wells distributed all over the state. With an average value of 7m from the surface, groundwater is shallow towards the coast and deeper inland.

Yucatán is characterized by a tropical weather with a widespread precipitation regime that can fluctuate between 200-400mm along the coastal area to 1000- 1200mm (Delgado *et al.*, 2010) (Figure 8.b). Data from 66 climatic stations shows a cumulative precipitation with an average annual value of 1087 mm per year (Figure 9). Some previous studies, mainly focus on vulnerability and nitrate pollution, have already estimated some recharge values as precipitation percentage, assigned by the municipality (Pérez Ceballos, 2003).

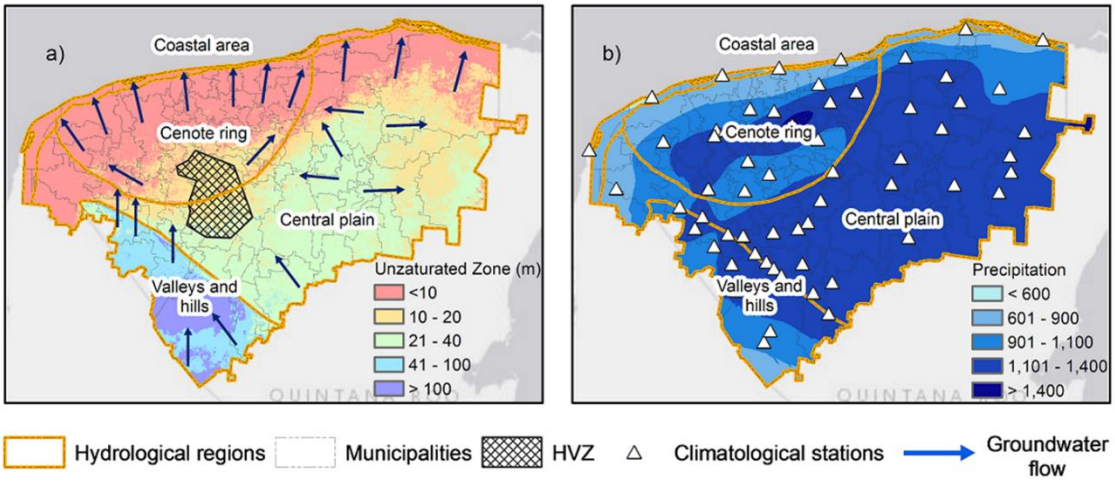

Figure 8: Water table levels (a) and precipitation spatial distribution (b). Source, Moreno, 2017. Maps elaborated with available data from CONABIO, INEGI AND SEDUMA.

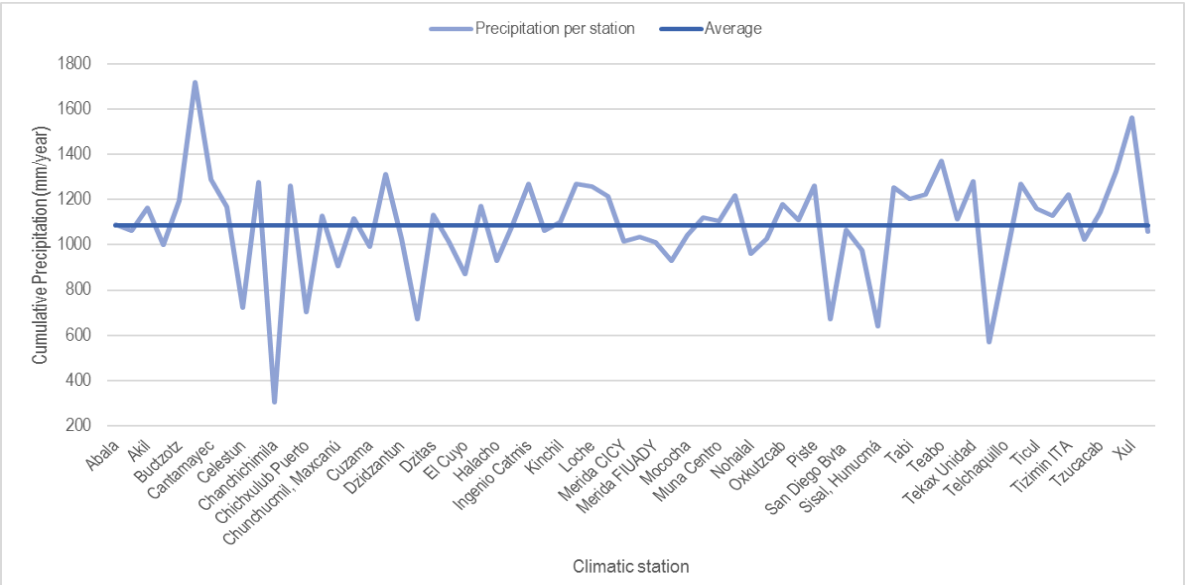

Figure 9: Annual precipitation for each of the 66 climatic stations. Data from 1995 to 2015 and its average value. Digital data sets provided by CONAGUA 2015.

Average annual precipitation from the climatological stations is presented in Figure 10, and it shows that the wet season occurs from May to September while the dry season from October to April, with maximum values, presented mostly on September.

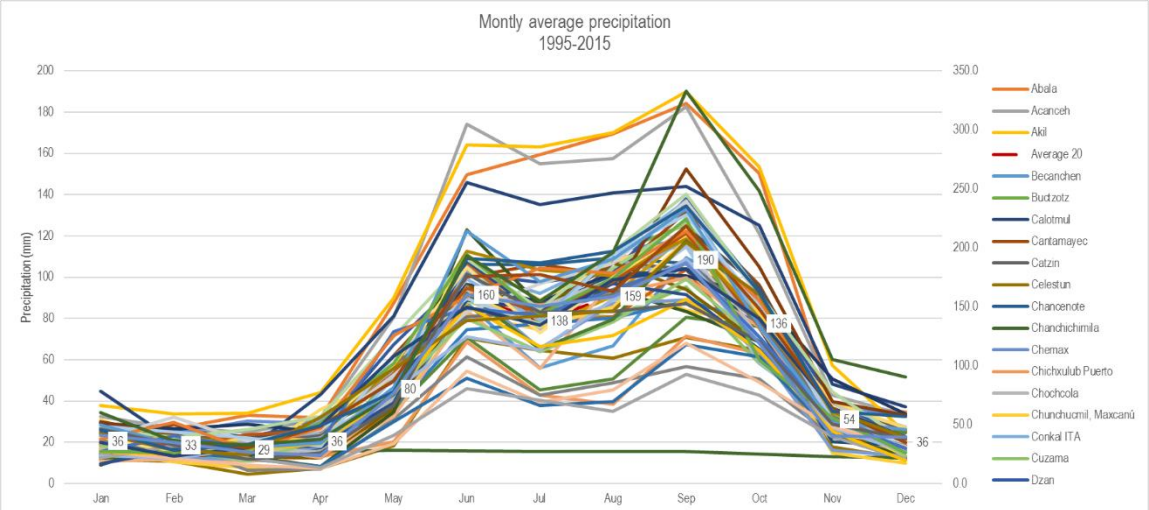

Figure 10: Seasonality of annual average precipitation in Yucatán peninsula

The seasonality also responds to a known hurricanes season that widely impacts the aquifer and backs ups the idea that the aquifer responds rapidly to the recharge process. It has been reported that after hurricanes, the water table rises almost instantly (within a few hours), for more than one meter of difference (Socki and Hughes, 2015).

Karst systems have heterogenic dynamics when it comes to the recharge process. The working assumption in this work is that recharge is the main driven of any transport process of pollutants from the surface towards the unconfined free aquifer of the study area. Therefore, a depth understanding of all the related process is needed. Is highly accepted that water table depth is mainly driven by the recharge processes along the whole aquifer and especially susceptible high precipitation events, except for the near coastal area, which may be more influenced by the tide dynamics (CONAGUA, 2002, 2012; CONAGUA and C.V., 2004; CONAGUA and Costera-IC, 2009, 2010; Bauer-Gottwein, *et al.*, 2011; CONAGUA and Betsco Consultants, 2011). In contrast to many sources, in this project we used precipitation patterns computed from figure 9 and 10 (page 19) -the resulting map, figure 55, see appendix 3-, which resulted in slightly different precipitation pattern and was used in further steps of the project.

Some recharge estimations based on hydrological water balance have been recently computed by the national water authority and are showed in table 2.

Table 2: Simplified water balance of the Yucatán karst official data. Source: (CONAGUA, 2018)

Total annual average recharge (Mm^3 per year)	**Surface area (km^2)**	**Discharge (Mm^3 per year)**	**Available groundwater (Mm^3/year)**	**Extracted water for human purposes (Mm^3 per year)**
21 813.4	124 409.1	14 542.2	2 842.7	4 448.82

Recharge in the area has a wide range of estimations, (table 3). This data is later used to compare discharge estimations given by the model and to analyze how our own computations behave through the model.

Table 3: Recharge data for the study area

Recharge express as a % of mean annual precipitation	**Source**
12% in the southwestern part of the modeled area 10% in the southern part, because of a thicker soil layer 20% the rest of the area	(González Herrera, Sánchez y Pinto and Gamboa Vargas, 2002)
80% of infiltration (see equation 1)	(Gómez *et al.*, 2018)
Approximately 25.3km3/year	(Parra *et al.*, 2015)

Unique characteristics are the flatness of the terrain, the existence of limestone lithology all over the aquifer and the fact that most precipitation percolates downward to the aquifer due of loss in evapotranspiration processes (Gonzalez-Herrera *et al.*, 2014). Given the specifics of the area and the fact that there are no surface water bodies, it is possible to assume that:

$$Infiltration = Precipitation - Evapotranspiration \qquad (1)$$

The simplified water balance (equation 1) would be then corrected for the actual amount of percolation that reaches the aquifer. Studies have already concluded that it is the recharge processes which

determines in great length how does the water table reacts (CONAGUA and Costera-IC, 2009; CONAGUA and Betsco Consultants, 2011).

2.4 Political features: municipalities, population and Mérida Metropolitan Area (MMA)

When it comes to its political division, Yucatán has 106 municipalities (INEGI, 2016). The ICR, also known as the Chixchulub sedimentary basin (Socki and Hughes, Hughes and Socki an Hughes, 2015), contains 64 municipalities, 6 of which are part of the Mérida metropolitan area (Figure 11a). In this area is located the Mérida municipality and the Merida city, capital of the state, where at least 57% of the total state population is concentrated. By 2015, the total population was around 1.9 million (Figure 11b).

Due to this fact, most urban pollution is concentrated in the metropolitan area due to the current lack of a proper sewage system (Arcega-Cabrera *et al.*, 2014). Local studies have assessed both the presence and the possible vulnerability implications of nitrate pollution in the Yucatán aquifer (Pacheco A. and Cabrera S., 1997; Pacheco *et al.*, 2002; Pérez Ceballos, 2003; Gonzalez-Herrera *et al.*, 2014; Torres, M. *et al.*, 2014; Rojas Fabro *et al.*, 2015). Most of them conclude that some areas have already exceeded the permissible concentrations within human consumption water quality standards.

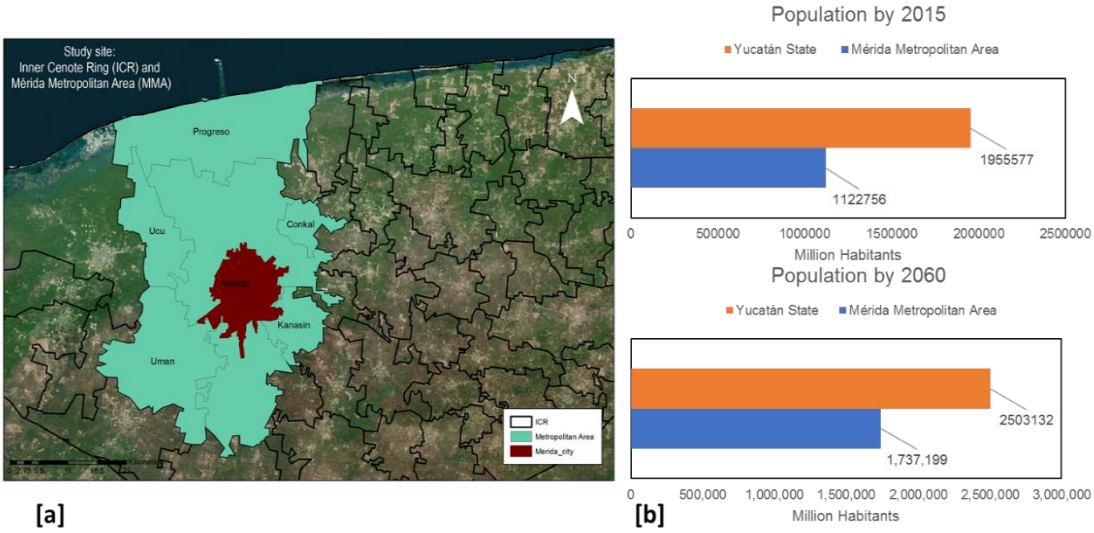

Figure 11: a) Mérida Metropolitan Area and b) Population by 2015 and 2060 (forecast) comparison between MMA and rest of the State, Data from INEGI 2015.

Most pollution that reaches the aquifer would come from diffusion infiltration that occurs due to the lack of a sewage system. Generated wastewater is deposited into septic tanks that eventually leak. Some areas use injection wells taking wastewater and place it in the saline interface of the aquifer (Marin *et al.*, 2000). As stated before, the main problem of Yucatán´s water resources are more related to quality and not with the exploitation status. This is mainly because of a generalized lack of wastewater management infrastructure -sewage and water treatment plants- and the existence of unaccountable artisanal septic tanks that leak directly into the aquifer (Torres, M.C. *et al.*, 2014). Population mostly

concentrates along the metropolitan area, which currently concentrates more than 57% of the total state population (Figure 12) and will continue as a tendency for the upcoming years.

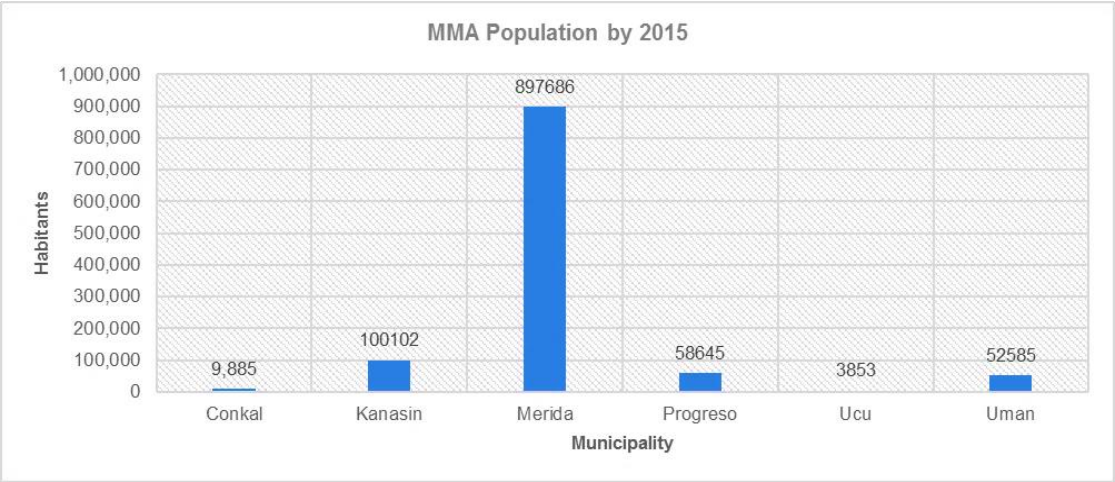

Figure 12: Population distribution in MMA

2.5 Water consumption and wastewater generation: pollution forecast

Extraction for human consumption does not jeopardize the aquifer water availability and around 7.5 million m^3 of groundwater per year are extracted but are quickly recover through constant and rapid recharge processes.

Extraction volumes represent 58% of the peninsula annual withdrawal and the aquifer remains almost undisturbed as can be seen from the higher availability of water *per cápita*, which is quite high compared to the national average, with about 7600 m^3/person/year (Rojas Fabro *et al.*, 2015). This is directly related with the fact that most of the area acts as a recharge zone – due to the fractured and karstified level of the rocks - particularly high in the cenote ring, a line with a high occurrence of sinkholes. Features that preserve the water resources in terms of quantity, also increase the vulnerability of the resource in quality terms.

Available data suggested that from the total amount of supply water, 40% gets lost due to pipe leakage and can be accounted as recharge again, which has already been done when reporting water consumption *per cápita* and has to be consider on the model conceptualization, mainly because recharge in the city does not occur in the same amount and rates than in the rest of the study area, where not such high levels of imperviousness due to urbanization have been reached.

From the amount of supply water, it has been estimated that 80% will leave as wastewater and most of it will not be treated although pollutants concentration would be buffered by the artisanal septic tanks all over the city as natural attenuation occurs in the septic tanks.

Given that there is not enough data to assess the real concentration that water from septic tanks enters the natural system when leaking or the residence time of the water in them, we will assume as initial concentration the inlet standard concentrations of any water treatment plant when available or the detected nitrated concentration for the field campaign reported by Pacheco (2002). Although pollutants suffer from degradation when temporally retained in septic tanks, for modeling purposes, we will use the same concentrations reported. The location of the municipalities will be defined as a recharge point [4] with a specific nitrate concentration as an initial value to run the model, except for the Merida case, that would be simulated a 2D object as infiltration basin. Table 4 shows the available data for the metropolitan area when it comes to water consumption and the calculations made with the previous assumptions.

Table 4: Consumption and wastewater generation in the MMA

Municipality	**Population (2015)**	**Area km^2**	**Water consumption (m3/d) [1]**	**Generated Wastewater (m^3/d) [2]**	**Water to septic tanks (m^3/d) [3]**	**Water to septic tanks (m^3/s) Recharge rate [4]**
Conkal	9 885	57	2352.368	1881.89	1237.35	0.014321132
Kanasín	100 102	73	27696.500	22157.20	14428.77	0.166999645
Mérida	897 686	858.41	247240.200	197792.15	166362.98	1.925497456
Progreso	58 645	270.1	14630.190	11704.15	10655.46	0.123327062
Ucú	3 853	193	726.968	581.57	212.33	0.002457556
Uman	52 585	234	12975.480	10380.38	5463.20	0.063231427
MMA Population	1 122 756					2.295834278
Yucatán Population	1 955 577					

A special stress is expected if we analyze any potential pollution towards the coast and the other MMA cities, specially Progreso. This coastal city is the third most populated city in the MMA, but it may be more vulnerable to pollution than other cities due to the groundwater flow patterns. As most regional numerical models suggest, all the groundwater flow that does not deviate towards the sea via the Cenote ring is discharge along the uniformly (Socki and Hughes, 2015) and follows a Northern- South path that will lead to Progreso, given the hydraulic gradient of the area.

When it comes to pollutants seasonal behavior, nitrates can serve as an example. Time series provided by CONAGUA show a relationship between nitrate concentration in relation with dry and wet season (Figure 13).

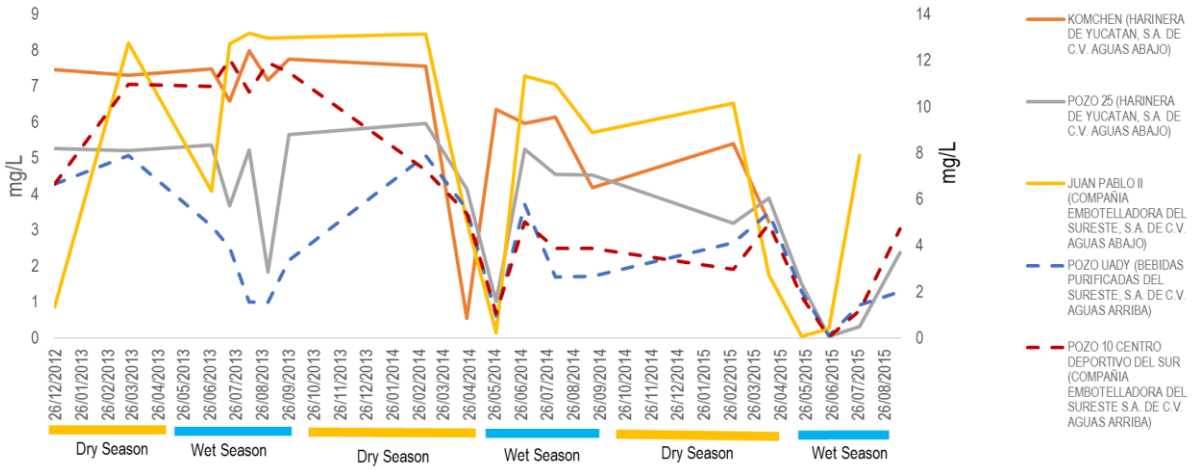

Figure 13: Time series for nitrate concentration trough seasons

There is not a perceptible tendency except from the fact that in upstream samples, nitrate concentration is in most cases lower than downstream, but the concentrations in the same wells vary considerably through time. Nitrate sampling points for some fieldwork campaign is showed in Figure 14, and we have highlighted the ones that were feed into the model. The main limitation of these values is their accuracy, for they are average values from a single campaign and there is no record of the depth at which they were measured. Nevertheless, using ArcGIS Tools, we build a spatial distribution map of Nitrates as a visual aid.

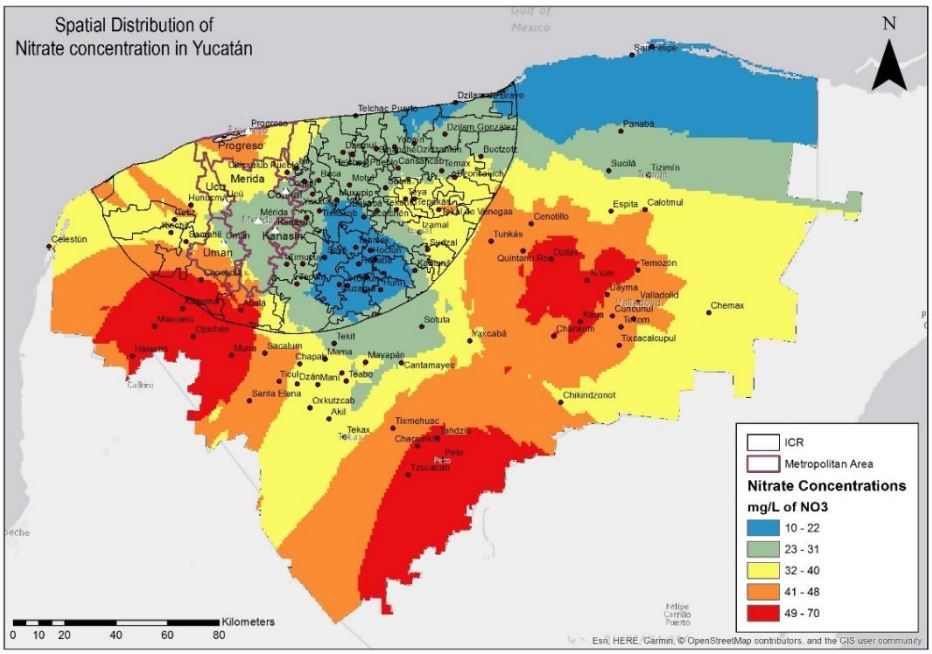

Figure 14: Nitrate spatial distribution in Yucatán. Kriging raster created with data published by Pacheco, 1999.

Given the expected heterogeneity and anisotropy of the area, interpolation tools are not the best approach to estimate known concentration (Zwahlen, 2003), but with the available data, we wanted to

shade some light with regard the pollutants spatial distribution and its possible correlation with human activities. These reported rates are not considering an increasing NO_3 trend concentration which will come as more as economic and population grows. Nonetheless, it seems estimations for the current situation and the NO_3 distribution may work as a good first approximation. Data show by (Pacheco, et.al., 2004) also contributes to assume that averages NO_3 concentration do not go above 10 mg/L yet (see figure 57, appendix 4).

2.6 Focus area: MMA

Given all the previous considerations, we decided that the focus area of the modelling part will be MMA (figure15), given it concentrates more than 57% percent of the population, has a running problem with sewage and proper water waste disposal and is located close by a high density agricultural developing area, which suggest nitrate pollution is a wide possibility.

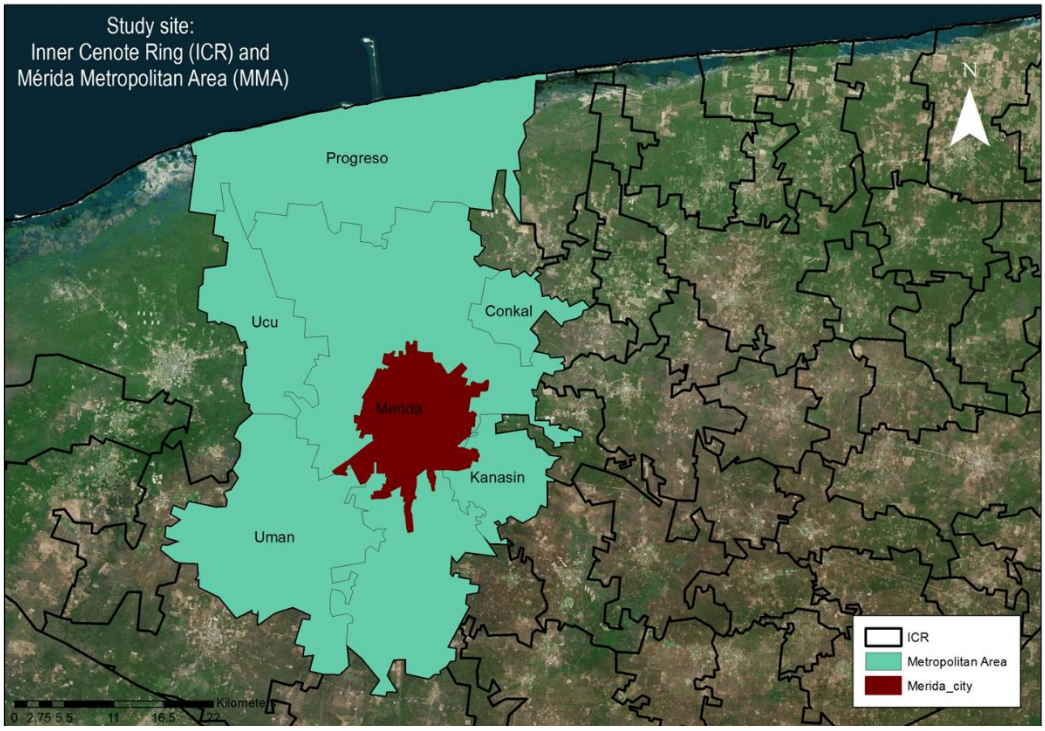

Figure 15: Focus area for modeling purposes, Mérida Metropolitan Area: Mérida city and suburbs, Progreso, Ucu, Conkal, Uman and Kanasín municipalities.

This possible pollution is directly related with the existence of artisanal septic tanks. These septic tanks have a unknow residence time by itself which helps to lower the initial concertation of many pollutants, such bacteria or CBOD (carbonaceous biochemical oxygen demand), but lack of data does not allow us to state the amount of degradation of any pollutant in this stage. Therefore, the recharge rate for each point would be used as point recharge to see the extent of the plume, but it would also be adjusted to the area of each municipality.

Progreso is the third most populated city within the MMA (see Figure 12, Section 2.4), but furthermore, is the only site between the modeled initial concentration that already excess NO_3 drinking water standards – México, 10 mg/L, according to NOM-127-SSA1-1994, modified in 2000 - and effects of ocean pollution have already been reported (Pacheco and Cabrera, 1997; Gonzalez-Herrera *et al.*, 2014; Botello, 2015).

There is, then, a direct correlation between wastewater generation and population, as it can be seen in table 5, where some data for transport model has been estimated based, mostly, on consumption of water.

Table 5: Data used for transport estimations in MMA: Population, NO_3 know concentration, and recharge rate obtain from wastewater generation rates

Municipality [A]	Population (2015) [B]	Initial NO_3 concentration (mg/L)	Area km2 [D]	Water consumption (m^3/d) [E]	Septic tanks (m^3/d) [F]	Water to septic tanks (m^3/day) [G]	Water to septic tanks (m^3/s) [H]
Conkal	9,885	29.7	57	2352.368	1237.34581	1237.34581	0.01432113
Kanasín	100102	39.2	73	27696.5	14428.7693	14428.7693	0.16699964
Merida	897686	28.0	858.41	247240.2	166362.980	166362.980	1.92549745
Progreso	58645	78.0	270.1	14630.19	10655.4581	10655.4581	0.12332706
Ucú	3853	29.1	193	726.968	212.332821	212.332821	0.00245755
Uman	52585	14.81	234	12975.48	5463.19530	5463.19530	0.06323142
MMA Population	1 122 756						2.29583427
Yucatán Population	1 955 577						

2.7 Literature review

Karst aquifers are especially vulnerable to pollution given there are high transmissivity rates because of the existence of preferential flow paths which allow water – and any pollutant it might carry- to travel fast and far. They are also characterized for little to nothing buffer areas when it comes to the lithological composition which reduces attenuation processes. These features make them both vulnerable and more difficult to study. In this section, we mention some of the important works related to the central topics of the master thesis.

2.7.1 Residence and traveling time in an aquifer

Few studies have been performed when it comes to including or even assessing the residence time or the traveling time of pollutants (Dedewanou *et al.*, 2015). For instance, Kralik and Keimel (2003) propose a new approach considering the time of traveling and input, mainly recharge, to assess the vulnerability or an area. Figure 16 shows the subfactors assess in the index.

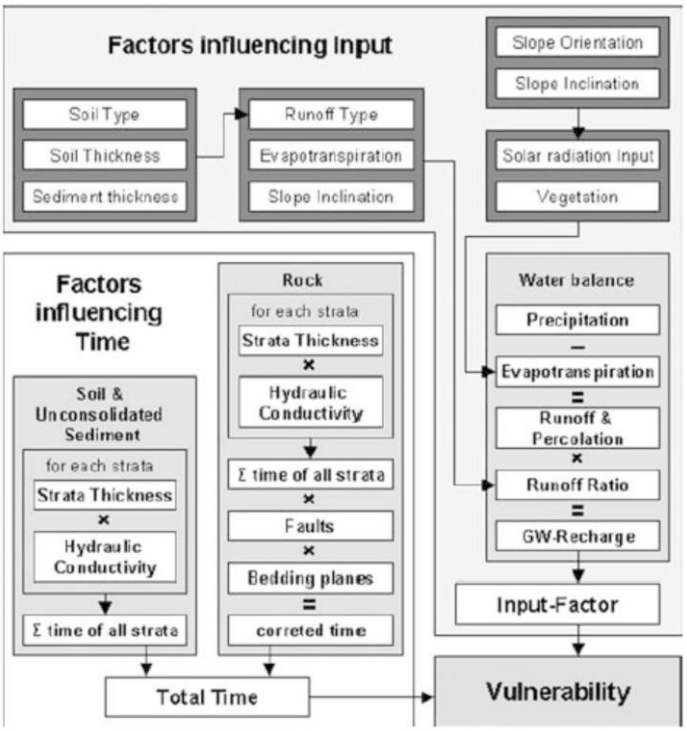

Figure 16: Input and time method to include time traveling into vulnerability assessment methods. Source: Kralik & Keimel (2003)

Although the index states residence times, it estimates this parameter as a dependent parameter or physical features and does not tackle any sorption approach, which wen modeling can be done.

1. The pollutant can be studied as an ideal tracer -mainly low pH and temperature dependency, low sorption effects, high chemical and biological stability and photolitically stable (Wenninger, 2017)- thus the only vulnerability that is been assess is the intrinsic one.
2. The focus of this vulnerability assessment method relies on the pollutant reaching the water table (resource vulnerability). This implies that only traveling time from the surface to the aquifer.

Others consider time as a function of dry and wet season and events (mainly dependent of high recharge phenomena and design vulnerability indexes depending on how an area is located from a recharge zone (Brosig *et al.*, 2008), and heavily relies on hydraulic gradient values, slope gradients, and infiltration been driven by preferential infiltration areas.

2.7.2 Recharge and saline-fresh water interface

Few studies have been done when it comes to saline intrusion in the Yucatán area. The most deal with the dynamic of the mixing zone. Nevertheless, it seems that the recharge process and the sea level have a high influence on the saline interface location (Parra *et al.*, 2015). For more details on recharge values as a possible input into the model, we gather several reported data that can be seen in table 4. The relationship between the rapid recharge rates has been studied by Escolero et.al. (2007), and it points out to a deeper study in the interactions between high amounts of recharge and the location of the saline mixing area as well as the saline lens, but only in relationship with high and rapid amounts of recharge, but not with average conditions. The relationship between the rapid recharge rates has been studied by Escolero et.al. (2007), and it points out to a deeper study in the interactions between high amounts of recharge and the location of the saline mixing area as well as the saline lens, but only in relationship with high and rapid amounts of recharge, but not with average conditions.

Figure 17 shows the approximate position of the fresh, brackish and saline lens below Mérida city, which accounts for at least 60% of the population in the area. Other sources describe the saline intrusion lens in the Yucatán aquifer as the depicted in equation 1 $di = 40 * dx$ where dx is the elevation above mean sea level and di is the depth of the interface. In other sources (Perry & Velazquez-Oliman, 2003), the water table level is more controlled by the sea level than recharge processes, although most of the influence is focus near the coast.

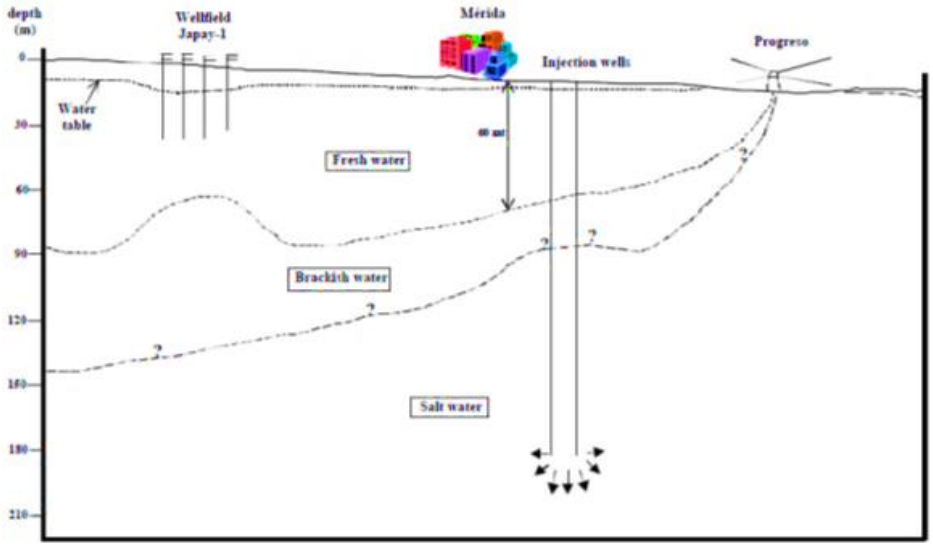

Figure 17: Position of the water lens below Mérida City. Source, Marín (2000)

2.7.3 Previous modeling studies

There are few studies that have taken upon the task of modelling groundwater flow in the karst system and have been used as a primary source of some general parameters for the setting up of the present groundwater flow model (González, et.al., 2002; Pérez Ceballos, 2003; CONAGUA and Costera-IC,

2009; Gondwe *et al.*, 2010). Between the main modeling remarks, calibration seems to respond more to recharge and discharge settings than to the inherent heterogeneity of the aquifer (Sanchez, 1999), although one may argue that the scale and the EPM approach may also play an important role in not reflecting the whole influence of local conduits in residence time.

The idea of modeling using layer discretization has also been at some extend teste and best results for it have found that combining a lower conductivity layer with a higher conductivity layer may lead to good calibration, as wells as to support steady-state simulations (Marín *et al.*, 2001). This highly conductive layer seems to work as a bulky path that dominates groundwater flow towards the coast and is not only used as a numerical simulation feature but is supported by empirical data (Bauer-Gottwein, *et al.*, 2011)(Buckley *et al.*, 1994). Nevertheless, most studies coincide in the conceptualization of the system, describing the whole area as a recharge catchment, with lack of surface water bodies and where groundwater flows are mostly determined by hydraulic gradient and the anomaly that the cenote ring, as a drain, plays within the system, conducting water towards the sea in a preferential and dual drain system (see figure 58, Appendix 5).

3 Methodology: conceptual model, working assumptions, and input data sets for Model Muse

This work aims to estimate residence time and pollutant behavior applying a conduit flow process package (CPF) unlike previous numerical models that have simulated groundwater flows in Yucatan using equivalent porous media approaches (EPM) (González et.al., 2002). Results obtained in this work will serve as a basis to couple the best groundwater fitting model with a transport model to assess the Yucatan groundwater vulnerability against surface pollution.

The current conceptual model of the area is given by (González et.al., 2002). Most of the aquifer, including the focus area, is an unconfined aquifer, depicted as a freshwater lens floating above saline water (Figure 18). The exception to the unconfined aquifer being the hydrological area along the coast that is classified as an aquitard with low conductivity rates and low recharge rates, but for modeling purposes, would not be included in the model.

Most approaches do not consider saline intrusion exerting an influence over the freshwater lens behavior. Recharge inconsiderate main factor influencing the water table with the exception of coastal areas, where tides do have a higher influence than recharge (CONAGUA, 2002).

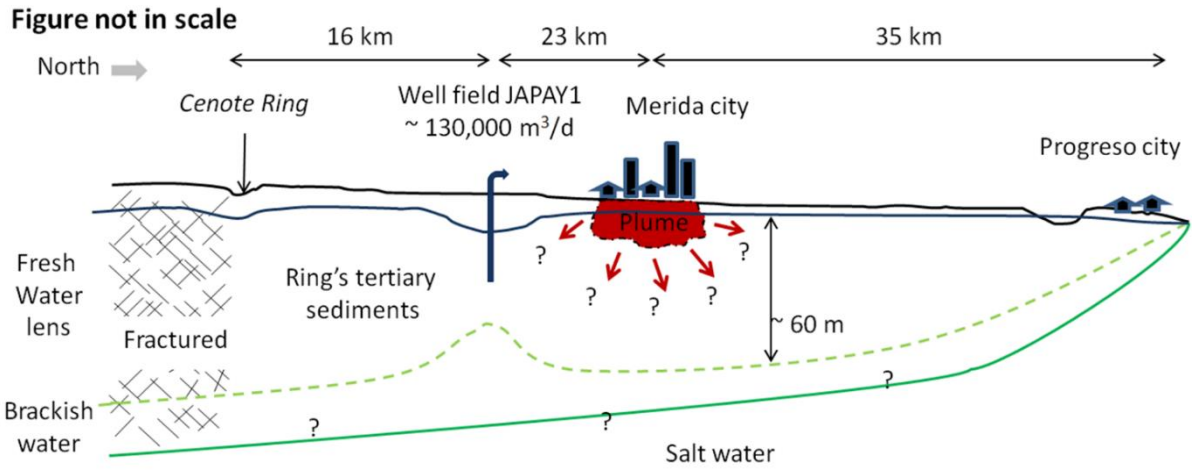

Figure 18: Current conceptual model for the study area, from coastal region to the Chixchulub formation. Source (Moreno, 2018 modified from Marín, 2000).

Given the particularities of the karst systems, there are many approaches that are being used to model groundwater flow in karst aquifers which have both advantages and disadvantages (Kunianski, 2016). Is beyond the scope of this work to go through all of them and describe the principles that make them work. Suffice to say that CFP package in model muse can solve the conduit conundrum using two different understandings of the same phenomena (high conductivity layers and conduit mapping). This work solely focusses on the layers defined in the model.

3.1 Model set up

3.1.1 MODFLOW for karst

A MODFLOW package for karst systems was developed in 2005 and has been used for some modeling approaches. The main problem with MODFLOW and other codes developed to solve groundwater flow equations, is that Darcy´s law does not accurately describe flow where turbulent and not laminar conditions exist. The code package created to solve this problem is known as Conduit Flow Process (CFP) package (Shoemaker *et al.*, 2005) and provides two different tools to approach the karstic features: CFP 1 will model specific conduits as pipes while CFP2 will define turbulent flow at any defined preferential flow layer. They are hybrid models that couple continuum models -simulating porous rock-, with a discrete pipe or flow models – that describe the specific karst features- (Shoemaker *et al.*, 2005; Reimann and Hill, 2009; Reimann, 2012)

Some disadvantages of the CFP package, regarding pollution studies, is its incompatibility with MT3DMS. The MT3DMS is a transport model compatible with MODFLOW code, which uses flow solutions (only for laminar flow) to simulate a wide range of transport phenomena, such as advection, dispersion/diffusion (Zheng and Wang, 1999). Therefore, to analyze pollutants behavior and residence time, in this work two approaches were used:

1. CFP was just developed with particle tracking, with gives us a general idea of the residence time of any particle in the aquifer, without considering transport processes.
2. EPM was then run and adjusted with the CFP parameters to run MT3DMS and nitrate data to have pollution plumes within the study area.

The CFP was run to analyze particle tracking, which only takes into consideration advection phenomena. Some new developments are being made at TU Dresden university to allow the CFP MODFLOW code to run with transport model, at least when using preferential layers as the main feature.

To set up the model, three stages were built to properly assess stressors impact on the karst system.

1. Using constant head boundaries,
2. Activating the recharge package and model
3. Using pumping wells located at the south of the Mérida city.

The comparison was made between different stages to estimate water budgets and to assess the impact of stressors of the system, establishing a based line for the following calibration.

Once the model was run with the original settings, the results were mainly heads, both simulated and compared with current water table data and water budget results, such as discharge. After the model set up, manual calibration was performed to match as close as possible observed and simulated heads. In a further section, we would discuss some limitations of manual calibration and other possible solutions

such as PEST or UCODE. Some steps towards the implementation of this sort of calibration were taken and are reported in the further steps section.

Calibration was done for both CFP and EPM, but this work only shows CFP data. Equivalent porous media was calibrated for running transport, and CFP was calibrated before particle tracking. When each simulation has been run, the water budget complies with an acceptable discrepancy percentage, lower than 0.1%.

3.1.2 Model Assumptions

The success of any groundwater model relays on the definition of the conceptual model and the quality of the input files and parameters. To build our model, some specific considerations regarding some parameters were made. One of the basic assumptions for any Darcy Law based model is that temperature, density, and viscosity must remain constant through the model -except for saline models.

Most gathered data suggest that temperature in the system is highly influenced by the recharge processes and does not considerably change through the vertical dimension: this is important given that the model takes into consideration the temperature and viscosity of the liquid to solve the groundwater equations for CFP package. Temperature data s obtained on a fieldwork campaign depicts profile temperatures of 5 studied wells (CONAGUA, 2002), which support the idea that temperature does not change significative along the vertical profile, although it varies rapidly from 0 to 8 meters depth, always staying between 26 to 29 °C (Figure19).

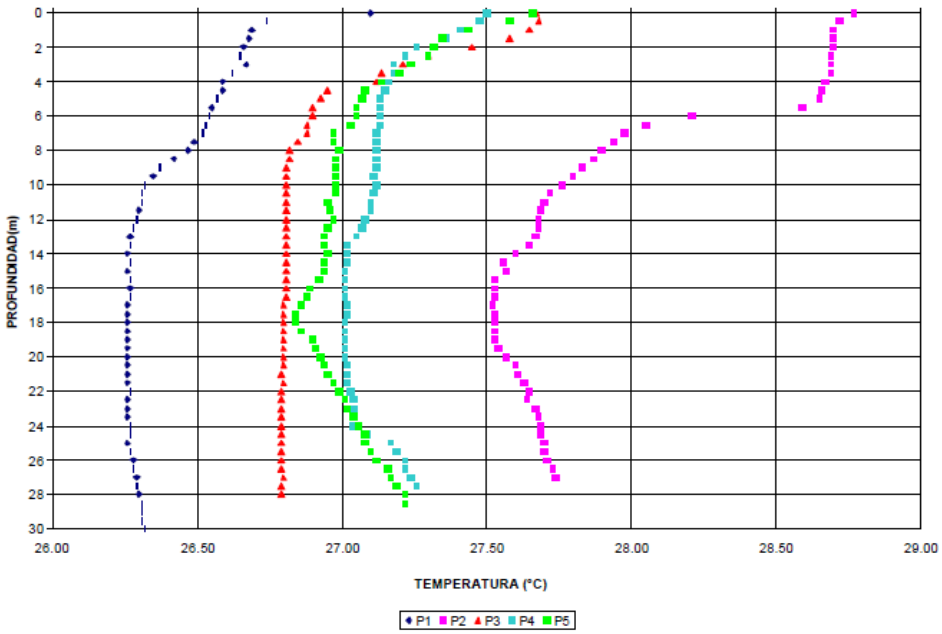

Figure 19: Temperature profile. Source (CONAGUA,2002)

Some studies suggest that recharge and the distance to the coast are the main factors that impact the water table level and its relationship with the saline interface, especially in relation to high recharge

events, such hurricanes. For the density and viscosity part, the saline interface- that may have a small impact in the water density, is detectable only after 38 – 48 m depth where the mixing zone begins (Escolero *et al.*, 2007). Some other sources suggest even 58m below Mérida City, and even some supply wells are installed more than 65m depth.

Transport in karst aquifer is simulated with EPM approach given a less developed karst at the inner sedimentary basin given what we know about the degree of fractured media; besides, we also try to compensate by using high hydraulic conductivities to induce Reynolds numbers as high as possible (Shoemaker *et al.*, 2008).

We opted for steady-state capabilities but decided to run 12 different stress periods to still account for the different recharge inputs responses. Though a whole simulated period, we considered that storage does not significantly change through time, although some trial runs may be done in the transient mode for transport when using average recharge packages. This assumption is based on the following facts:

1. CONAGUA has classified the aquifer as underexploited and the amount of water that is extracted for human purposes represents less than 1% of the total water budget of the system.
2. Available time series of head values suggest that seasonal variations of head occur, but not a significant downward trend has been spotted through the years. Head change according to recharge inputs and the system recovers rapidly, so storage, overall, does not change (see Figure 20).

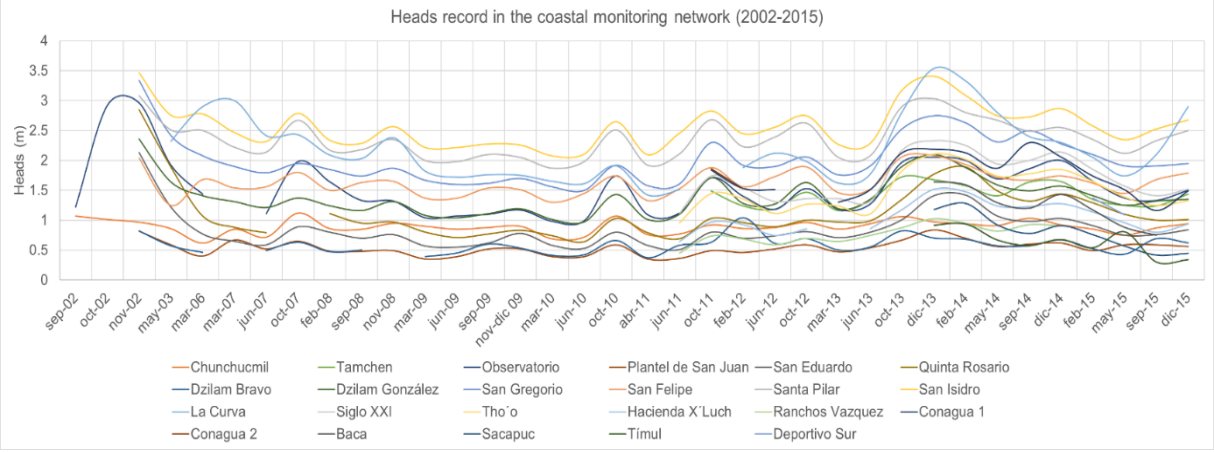

Figure 20: Evolution of head values over a short time series on the coastal monitoring network, 2002 to 2015. Source: Piezometric data from Monitoring Network. CONAGUA, 2015

The CFP package has several options specially designed for karst aquifers with many different settings when it comes to the description of the conduit systems than escalate in both complexities and needed input information. This work is among a few others (Xu and Hu, 2016) that assess the same region using CFP approach other than EPM for groundwater flow and is useful to define specific requirements for

CFP package that EMP models do not need as input data: as the CFP approach has at least 2 different ways to solve the conduits problems, it was decided to use the simplest one: layers of turbulent flow embedded with laminar flow zones (known as CFP 2).

Some studies suggest the existence of at least three different preferential flow paths located at various depths of the aquifer. Such layers are approximately located at 11 to 12, 15 to 16 and 29 to 32 meters depth (Sanchez, 1999). Given the available information, it possible to assume that at least one of those paths exists, and that can be modeled as a layer in the CFP.

The saline lens varies in thickness along the study area and it can be found between 18 m close to the coastal area and more than 110m depth at the south, more than 110km from the coast towards the cenote ring. This means that, for modeling purposes, we assumed that it would not have a great impact over the freshwater lens, except in the coast, and therefore, the saline interactions with not be taken into consideration in the first run. These assumptions seem to be possible if we look at some local studies (CONAGUA, 2002; CONAGUA and C.V., 2004; CONAGUA and Costera-IC, 2009, 2010; CONAGUA and Betsco Consultants, 2011).

Regarding transport, some residence time models include the following assumptions according to Dedewanou *et al.*, (2015):

1. The high vulnerability is a couple with a short residence time
2. Instantaneous release of a conservative contaminant. In the specific case of Yucatán, a widely and recent monitored one is nitrate concentration. Nitrate is a conservative pollutant.
3. The use equation would be an advection-dispersion equation
4. The model would not take into consideration retardation and degradation processes.

In table 6 the model summary can be found, although each input element of the model is broadly described in the following chapters. All input parameters are converted to m/s. For some input parameters were originally created in other units – for example, recharge per month was computed in mm per day- then using the Model Muse calculator tool, the units were adjusted.

Table 6: Model summary. Parameters and short explanations

Original parameter or package	Values
Layers: 3 convertible layers and 1 confined layer which is defined to the surface and has different depth horizons from the surface.	Layer 1: DEM -10 meters Layer 2: (DEM- 35) * 0.3 Layer 3: DEM- 35 meters This layer is then discretized to depict the beginning of the saturated area and the preferential flow path that tries to account for the most relevant karst feature. Layer 4: DEM -80 meters The 80 meters depth for the aquifer would only account for the freshwater lens. As stated before, we are only focusing on the upper part of the aquifer, regardless the saline lens in the model. Convertible layers mean that the cell can be empty at any point of the simulation while confined layer means the head remains is constant in that cell and cannot go dry.
Hydraulic conductivity per layer: Given that the CFP implies that we need one layer of preferential flow, we have decided to define layer 3 most conductive area, Values are suggested by González in a previous numerical model where the best calibration was obtained. The highest K= 1.115m/s and, valued that would be assigned to the preferential layer	Layer 1:0.1 m/s Layer 2:0.1 m/s Layer 3: 1.115 m/s Layer 4: 0.1 m/s
Boundary conditions • **Constant head at sea level in 0m** In further steps, and to adjust the conceptual model after feedback, some trials were run with GHB package (a general boundary package, which also depends on conductance). • **Constant head at the south of the model**	Constant head at sea level: 0 m. The discharge area was defined based on some studies that suggest that this area is quite variable and can go between 5 to 18 meters thick. So, in the model, the formula was defined as: Discharge area = (Model Top- 18)/2, trying to account for the small differences in the discharge area, and made them depended on the elevation of the terrain in the model top layer. This is an arbitrary boundary that does not match with any specific karstic, topographic or political boundary, at least in the MMA model. But, when running just particles for ICR, the boundary condition is the Cenote Ring itself. We did not put too much stress into this section, because we decided to zoom in on the MMA. This boundary condition acts as natural drainage to the aquifer that redirects the water flow from inland to the ocean and concentrating the discharge of the whole aquifer in the outlets of the

3.1.3 Recharge from field data

Recharge estimations can be performed by many approaches. In this work, two different approaches would be used to estimated recharge amounts or rates: one empirical and one spatially based method. Using those values (annual averages), we estimated the recharge for the whole aquifer based on the iDW tool from ArcGIS. Figure 21 shows the final annual recharge for the focus area based on these values.

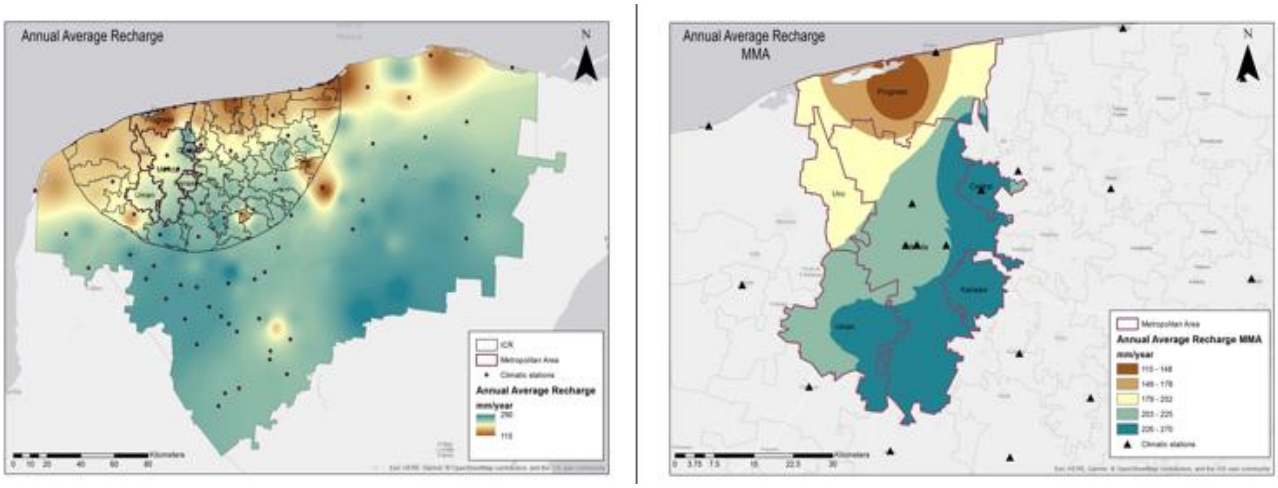

Figure 21: Annual average recharge. Interpolation using iDW tool in ArcGIS 10.3 based on point data publish by Pérez (2003)

The interpolation tool was applied for the whole Yucatán state, but then the mask tool was used to clip just the data relevant to the study area. The average value of recharge is around 212 mm per year, although is highly variable between the coastal area and inner land, mostly explain both by the precipitation regime and the existence of a semi-impermeable barrier along the coast with unspecified – yet- width. It is important to note that for practical porpoises, the whole Yucatán state gets conceptualized as a recharge basin, with predominant diffuse infiltration patterns and some located point source infiltration, like sinkholes (CONAGUA, 2015).

3.1.4 APLIS methodology

APLIS is a spatial tool that can use GIS software to estimate recharge (formula 3) using the following input layers (Andreo *et al.*, 2017; Marín, 2015): altitude (A), slope (P), lithology (L), concentrated infiltration exokarst features (I), soil type (S) and hydrogeological characteristics (F_h) and they follow formula 1:

$$R = \frac{A}{\frac{A + P + 3L + 2I + S}{0.9}} * F_h \qquad (2)$$

R would be the infiltration rate which then would be multiplied by the annual rainfall of a given period to estimate the actual recharge on a given grid. One of the advantages of the APLIS approach -and reasons to use it- is that takes into consideration the intrinsic characteristics of the karst settings and its application keeps close resemblance with the vulnerability methods (Andreo *et al.*, 2017). Each input

layer is rated using the rating tables contain in Navarro (2013) and the recharge rate is computed with formula 2. For each parameter, we have selected and assigned a rating value valid for the cenote inner area. While Altitude (A), slope (P) are straight forwards quantifiable -which means no much room for subjectivity- Lithology(L), Infiltration landforms (I) and Soils (S) are not. Nevertheless, when it comes to infiltration landforms, the options are quite limited.

The altitude value is 1 for the whole index, given that most of the terrain is locate below 200 meters, except for a small hilly area at the south of the state, which is not part of the study. Table 7 depicts the highly related slope ratings and the ones that were assigned for this purpose. The inner cenote has an average slope of 1.03%, which account for low hydraulic gradients. This would seem to indicate that the groundwater flows maybe be stagnate, but given the existence of preferential paths, most models assume traveling distances of more than 90 km per day as hydraulic conductivity.

Table 7: Altitude (A) and slope (P) ratings for the study area

Altitude An (m)	**Rating**	**Slope P (%)**	**Rating**
≤ 300	**1**	**≤ 3**	**10**
300-600	2	**3 to 5**	**9**
600-900	3	**5 to 10**	**8**
900-1200	4	**10 to 15**	**7**
1200-1500	5	15 to 20	6
1500-1800	6	20 to 30	5
1800-2100	7	30 to 45	4
2100-2400	8	45 to 65	3
2400-2700	9	65 to 100	2
>2700	10	<100	1

Lithology parameter (table 8) is also quite important both in definition and weight. It has been clearly established (Bauer-Gottwein, *et al.*, 2011) that most of the peninsula is formed by different degrees of karstified limestone weather though different processes.

Table 8: Lithology (L) ratings for the method and for the study area

Lithology	**Ratings**	**Yucatán rate**
Limestones and dolostones, Karstified	10 or 9	**9**
Limestones and dolostones, fractured, slighted karstified	8 or 7	**7**
Limestones and dolostones, fissured	6 or 5	**5**
Gravels and sands	4	No
Conglomerates	3	No
Plutonic and metamorphic rocks	2	No
Shales, silts, clays	1	No

For the purposes of this work, only three major categories have been used to compute the index, karstified, slightly karstified and fissured. These three categories were compared with previous karstification GIS maps. Most of the karstified area are comprehended in the high-density cenote area, mainly the ring, while the slightly karstified area is the ones where most fissure surfaces and dolines, but not sinkholes, are located. Finally, the fissured area, although does not complete accurately depicted by it, has been compared with most of the inner ring, which is a sedimentary basin, younger than most of the peninsula and that has yet not been weather in such degree as the rest of the peninsula and coastal area. Infiltration landforms is another non-quantitative assessment of the area and it's highly correlated with the karstification parameter. For the index, there is only three possible infiltration paths, each one related to a karstic landform (table 9), and those are also classified according to the karstification map on Figure 56 (see Appendix 3). The method overestimates the recharge in the sinkhole area and may underestimate the recharge in the whole sedimentary basin. While the recharge patterns seem to mainly depend on the precipitation regime, the recharge dynamics in the APLIS method are more dependent on the intrinsic characteristics of the inner area. Therefore, most of the study area will have a less recharge rate depending on the hydrogeological settings.

Table 9: Infiltration landforms

Infiltration landforms	**Ratings**	**Yucatán rate**
Abundant infiltration landforms	10	Karstified areas
Moderate infiltration landforms	5	Slighted karstified area
Scarce infiltration landforms	1	Fissured

Finally, soils parameter is covered in table 10. Although the tag classification is not the same, some soil equivalences were made using FAO soil definitions (FAO- Food and Agriculture Organization of the UN, 2018). Not all the soils that have been found in the state are comprehended in the inner area.

Table 10: Soils for APLIS methodology and the study area

Soils (S)	**Rating**	**Soils in Yucatán**	**Rating for Yucatán**
Leptosols	10	**Considered the equivalent for Litosol and Rendzina**	**10**
Arenosols and xerosols	9	Not found	*
Calcareous regosols and fluvisols	8	**Regosols**	**8**
Euthricregosols and solonchaks	7	**Solonchak**	**7**
Cambisols	6	Not found	*
Euthriccambisols	5	Not found	*
Histosolsandluvisols	4	**Luvisols**	**4**
Chromicluvisols	3	Not found	*
Planosols	2	Not found	*
Verisols	1	Not found	*

The implication of soils being mostly Litosols and rendzinas are that organic layer is poorly developed. Once all the parameters are computed, we use the raster calculator tool for the APLIS rate, which sums all the previous layers for the index and multiplying them for its weights (Figure 22). For practical purposes, we estimated APLIS for the whole state and the clip it for the study area using the extraction by mask tool.

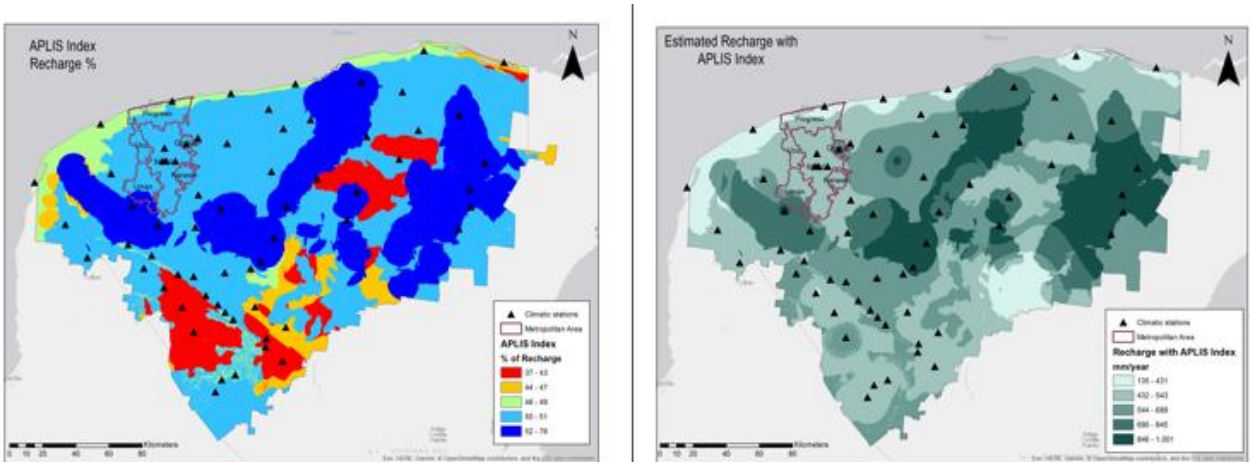

Figure 22: Recharge Index in % and mm/year for the Yucatán area estimated with APLIS GIS-based methodology

We have estimated a recharge rate that can be applied to any precipitation data and this is the advantage of the APLIS methodology. The rate can be applied to any given stress period, such as each month. Using the recharge data, we estimated twelve recharge values, one for each month, that would be saved as ASCII files and then feed as input files into the groundwater model. This method varies greatly in comparison with other estimation data and needs to be validated with field measurements to see if it is possible to apply it without any modifications in the Yucatán area.

Nevertheless, the overestimation may be useful when assessing high impact phenomena such as hurricanes, when high recharge rates have been recorded. The final recharge rate can be seen in Figure 22 also shows an average value of 56%, and highly overestimating the conservative values of 9 to 20% of other sources. Fair to say that the recharge rate was applied to a time series of precipitation data that also reflect high values of presentation in some areas, when compared it with reported values in other studies, although the average value remains, an overall, similar, with 1089 mm per year of annual precipitation. One major disadvantage of the method is that does not consider vegetative cover to assess possible interceptions of the rainfall and therefore it will always overestimate recharge.

3.2 Packages and input files

Figure 23 shows the general path that was following to go from GIS base data sets to compatible data sets for MODFLOW/ Model Muse interface to build and run a groundwater modeling. All datasets were used for CFP and EPM and only the ones related with transport process are solely limited to EPM. From the data sets, GIS spatial distribution files were composed and then transform into ASCII or shapefiles compatible with Model Muse GUI.

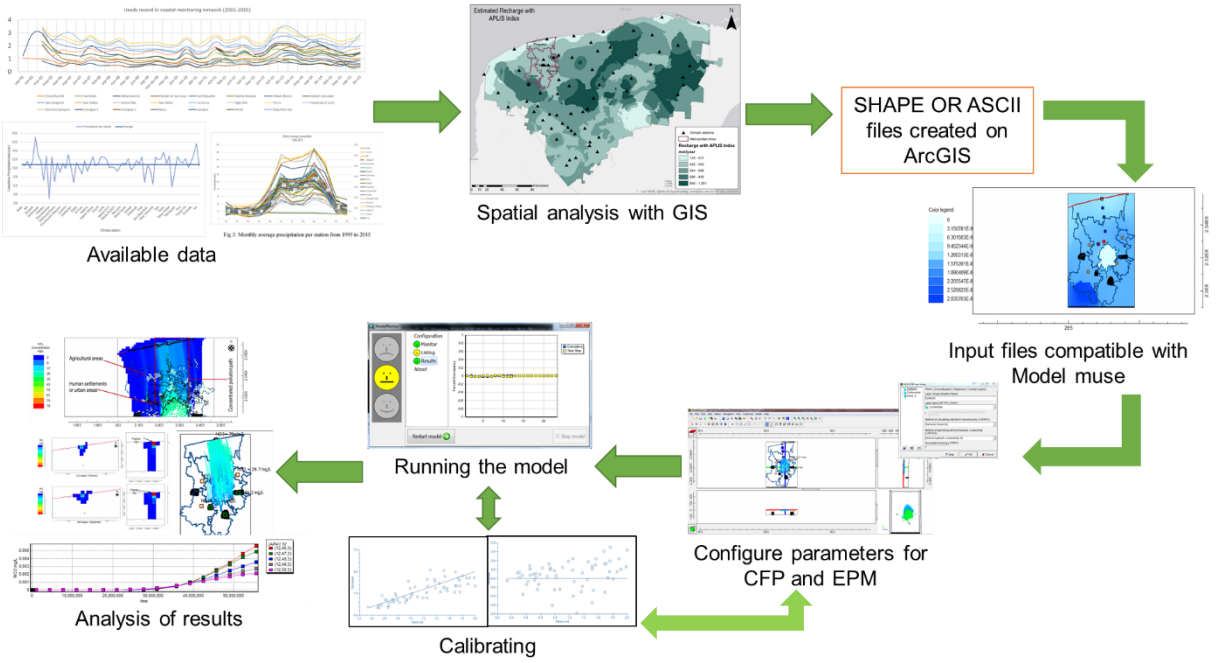

Figure 23: General methodology follow to create input files for Model Muse GUI.

3.2.1 Layers and hydraulic conductivity

This section justifies the layer selection and features. Karst system is complex and dynamic. A complex element in any karst is the epikarst feature, a buffer layer on the top of the aquifer that can be both a protective or a highly vulnerable area, mainly depending on the recharge dynamics. One of the principal assumptions of this work is that on the dry season -and given the limited amount of recharge- the pollutants may stay in the epikarst area for a while and do not reach the aquifer completely; but, when wet season starts, and the amount of water travelling from surface to groundwater increases, so thus the pollutant concentration, as the water flushes the concentrated pollutants that may have stay back at the epikarst. Is beyond the scope of this work to simulate the epikarst interactions, but as an inherent formation of karst features, it is being considered in the conceptual model as the top layer of the model. This epikarst layer has been describing in many works as a high resistance layer at the top of the aquifer that is also quite permeable given the density of fractures, conduits and other karst formations (Zwahlen, 2003; Reimann, 2012) in our case, it was defined.

We decided that a four-model layer would be appropriate. The intent was to simulate:

- the epikarst.
- a small change zone between the unsaturated and saturated area where the table water is located.
- the preferential path as part of the CFP approach -which constitutes a saturated zone.
- and the rest of the aquifer.

The discretization would follow the distribution showed in Figure 24, which depicts penetration times of some drilling done along with a transect area from the inner land towards the coast on a south-north direction given by some local studies (CONAGUA, 2002).

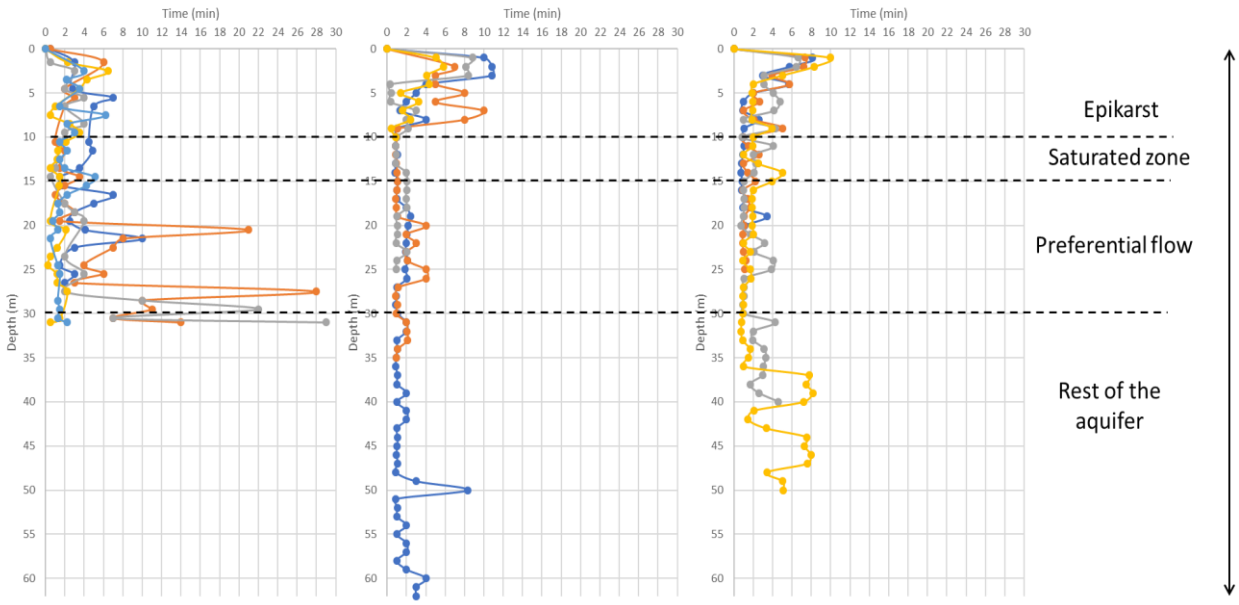

Figure 24: Depth profiles of penetration times as an indicator of different aquifer layers

These vertical profiles depict the penetration times of the drilling equipment and are being used as an indicator of the soil matrix, and also support other sources that suggested preferential paths may exist in the area, where bulky high hydraulic conductivities are shared (Sanchez, 1999; Buckley *et al.*, 1994).

It is assumed that the higher the penetration time, the more compacted the soil matrix is. Following on that, it is possible to assume lower porosities both total and effective, and therefore, higher hydraulic conductivities. So, a more compacted terrain would have a lower hydraulic conductivity whereas a more porous media (with small penetration times), would probably have high porosities and high hydraulic conductivities.

In the model, the discretization has been achieved by importing a DEM ASCII file created in GIS software and interpolating the cell using fitted surface in model muse to get model top elevation and then defining the thickness of each layer. Then, each layer gets the thickness defined using the formula editor as shown in table 11.

Table 11: Layer thickness definition

Layer #	**Formula**
Layer 1	Model top (DEM) – 10 m
Layer 2	(Model top – 35 m) *0.3
Layer 3	Model top – 35 m
Layer 4	Model top – 80

The final depth was defined as 80 m. Below Mérida city, some studies have estimated that the saline interface may be located at around 58m depth and given that the focus of the work has been placed in the metropolitan area, this depth may be representative enough. For the porpoises of the model, the layers are simulated from 0 to 80 m depths, and in the first glance, the saline intrusion is not taken into much consideration, given the scope of the modeling part.

The hydraulic conductivity, K, was the same used by González et.al. (2002) and Pérez Ceballos (2003). The hydraulic conductivity was estimated from previous flow models of the groundwater flow in the area, by assuming EPM behavior.

The CFP package requires to define the void diameter of the flow layer, which was set in 0.9 as well as critical Reynolds numbers. These numbers were maintained in 2000 and 4000 as the default settings in the program. For CFP package, critical Reynolds numbers are the ones that the code defines to make the shift between laminar and turbulent flow. So, the final working discretized model is showed in Figures 25 and 26. After calibration is possible to have new modifications to the conceptual model, especially as it is one of the goals of calibration: to test if the original assumptions were as close as possible to the reality. In the end, modeling is just a simplification of an otherwise complex reality (Reimann, 2012)

For both CFP and EPM, the same input files were used. Most of the input files are formatted as shape or ASCII and were created with ArcGIS software and the shared packages are depicted in table 12.

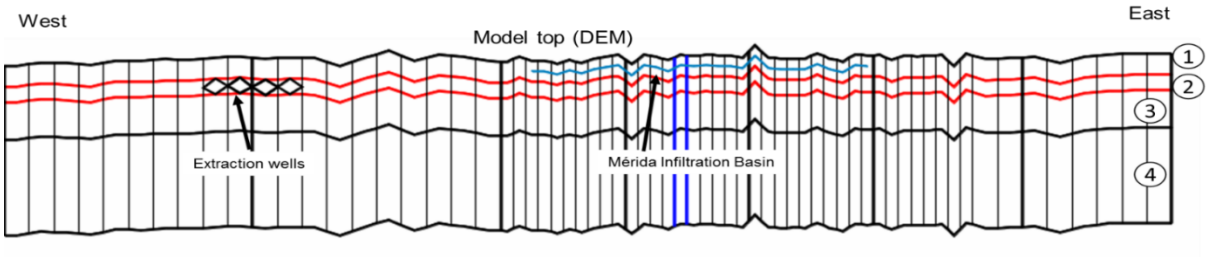

Figure 26: Cross-section from West-East direction

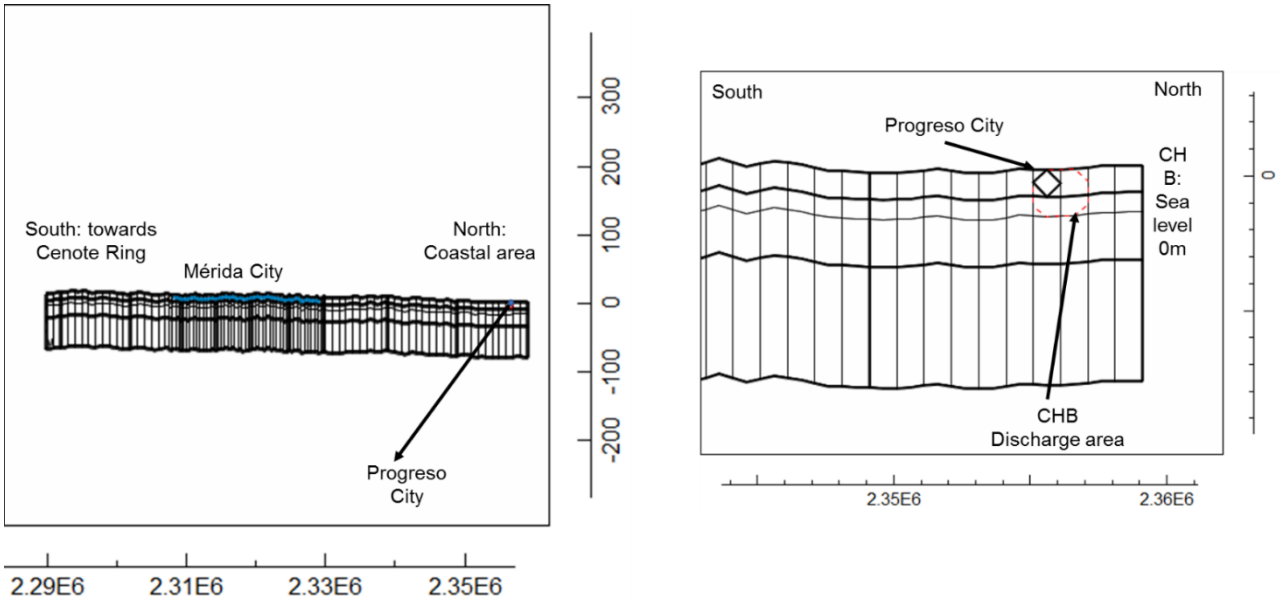

Figure 25: Cross-section North-South view and close-up to Progreso and discharge area

Table 12: Packages included in each approach

CFP	Packages	EPM
Yes	CHD	Yes
Yes. Shapefiles of MMA Mérida City as an infiltration basin, no natural recharge simulated	Recharge	Yes. Shapefiles of MMA Mérida City as an infiltration basin, no natural recharge simulated
JAPAY Pumping wells for abstraction from I to IV	Wells: Pumping	JAPAY Pumping wells for abstraction from I to IV
Not compatible	MT3DMS	Yes Further details in the specific section

3.2.2 Constant head and initial MODFLOW heads

Constant head to the coastal area: Constant head boundaries were defined both at the south and the north of the model. North, towards the coast, constant head of 0m, which is sea level at the coastal area. The discharge area towards the sea has a different thickness along the coast and a deepness that ranges from 5 to 18m (Sanchez, 1999). There is no conclusive data for its definition, so we decided to run the first model defining the thickness by the formula stated in table 11 (see 3.4.1). The deepest point, according to the layer definition, would be at 10m, what a variable discharge area, depending mostly on the elevation terrain.

Constant head of inner area (figure 27): for the metropolitan area, the constant head at the south, towards the cenote ring, was set using an ASCII file obtained from an existing Raster of average heads in the area, which ranges from 0 to 5 m over sea level.

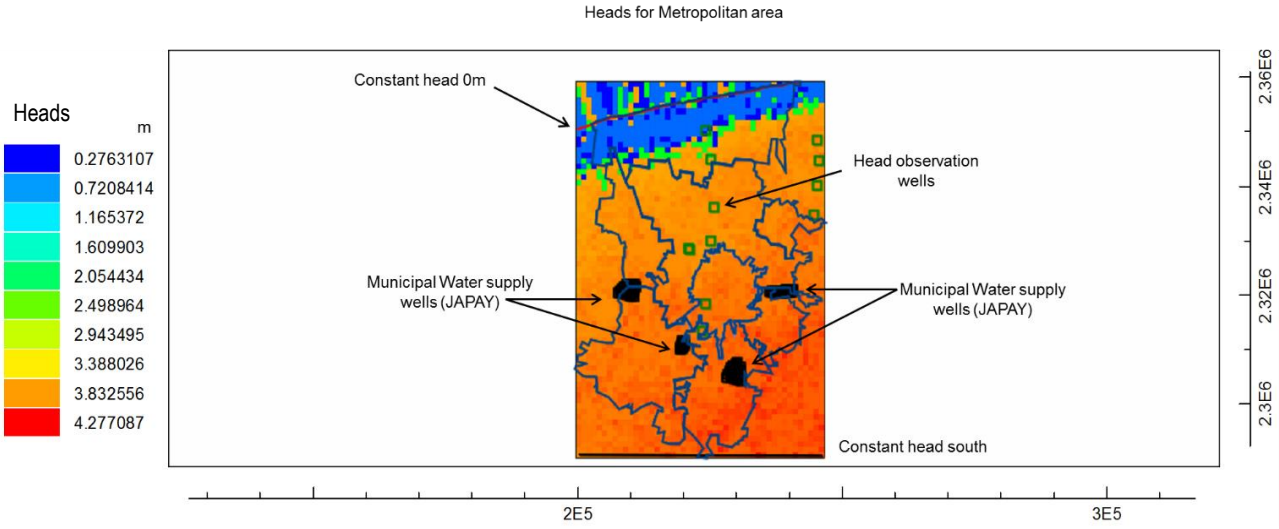

Figure 27: Constant head boundaries and head observations

This file may have some small divergence from the real situation, given that was estimated using a relationship between some water levels and the DEM of the area.

For the initial MODFLOW head, a different (Figure 28) ASCII file was used, this one computed using iDW tool and the most reliable observations given by the water authority, an available time series from 2002 to 2015 with recordings, on average, every 4 months. This is because, when running with averages heads from 0 to 5 meters, the solver never could meet convergence and the water budget was never satisfactory.

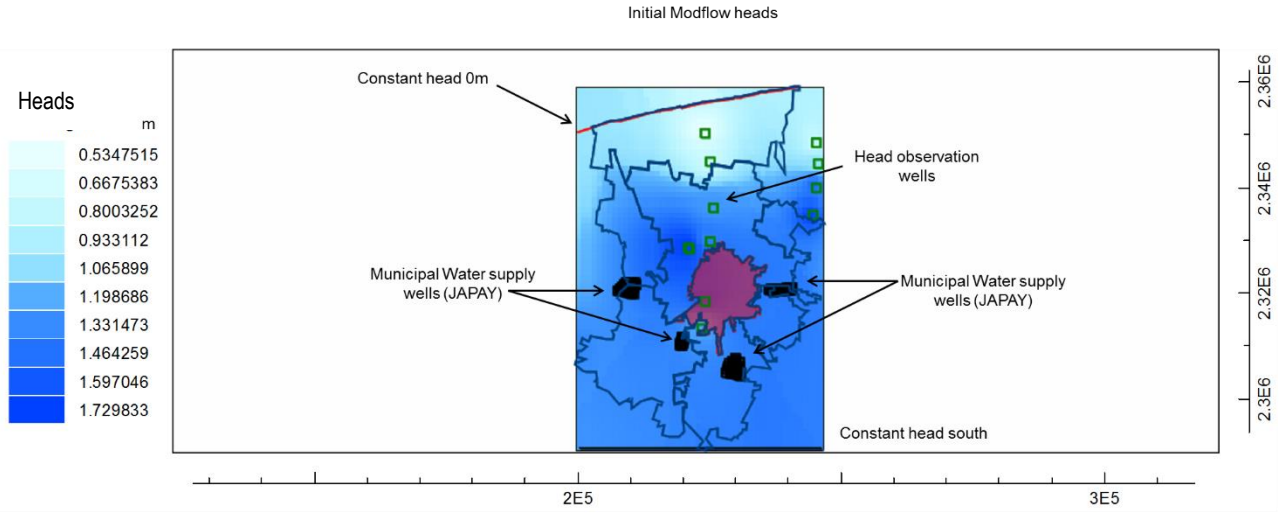

Figure 28: Initial MODFLOW heads for both models

3.2.3 Recharge package

Recharge was computed using the recharge rates estimated with the APLIS methodology month by month and running the model using 12 stress periods, each one of them of 1 day (84600 seconds), as a representation of each month in steady state condition.

Upon calibration, most of the recharge seems to be highly overestimated with GIS methodology for most of the area, except in the coastal area, where heads are still too low when comparing to recharge. It can be possible that tides have a bigger impact on the fresh lens height. The 13th used recharge file was created within model muse by computing a daily average out of the 12 individual stress period packages. This package was used only after each individual stress period package to simulate transport under average conditions

Figures 29 and 30 show the tendency in a dry and wet season of effective recharge in mm per day that was introduced into the model. The input ASCII files were then treated with the formula editor to compute the rate in m/s, to keep the congruence of units through the model.

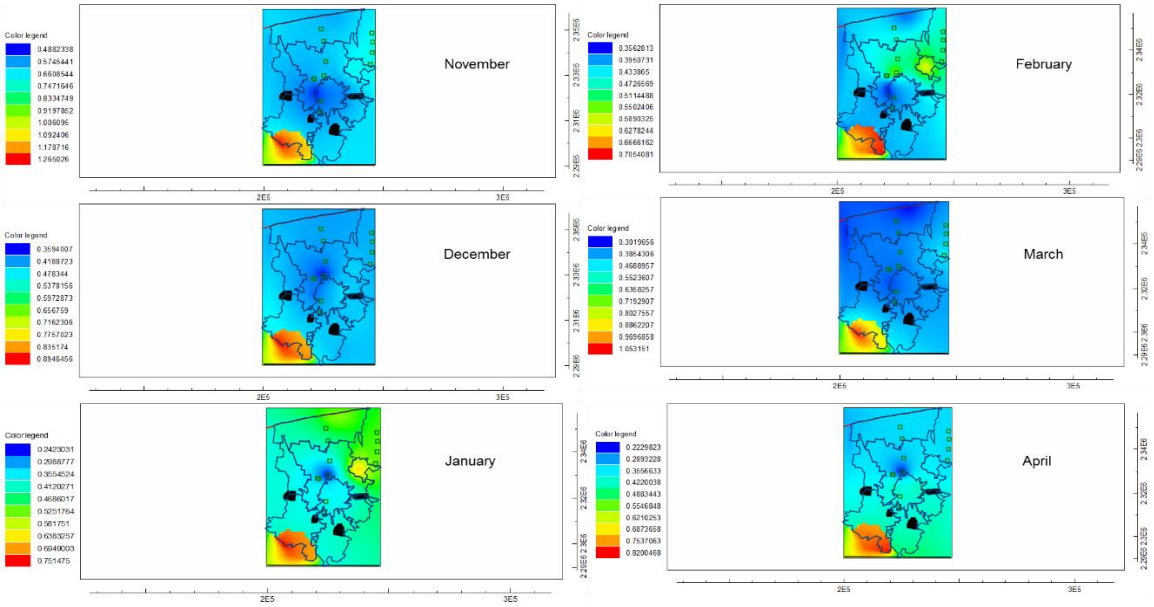

Figure 29: Input recharge files in mm/day for dry season (November to April)

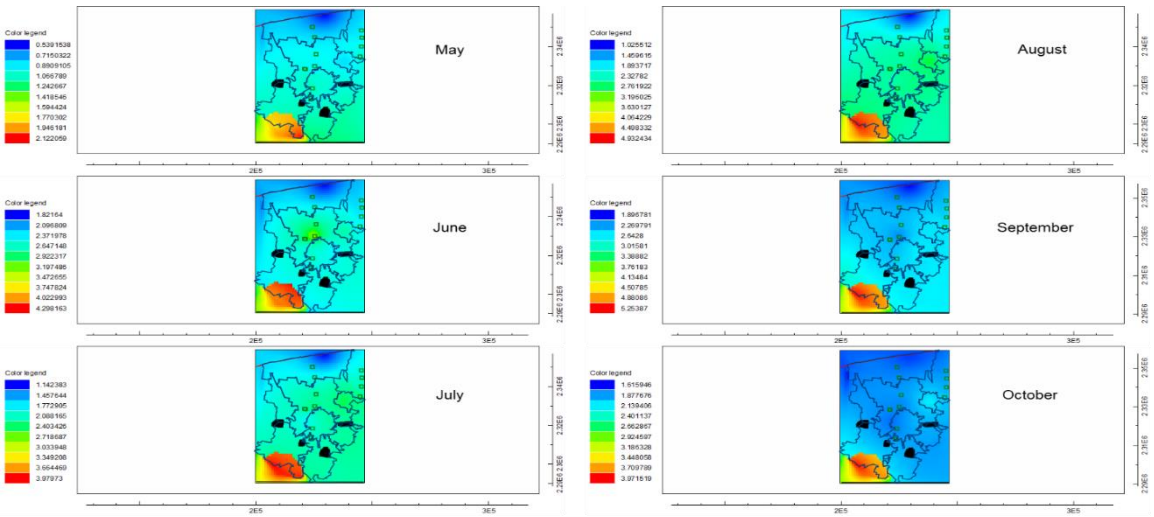

Figure 30: input recharge files in mm/day for wet season (May to October)

As it can be seen in (Figure 31), Mérida does not report any recharge. We decided to not simulate recharge in this area from the input files due to the high degree of urbanization but included a recharge package using 40% of the supply water that gets lost because of pipe leakage. This is because, as part of the conceptual model, Mérida is conceptualized as a recharge package with the losses of the drinking water distribution system.

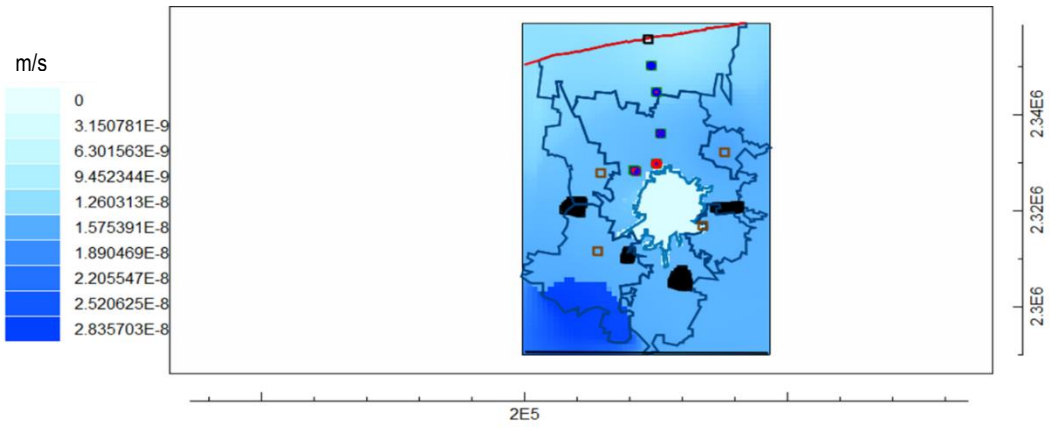

Figure 31: Average recharge for transport model, 13th stress period

3.2.4 Well package

The location and pumping rates of the municipal well fields are known and are shown in figure 32 and are the wells that supply the metropolitan area.

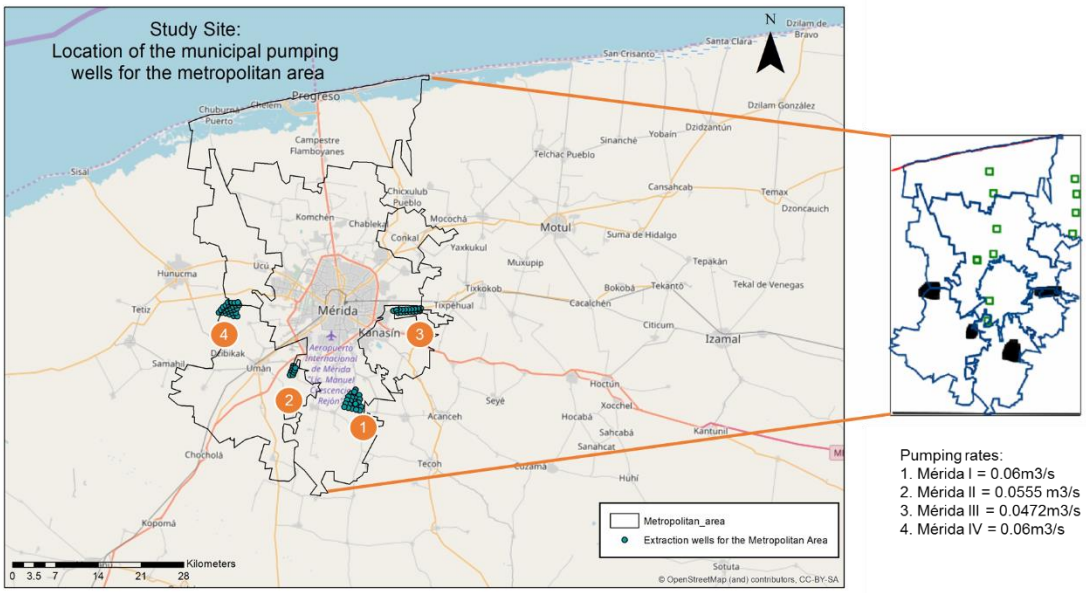

Figure 32: Location of the municipal wells

This wells exclusively supply drinking water for the city, while other communities within the metropolitan area have different wells that are not model here, mainly because most abstraction comes from this fields. The wells are located between 37 and 38 meters in depth, which means the drinking water comes

from the third layer of the aquifer, below the preferential path. This wells only supply water demands from Mérida City. The rest of the communities have local wells that are operated either by municipalities or private owners and most of them are not mapped.

3.2.5 Time discretization

Every simulation was run in the steady state given the fact that: i) the aquifers recover within hours according to many local studies and ii) the storage does not change on average for a hydrological year, as stated in the water table behavior section. Therefore, the time discretization was solely defined as one-day duration of the 12 months, just to assess the impact of the recharge per month. It can be seen more closely when it comes to water budget that in fact to transport processes. This is limitations of the model and would be discussed with more detail in the limitations section. Table 13 shows the duration of each stress period in seconds, days and years. Each period corresponds to a month and the simulation is been run by the calendar and not a hydrological year.

Table 13: Time discretization for models

Stress period	End time (seconds)	Days	Years	Month
1	86400	1	0.00274	January
2	172800	2	0.005479	February
3	259200	3	0.008219	March
4	345600	4	0.010959	April
5	432000	5	0.013699	May
6	518400	6	0.016438	June
7	604800	7	0.019178	July
8	691200	8	0.021918	August
9	777600	9	0.024658	September
10	864000	10	0.027397	October
11	950400	11	0.030137	November
12	1036800	12	0.032877	December
13	Variable time for MT3DMS in years (1, 2, 3,4,5, 10,15,20,30, 60), depending on the model. See table 11			

In table 14, time for transport models is included. We decided to model up to 60 years in order assess if some forecast is possible, although it is likely that the model still does not account for many features and therefore is not robust enough to do an accurate forecast. More details will also be discussed in the limitations section.

Table 14: Time discretization

Years	Seconds
1	31557600
2	63115200
3	94672800
4	126230400
5	157788000
10	315576000
15	473364000
20	631152000
30	946728000
60	1893456000

3.2.6 Particle tracking

Two places were defined as the origin of the particles: the constant head at the south of the MMA, where the CHD boundary conditions were set and the whole Mérida infiltration shape. The first one was selected to see the time it would take for some particles to reach the coast and to assess the effects of the pumping wellfields into the particle paths. CHD as the initial place for particles also helps to evaluate if the preferential flow path (layer 3) has a higher particle density because that would point out to the influence of the karstic characteristics. The second one was defined as most pollution would come out of the metropolitan area and travel, thus following the groundwater paths. This would also indicate which proximate areas to the city are most vulnerable when it comes to the diffuse pollution generated in the city itself. The original settings for the particle tracking are described as follows. We used version 6 of MODPATH, defining that recharge would be placed in the top active cells, which allows for some cells in the first layer to go dry and finally the particle tracking was set in a forward direction.

1. Sources of particles:
    a. Southern constant head (close by the Cenote Ring)
    b. Mérida City infiltration basin
2. IFACE: Flow into boundary cells: internal
3. Initial particle placement: Grid. Numbers of rows and columns in X and Y direction 1 and 4 in the Z direction.

Additionally, we run a backward direction particle tracking from the pumping wells, to double check if any of them would carry out particles, especially coming from Mérida City.

To assess how pumping rates impact groundwater flow in the study area, we performed several runs for particle tracking. There is a new version of transport that can be a couple with CFP 2 (preferential flow layer approach), that may be explored in future works, recently developed (Reimann, 2012).

3.2.7 Transport with EPM

Dual porosity consists of both possible porosities in the aquifer, the primary one, given by the soil matrix and secondary, given by the existence of conduits- secondary solution- of regional fracturing (Shoemaker *et al.*, 2005). All the default values for transport were used and the activated packages for MT3MS were: BTN, ADV, DSP, SSM, and GCG. Even thou unit of the model was grams when used in the model the output would be in g/m^3 or mg/L. The species particle was nitrate, the selected solver was a hybrid MOC and the only change was the maximum number of particles allow, which went from 75000 to 150000.

Transport model was simulated under two different settings: Long-term transport model was run in the 13^{th} stress period, as the only one transient, over a period of 60 years, discretized as stated in table 11, with some output modifications to account for various periods of time and we used an average annual recharge computed out of the 12 recharge input files.

When it comes to nitrates, we used recharge package for Mérida City as an infiltration basin. Data for the recharge rate can be seen in table 5 (section 2.6). 80% of the consumed water goes as wastewater and most of it reaches the on-site artisanal septic tanks. The septic tanks have a unknow residence time by itself which helps to lower the initial concertation of many pollutants, such bacteria or CBOD (carbonaceous biochemical oxygen demand), but lack of data does not allow us to state the amount of degradation of any pollutant in this stage. Therefore, the recharge rate [H] for each point would be used as point recharge to see the extent of the plume, but it would also be adjusted to the area of each municipality.

3.3 Calibration

3.3.1 Water budget analysis

Recharge process plays a fundamental roll in the water budget of the study area, with at least 30% of the contribution to the final discharge (figure 33). Despite the main flow source towards the aquifer one coming from the rest of the aquifer, the recharge is the driven hydraulic process when it comes to the aquifer behavior. Analyzing inputs and outputs of the model, when recharge increases so do the discharge head in the ocean.

The data seems consistent with discharge and such the tendency is showed in Figure 34, assuming each day is a representative average day within a calendar year using recharge data calibrated from the model.

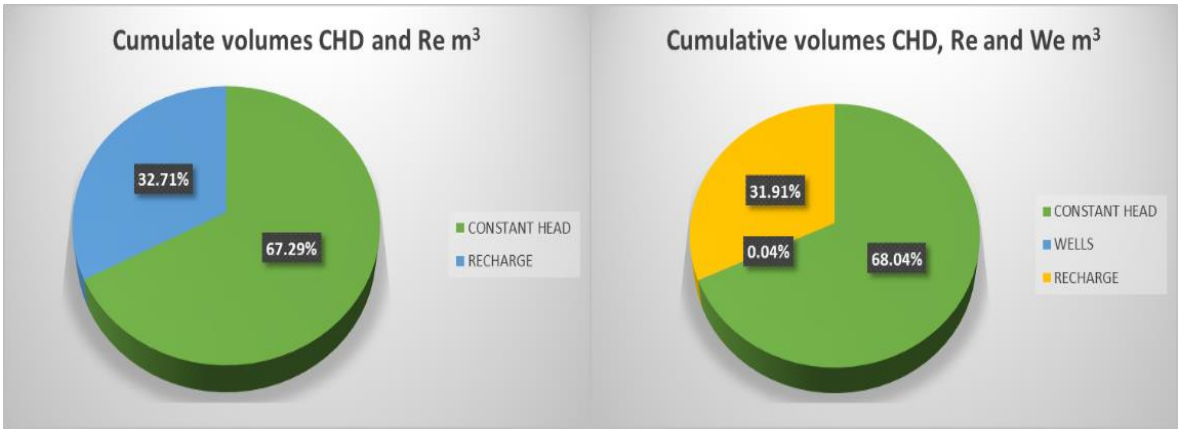

Figure 33: Comparative percentages of recharge contribution to water balance, CFP

Figure 34 (see above) also shows how when recharge increases, so do the discharge. Recharge can increase up to 6 times higher in the humid months (June and September) in comparison with the driest months (March and April), which in some cases represents a single increase of recharge up to 6% per stress period.

The simulation and the time discretization accounts for 12 stress step periods that resemble a day in each month. This means is better to assess the water budget in terms of rates (m^3/s).

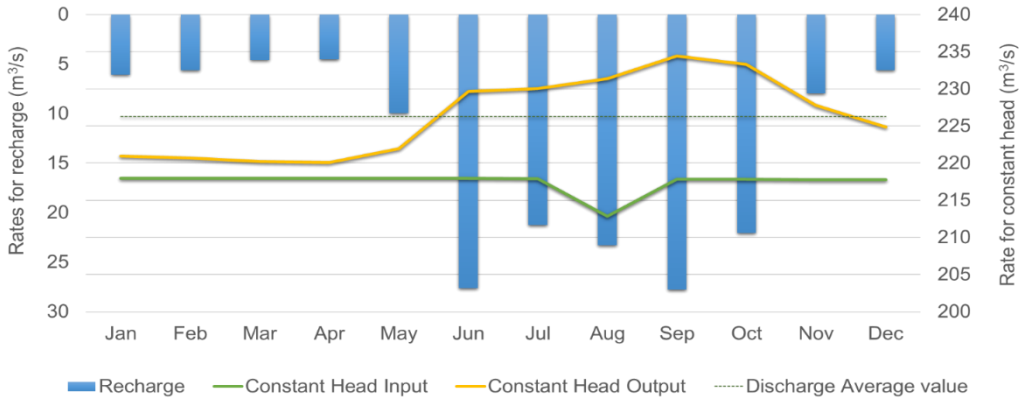

Figure 34: Water budget for each stress period. The output from a steady state simulation, all used packages activated. Average discrepancy < 0.003

If compared with table 2 (section 2.3), average annual recharge for the entire Yucatán peninsula is around 21 813.4 Mm^3 or 5.56E-8 m/s for each square kilometer. But model results (table 15) overestimate the discharge computations of CONAGUA by 2015.

Table 15: Discharge data

Discharge m^3/s	Source
5	Model results, discharge per $km^{2,}$
0.5 to 3.0	Source: Thesis numerical model Two values correspond to dry and wet season respectively
0.46	This value was estimated from the annual discharge computations presented by the water authority.

As expected, lower recharges rates are found in the dry months while higher recharge rates in wet months. Interesting to note how different recharge rates are among each other. This difference in recharge can also be used as a differentiation vulnerability parameter. Given the transport pollutant is influenced by higher recharge, months with higher rates may need different and special measures. This is also true when dealing with extraordinary natural events, such as hurricanes, that imply high recharge rates in shorter time frames.

3.3.2 Root mean square residual and HOB

When using a model muse and the HOB package, it is possible for the software to compare simulated heads with observed heads. The criteria we used to stop calibration was RMSE value. There are no uniform criteria to define what constitutes a good RMSE, so we define a threshold of 0.2500 to stop calibrating. Observed heads are the average of the time series available on the coastal piezometric

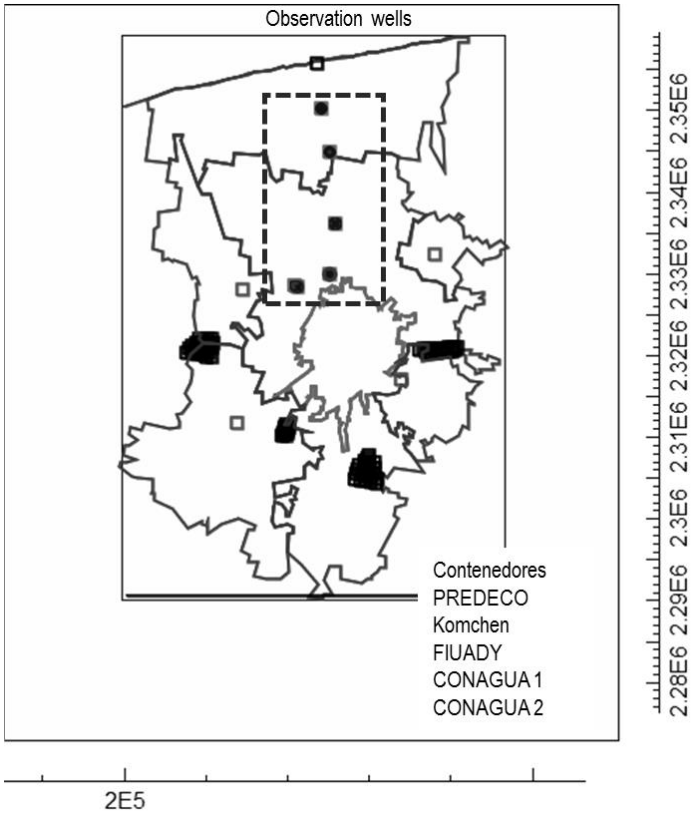

Figure 35: Location of the observations wells for the HOB package

network from 2002 to 2015 for given periods of time and the HOB points within the model are shown in figure 35. Table 16 shows the observed and simulated values recorded in the HOB points that were used for calibration purposes. The heads for the simulation with the best root square defined the stopping point of calibration. Some clarifications and further steps related to calibration improvement will be made in section 6.

Table 16: Observed vs Simulated heads for comparison

		Stress Period						
	Location	Jan	Feb	April	May	June	July	August
Observed heads (m)	FIUADY	1.4350	1.5590	1.6467	1.5267	1.0400	1.3650	1.0420
	Komchen	1.3767	0.9900	1.2600	0.9580	1.3750	1.4460	1.5600
	PREDECO	0.7333	0.6200	0.7100	0.5498	0.7700	0.8908	0.9333
	Contenedores	0.4767	0.5000	0.3300	0.4980	0.5400	0.6468	0.6433
	CONAGUA 1	1.7300	1.9850	1.9133	1.8000	1.3000	1.6900	1.5110
	CONAGUA 2	1.8600	1.5300	N/A	N/A	N/A	N/A	N/A
Simulated heads (m)	FIUADY	1.5427	1.5427	1.5426	1.5427	1.5436	1.5449	1.5464
	Komchen	1.1673	1.1671	1.1674	1.1702	1.1772	1.1787	1.1767
	PREDECO	0.6363	0.6356	0.6378	0.6485	0.6587	0.6585	0.6466
	Contenedores	0.3214	0.3207	0.3228	0.3329	0.3405	0.3399	0.3282
	CONAGUA 1	1.6252	1.6252	1.6251	1.6252	1.6260	1.6271	1.6283
	CONAGUA 2	1.6126	1.6126	N/A	N/A	N/A	N/A	N/A

The head values are stress period averages that were computed from time series of observed heads in the piezometric network operated by CONAGUA along the coast. At the beginning of the simulation, the behavior of the heads is showed in Figure 36 shows how the differences between observed heads and

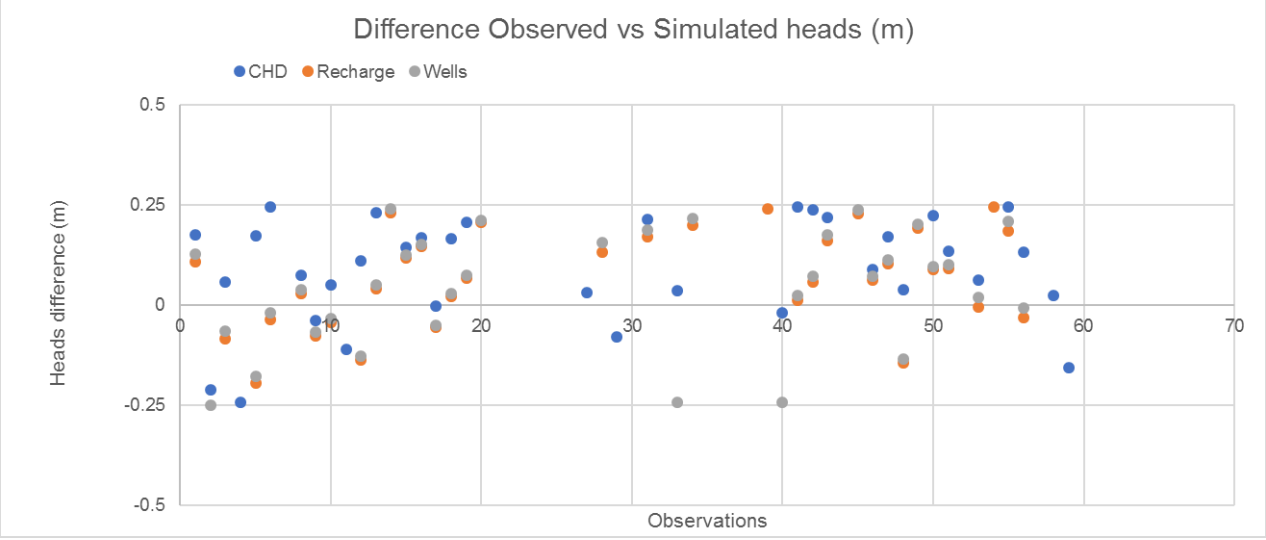

Figure 36: Difference behavior between observed and simulated heads

simulated changes over time. Over 35 out of 59 available values for comparison fall between ∓0.25m of difference between the observed and the simulated head while

Figure 37 at the beginning and at the end of the calibration process. They show the spatial distribution of the biggest head differences for the model. The idea of the visual inspection of the model is to detect if the error distribution is random or is a systematically located error. There are no specific criteria when it comes to calibration limits. Some HOB points were not included between the first calibration and the final one, given the changes in recharge package of model boundaries.

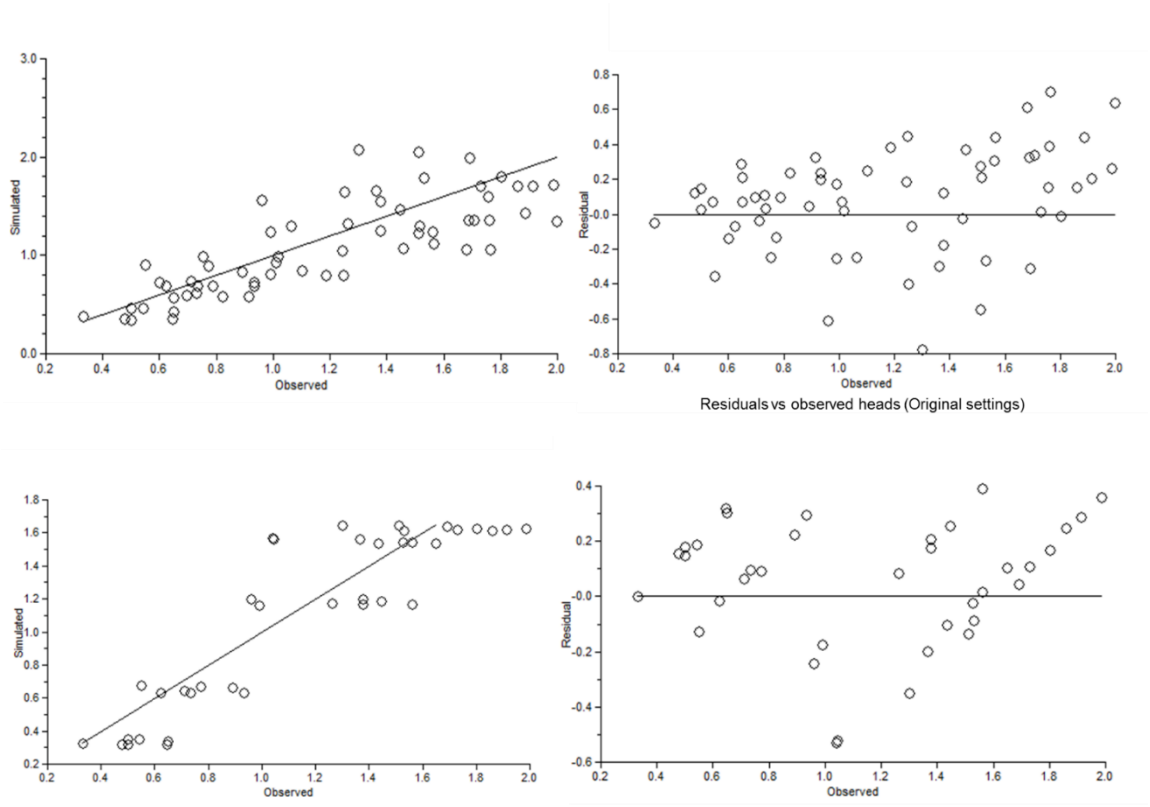

Figure 37: Statistical behavior of heads at the beginning and end of calibration of a steady state simulation with all packages activated. The final calibration implied to adjust the HOB package, which explains the difference in the value occurrence.

The idea of the calibration is to decrease the distance between the observed heads and the simulated ones. The monitoring tool of model muse points out to specific stress periods that reflect the bigger differences between both, so, after a uniform calibration of the chosen parameters, a target calibration may also be done to increase the accuracy of the model.

3.3.3 Calibration of CFP process

When calibrating a groundwater model, there are a few things to consider (Reily and Harbaugh, 1999)

1. Which are the parameters that would be selected? Mainly, the selected parameters are so due to the uncertainty related to them as well as the impact of the parameter in the outcome of the model. For this first step, we will calibrate two parameters: hydraulic conductivity and recharge rates. Even when we try to compute as accurately as possible the recharge rates, many are the factor that influences the process
2. What are the parameters that influence the most the model? This influence can be seen when running the different steps towards the complete model. First, as many guides suggested (Filippis *et al.*, 2017; Brikowski, 2013), the basic scenario is built, mainly the constant head-dependent flow, with no external stresses; then, the recharge process is added and finally the abstraction wells, in order to understand how the system behaves to external stressors.

Every calibration process, being an automatic or manual, has the same objective: to adjust the input parameters in order to fit the observed data (Gallegos, 2011). To calibrate our model, we selected two parameters that may be adjusted along the process: hydraulic conductivity (first Kx and then Kz, if the vertical infiltration is higher) and recharge rates. After some trial and errors run, it was evident that the modifications in the Kz magnitude were not significant enough, so the only parameter left for trial was Kx. We decided to not go above the suggested values of Kx found in literature given that they are already quite high even for karst standards (Marín *et al.*, 2001).

Given that the hydraulic conductivity is already high according to literature, we stop at the best root value without going beyond the suggested values of 1.115 m/s even though a slight improvement in the RMSR. Calibration is not only about the numerical values, but also to select values that are possible within the hydrological settings.

Calibration was stopped at RMRE= 0.2221 and the tracking particle model was then established. The best fit CFP parameters achieve by manual calibration are shown in table 17.

Table 17: Best fit calibration parameters

Parameter	Value	Comments
Recharge rate (m/s)	Coastal area= 2.5 times the original input file.	This calibration is numerical, but it would have to be further analyzed. We know that most of the coastal area has lower hydraulic conductivities and an important part of acts as a semi-unconfined aquifer, thus a higher recharge rate in this area is not quite compatible with the knowledge that we have.
	Metropolitan area (not including Mérida) = 0.2 times the original input file Rest of the area= 0.0025	This adjustment demonstrated that recharge rates were both underestimated and overestimated with the GIS methodology.

Hydraulic conductivity values (Kx)	Layer 1 Kx = 1 m/s Layer 2 Kx= 0.5 m/s Layer 3 Kx= 1.115 m/s Layer 4 Kx= 1 m/s	A better RMSE was showed with Kx for layer 1 and 2 In reverse order. Nevertheless, we consider that this configuration did not depict the initial assumptions about layer 1, epikarst formation.
Hydraulic conductivity values (Kz)	All layers 1.115 m/s	

Calibration was conducted as trial and error. That implies changing one parameter at the time and then, when the best RMSE was achieved (it did not increase), the following parameter would then change. The first modified parameters were Kx, followed by Kz and finally recharge. Besides observing the behavior of the RMSE value, the behavior of the parameters themselves was also plotted to display a tendency (See figure 59, appendix 6).

3.3.4 Tides effect

In the first version of the model, no precautions were taken for simulating the tide effect around the coast and at least 10 km inland. This was evident in the calibration process where most heads in the coastal area were higher than the simulated ones. This was overcompensated with high recharge rates. Nevertheless, as it can be seen in table 17 (section 3.5.3) where the final values are contained, the higher recharge rates were defined in a coastal area.

This was done more as a consistency step, where most areas were adjusted for recharge, but not because the model depicted accurately the behavior. In the coastal area, it is believed that recharge is not that high, at least for the following reasons: i) most of the aquifer is a free and unconfined, except for a small yet unidentified area along the coast where the confinement of the aquifer has been created by deposition of calcite trough transport processes, which will decrease the amount of recharge that actually goes to the aquifer (Bauer-Gottwein, *et al.*, 2011); ii) in this area, some studies have suggested that tiles are the major driven of the water table, mainly based on EC studies and not recharge dynamics (Escolero *et al.*, 2007)(CONAGUA, 2012).

Figure 38 shows EC profiles from some field campaigns that showed how the recorded EC increases where tides grow and decrease when tides retrieve, backing up this notion (CONAGUA and C.V., 2004). For that purpose, two changes were made to the original conceptual model.

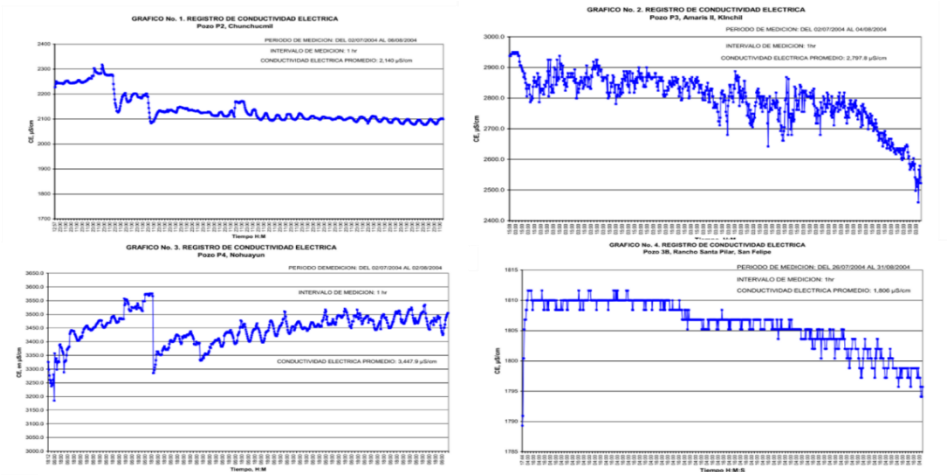

Figure 38: EC lectures that show tides effect over freshwater lens vertical location

For time reasons, the impact of the changes in the general water budget, transport, and particle tracking was not explored, but are fully discussed in the further steps section.

4 Results

4.1 Particle Tracking

Particle tracking reveals that given the current pumping rate, no huge effects are caused by the good fields that supply Mérida, except from the good field No. 4, located west of the city (figure 39). The model shows that the delay seems to affect only the particles concentrated in the third layer and most of the particles in the 1 and 2 remain undisturbed, mainly because the wells extracted water below 37m depth.

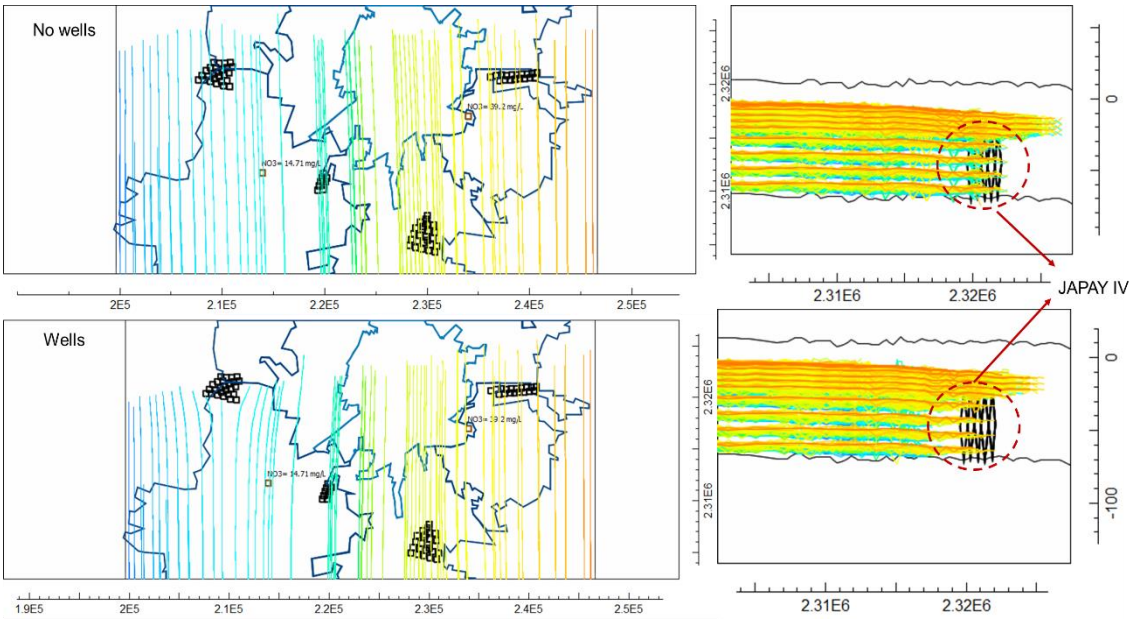

Figure 39: Impact of wells in particle tracking model

Figure 40 shows the particle paths through 10 or 30 years of simulation in CFP. If placing particles in the CHB at the south, particles take up to 7 years to reach the cost, 8 years to reach Progreso City and at least 10 years to end up at the discharge area and complete one cycle. Of course, particle tracking always depends on the particle release point. But, in general terms, particles travel through the aquifer will take shorter times to reach the coastal area.

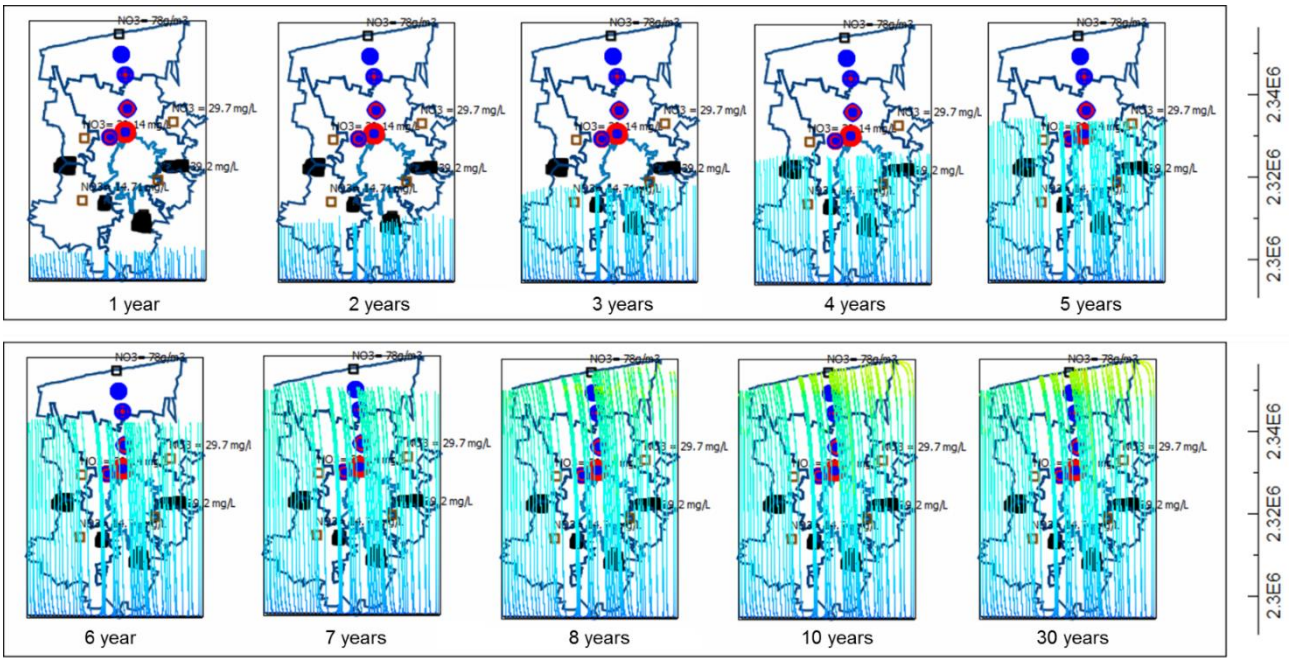

Figure 40: Particle times in CFP, no wells

The difference between the flow paths across the south-north direction is not as significant as the difference when it comes to layer distribution. With the introduction of the wells in the CFP model, the water follows two clear paths along the vertical axis, as it can be seen when comparing CFP with and without the WELL package (Figure 41).

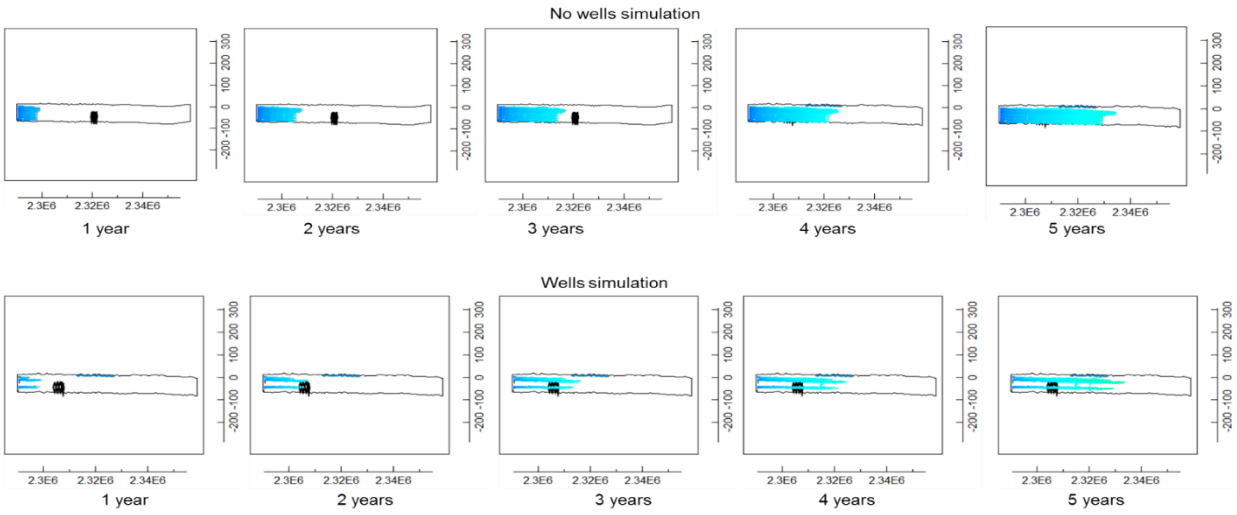

Figure 41: Comparison between simulations: with and without Well package.

By simulating particle tracking originated in Mérida City, we wanted to assess the possible impact of the pollution that is generated in the City towards the rest of the metropolitan area, Figure 42 show the evolution in the same time-scale as before and illustrates how much time will it take for any pollutant to reach the coastal area.

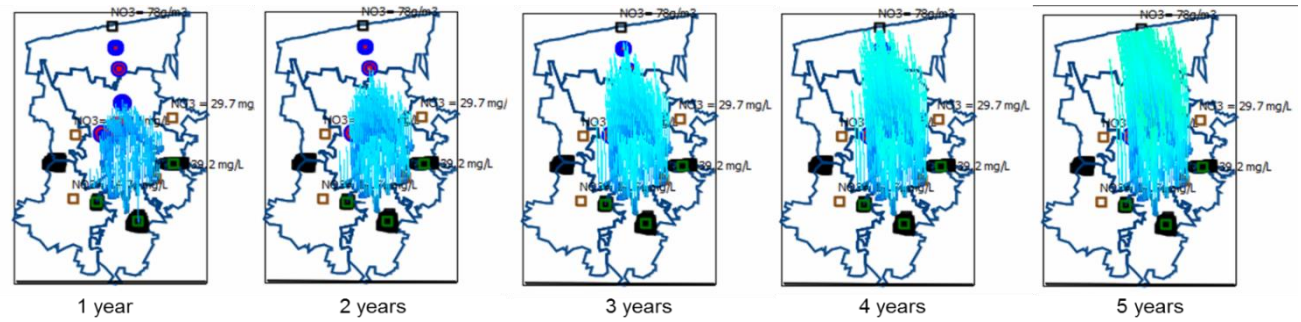

Figure 42: Particle tracking from Mérida City towards the coast

At 1 year of simulation, particles left Mérida city and reached the MMA periphery, passing through the first HOB- FIUADY (Mérida Autonomous University) and barely reaching HOB- Komchem, approximately 15 km away from Mérida city center, but around 6 km away from the first HOB. It means particles travel at a rate of 15 km/year. Then, after 2 years the particles delay and just reached the third HOB, PREDECO, that is located 9 km away from Komchen and 26 km away from Mérida, implying a moving rate of 13 km/ year. After 4 years, the particles would have reached Progreso city coastal city, located 35 km Mérida center, averaging a rate of 8.75 km/year.

Even thou the model has many limitations, results from particle tracking in CFP model can help us to estimate how long will it take for a pollution plume to move towards the coast and impact other areas, such as Progreso, and when compared to other particle paths, seems consistent to the site previous studies (Baur, 2011).

4.2 Transport model

In the current settings of the model, little can be said about the water dynamics in the unsaturated area. So, the most explored outcome is the one related to the residence time. Transport model was simulated under two different settings: Long-term transport model was run in the 13th stress period, as the only one transient, over a period of 60 years, discretized as stated in table 11, with some output modifications to account for various periods of time and we used an average annual recharge computed out of the 12 recharge input files

Figure 43 depicts low concentrations for the purposes of plume behavior. It is fair to say that the pollution plume extends broader in the vertical direction than in the horizontal one. The selected cells correspond to Progreso city, on the coast. This may be due to the best fit value for Kz is the highest conductivity value assigned to the model, the same as the preferential path. The Figures also reflect a clear impact of the recharge process. The plume concentrates between the first and third layer for the most part, and the higher concentrations are in the first 3 layers, where water table levels in the area are quite shallow.

Available data suggested that concentrations of NO_3 were already higher than the drinking water standards (Pérez, 2003), so the initial concentration was defined as the detected concentration in the field campaigns. When comparing both sites in different stress periods, Figures 43 (above) also shows how the pollution plume increases both horizontally and vertically with more recharge.

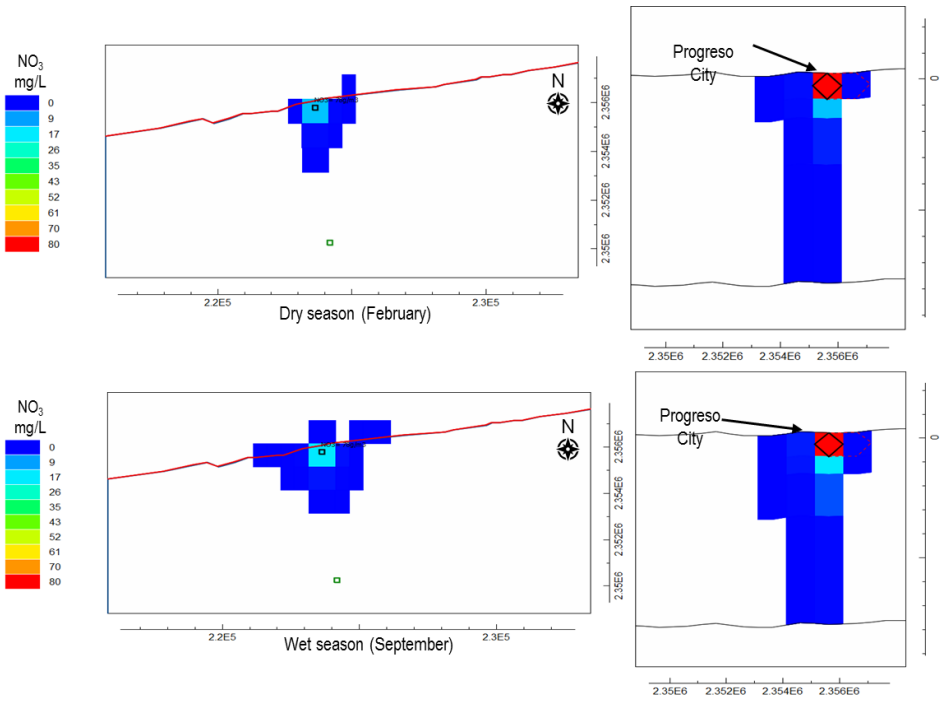

Figure 43: Influence of the recharge process on pollutant transport through two selected periods of dry (up) and wet (down) season

The last stress period depicts the average recharge through an annual cycle without consideration of different recharge zones. At the beginning of the transport simulation, plumes are constrained to the near areas where the point and diffuse infiltration takes place. By the end of the simulation, the pollution plume coming from Mérida city has reached Progreso City and two of the pumping well fields that supply drinking water to the city. This does not mean that currently polluted water is been pumped but suggested that, from the 4 well fields, JAPAY IV and I are the most vulnerable ones because they are reached by the plume (Figure 44). The result is consistent with the tracking particle model.

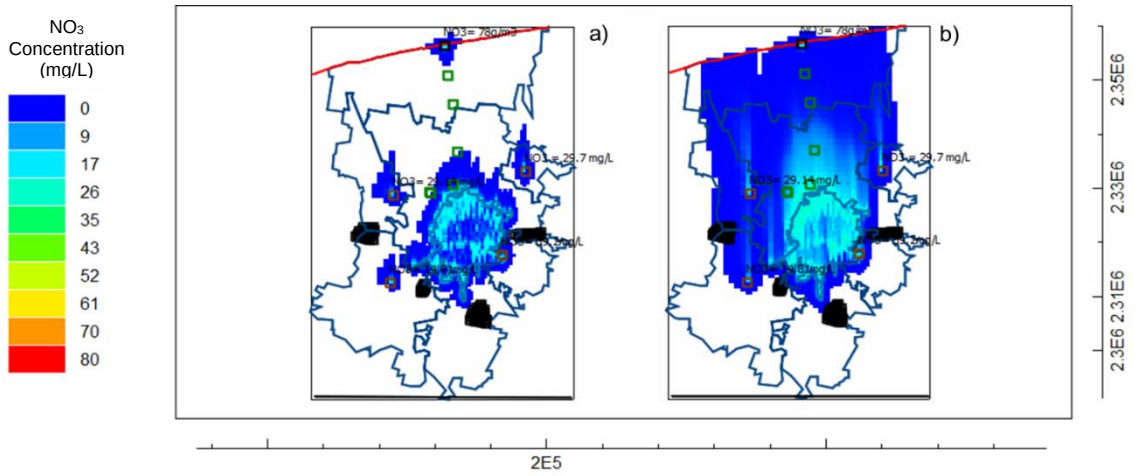

Figure 44: Beginning and end of the 30 years simulation of the transport model in Transient state for the 13th period.

The fact that the pollution plume reaches the field wells is even more evident looking at Figure 45. At the beginning of the simulation (left), is clear how the plume has just reached Mérida city and, in each town center -also consider part of the MMA- smaller plumes have also started to spread, all of them following the particle paths. After the end of the simulation (right), most plumes have merged and are not individually recognized. Pollution from Mérida has already reached the coast and Progreso City.

Available data cannot point out to a specific trend, although most studies suggested that nitrate pollution is an increasing problem in the region as seen in previous sections. Model results show that the pollution plume also travels downwards and reaches the bottom of the aquifer, even the area from where the drinking weather gets extracted although the concentration graphs do not show a significant increase of NO_3 in the pumping fields of the thicker layer. Figure 45 shows bigger concentrations in the layer 1 to 3 and how the plume has reached JAPAY fields 4 and 1, with more pollution traveling towards JAPAY 4.

Even thou the simulation gives low concentrations reaching both good fields and Progreso city, this is just a matter of the initial concentrations that were feed into the model, provided the current information.

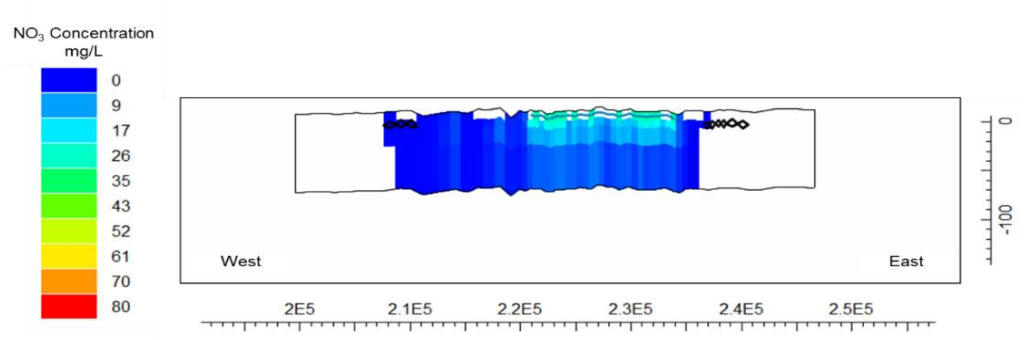

Figure 45: Pollution plume from East- West cross-section

If we look at the concentration curves (figure 46), we can see that it takes less than a year for the pollutants to reach the wells at detectable concentrations -around 300 days- from the moment the pollutant gets a release from any of the two potential pollution sources (Mérida city and Umán). Overall,

it seems that given the general groundwater path, the wells may never reflect high concentrations of NO_3 unless the concentration in the City increases significantly.

The pollutant moves through the system in the horizontal direction mainly through layers 2 and 3 -unsaturated- saturated area and the preferential path-. We would expect higher concentrations along the horizontal direction and mainly in the third layer given the high hydraulic conductivity, but it seems the transport related process influence the most the pollution plume.

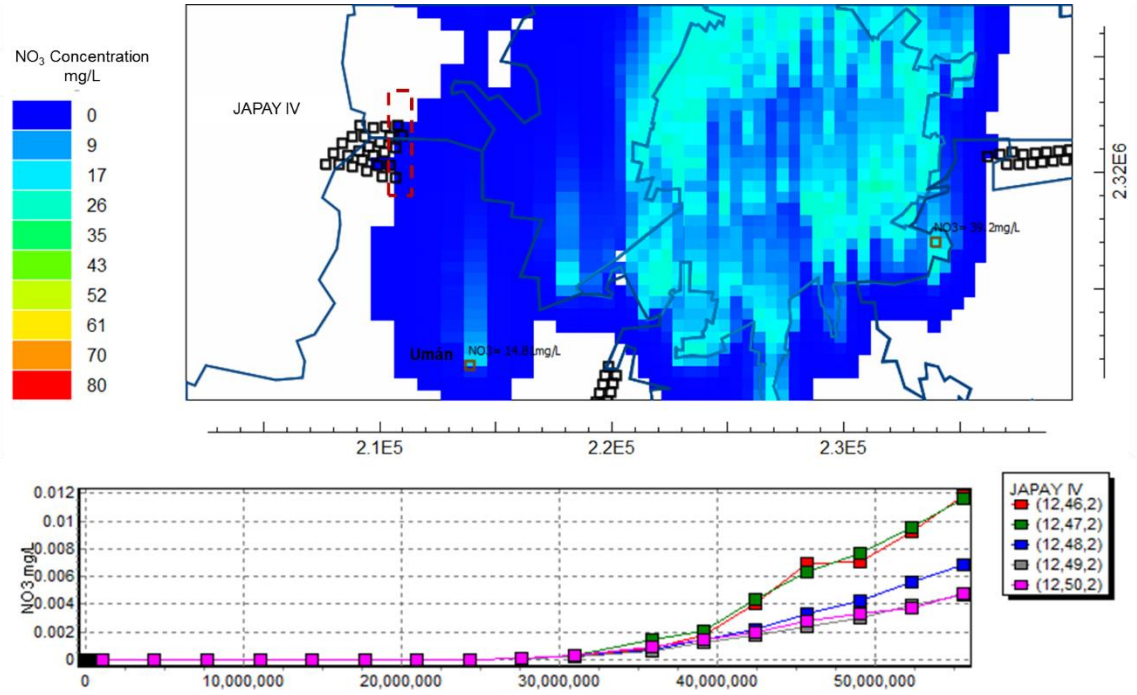

Figure 46: Pollutant plume and JAPAY first affected wells

Model results reflect that Layer 2 is the one that reflects the higher concentrations, given that vertical conductivity is higher than the horizontal one. If we compared the concentration graph in Figure 46 with Figure 47, layer 2 has a higher concentration than layer 3. This would imply that most pollution travels downward instead of horizontally, even thou we would expect some effect of the preferential flow path at layer 3.

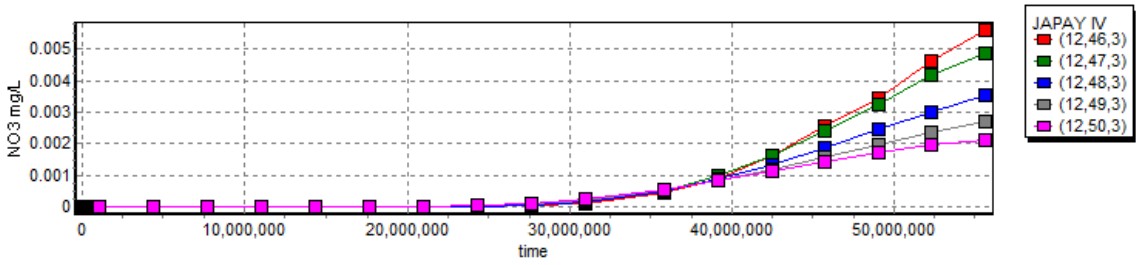

Figure 47: Concentration curves in layer 3, JAPAY first affected wells

The modeling results depicted in figure 47 also show that the concentration increases through time and follows an upward tendency, although it may take a long period of time and higher concentrations to pose health risk to population.

The pollution plume follows the groundwater path, so towards the coast nitrates are more concentrated than along the west-east direction. This can be assessed when we analyzed the same graphs but for Progreso City. How long does it take for the pollution coming from Mérida to reach the coastal city?

If we just focus on the pollution especially coming from Mérida City and run the model for 60 years on

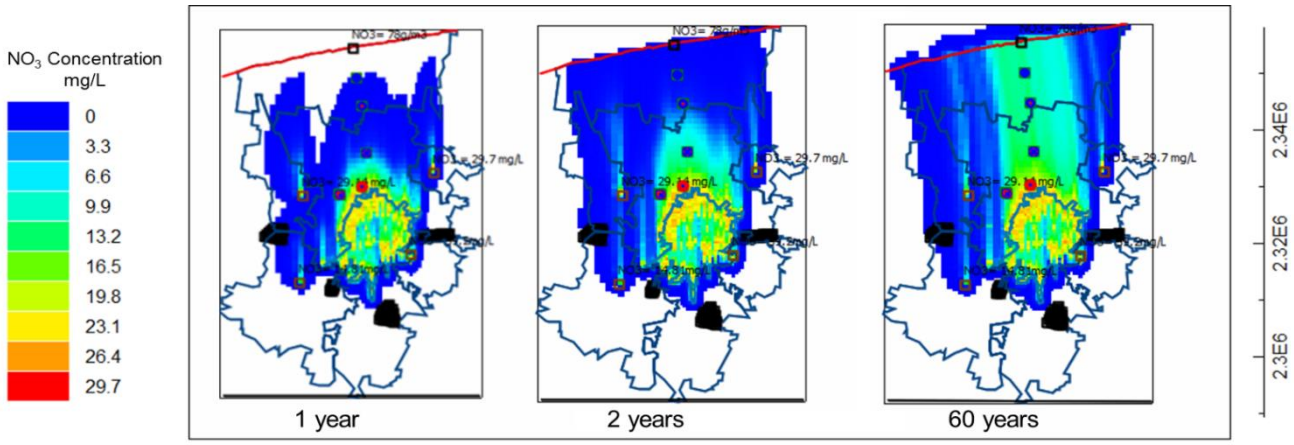

Figure 48: Pollution plume traveling from Mérida City to Progreso City

annual intervals, between the 1st and 2nd-year pollution has already reached the coastal city (Figure 48).

After 60 years of simulation, the model shows high concentrations of NO_3 coming from Mérida, with maximum values of 11 mg/L without considering the synergetic effect of the pollution already been released in the city. It is important to state that only one known concentration of NO_3 is used as an average input for the model, therefore results are in function of this maximum concentration. If concentration at Mérida increases, so the concentrations along the plume. So, we focus more on time it takes for the plume to reached specific areas than concentrations.

The travel transport model does not account for the synergetic effect of pollution coming from both Progreso and Mérida together explicitly. Nevertheless, according to concentration curves, it would be after 3 years that increasingly high concentration would be estimated in the area and mainly coming from layer 2 and 3.

The model shows that the recharge process has also an interesting influence on the concentration pattern of the nitrates along with the layers. Figure 49 shows a comparison between simulated concentrations in Progreso city -currently, the highest nitrate concentration recorded- and the layers.

First, concentration increases with recharge from July to November but also shows an upwards

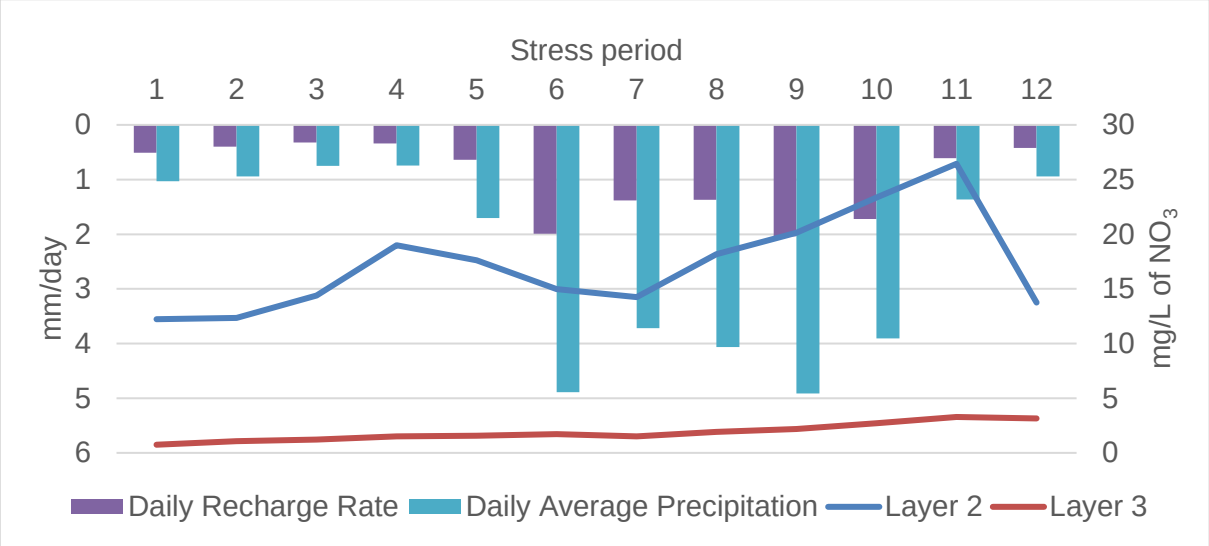

Figure 49: Relationship between recharge in each cell (Col 29, Row 4) and concentrations of nitrates trough each layer.

tendency from January to April.

Layer 2 is the one that responds directly to the recharge changes through the model, mainly because layer 1 and 2 is where the water tables are found and, therefore, the beginning of the transport model. Layer 2, in this case, is highly reactive to changes in the recharge package, responding with increasing concentrations of NO_3 when Recharge also increases, but reflecting a small lag – for instance, from October to November. In the mid time, layer 3 does not respond as actively as layer 2 although reflect an upward tendency in the NO_3 concentration. The average depth of layer 3 is 35 meters, starting even after 15 meters. This would mean that most dynamic behavior is limited to layers 1 and 2, while layer 3 responds less incremental transport process.

The average depth of layer 2 is a function of layer 3 and the elevation of the terrain (see table 11, section 3.4.1.) This backs up the hypothesis that recharge dynamics will play a high role in the increasing pollution of the aquifer but will need to be carefully analyzed and may point out to the suspected epikarst dynamics as a buffer and release function. To certainty assess that epikarst acts as described, simulations with explicitly UZF package must be conducted.

Nevertheless, the circular path would seem to suggest a flush effect that is more visible within the wet season. Moreover, the influence of the recharge process is restricted to the top layer 2, where the interface between the water table and the unsaturated area is. More than that, the NO_3 concentration remains constant through the simulation. For the specific case of Merida city, the plume also has an

interesting behavior (Figure 50). The pollution plume below the city concentrates mainly between layer 2 and 3 -layer 1 only when it has a water table level, given the transport model starts only when water exists in the model.

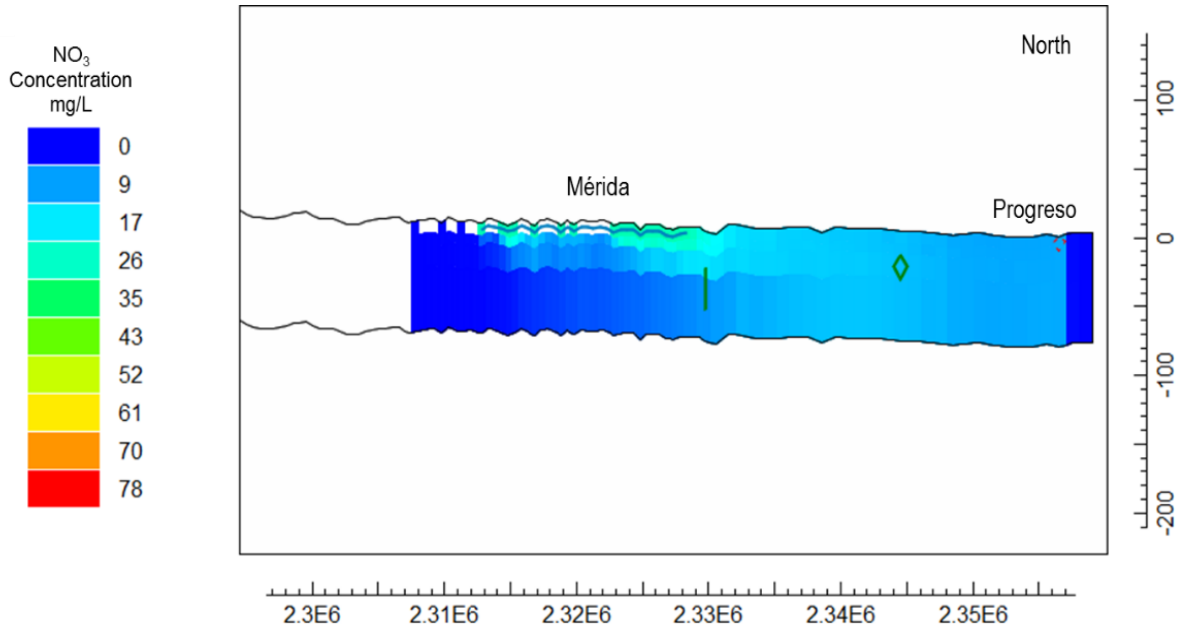

Figure 50: Pollution plume on a South-North cross-section.

This means that most of the north of the city has a higher concentration of pollutant than towards the south, which means that southern good fields may not be reached at all by pollution coming from the basin. This model results may suggest that the most dynamic area for pollution is located between Mérida and Progreso, although mainly between layer 1 and 2, with more diffusion at layer 3. This also may imply that, when coupling a saline model, the effects of the saline interface would not be noted on a regional scale, but rather in a specific area where the saline lens is quite close to layer 2.

The hydraulic gradient and the groundwater general path drags pollution to the north of the city and towards the coastal area and has higher concentrations compared with south of the city and it concentrates pollution in the area between North of Mérida and Progreso, less than 35km between them. Model results display in Figure 51 show the same behavior per layer. Layer 1 shows pollution initial state. Wherever the model finds the water table, the transport model starts running. White squares represent areas above the water table where simulation of MT3DMS cannot be computed because the cell is dry and are concentrated at the north and center of the city. This may partially explain why the most polluted area is found at the north, although mostly the pollution plume behavior is explained by the gradient itself.

Layer 2 and 3 have the highest concentration among the layers. Layer 4 is interesting because it would comprehend the depth at which most extracting wells are pumping drinking water.

So, what are the input times that will be feed into the IKAV project? After analyzing both particle tracking and transport, the critical times are shown in table 18, where the minimum time it takes for the pollutant

to reach the source area (considering pollution coming from Mérida City), even considering low concentrations. This precaution is motivated by the fact we still do not have enough knowledge of the undergoing process that leads to pollution leakage within the aquifer. Therefore, the initial concentration that was feed into the model is a sampling point that cannot account for the complete system.

Table 18: Summary of times for source vulnerability analyses

Source Vulnerability	Minimum estimated time	Maximum Concentration	Does it reach the maximum permissible levels?
Well Fields JAPAY 1 JAPAY 4	Less than 1 year, with low concentrations	On a 60 years simulation, the maximum concentration is 0.01mg/L from an initial concentration in Mérida of 28 mg/L	No
Progreso City	2 years for lowest recorded concentration and 4 years for concentrations higher than 5 mg/L without considering local pollution	On a 60 years simulation, maximum concentration is 11.8 NO_3 from the pollution coming from Mérida City	Yes
Mérida City	Most pollution travels north towards the coast, away from drinking wells fields 2 and 3	Maximum concentration remains the same as input if no changes are model	No
Observation wells cells (HBO) along Mérida Progreso transect (direction Mérida-Progreso)	FIUADY ~ 50 days Komchen ~300 days PREDECO ~ 365 days Contenedores ~ 730 days	Layer-dependent (see Appendix 8 for concentration curves that showed times).	No

Using the constructed model, we were able to describe residence time in more detail and we are confident that it may be included upon vulnerability analysis.

In Progreso, the pollution plume grows in length and width when recharge increases. The spatial distribution of the pollution plume suggested that most pollution is transported by the groundwater general paths that seem to diverge from the drinking water supply fields.

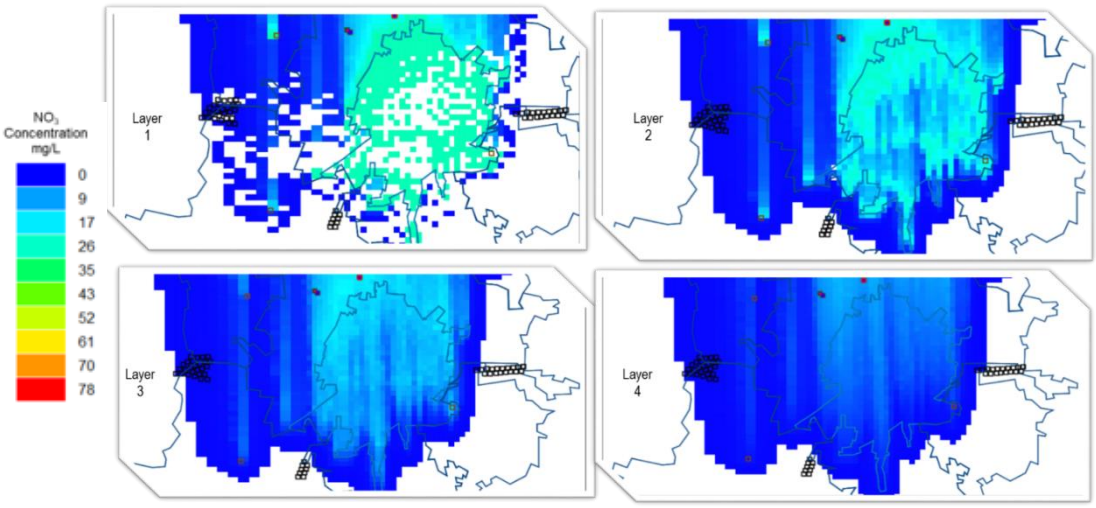

Figure 51: Pollution plume behavior of the four layers. Top view of the model with special attention at Mérida City

This may mean that it is possible that drinking water wells that are being used to supply the city do not get affected, at least the ones located at the south of the city. Nevertheless, there are many small communities that can be found scattered between Mérida and Progreso, which seems to be one of the major pollution paths. Those communities have shallow and artisanal pumping wells to supply drinking water and are, so far, unmapped and unaccounted for. These communities settled in the path of the pollution and could be susceptible to drinking pollutant water in a nearby future, assuming NO_3 concentration has not increased already. Results show that the pollution plume reaches the coast, but with a concentration close to 0, while concentration near Progreso city, which is located less than 35km away from Mérida reach up to 11 mg/L. This means that within 10 years, the concentration at the coastal area could increase least 50% of its initial concentration. Even though the hydraulic gradient is quite low, the plume moves exclusively up north, towards the sea in a preferential path that does not necessarily follow the preferential layer. Some concentration values seem to support the idea mainly 2 and 3 are where the most concentrate plume can be found, but the plume mostly follows the particle path.

5 Conclusions

Residence time and transport. Using the constructed model, we were able to describe residence time in more detail and we are confident that it may shade light upon vulnerability analysis. A central hypothesis was also partially supported. We stated that recharge would play a fundamental role in transport processes and that can be zooming in in specific cases, such as the one depicted in Figure 43, where the pollution plume grows in length and width when recharge increases.

The hydraulic gradient and the groundwater general path drags pollution to the north of the city and towards the coastal area and has its higher concentrations between Mérida and Progreso, in a very distinctive path. Most pollution travels faster towards the coast than in the west-east direction. This fact may be helpful when defining vulnerability zones in further studies.

The spatial distribution of the pollution plume suggested that most pollution is transported by the groundwater general paths that seem to diverge from the drinking water supply fields. This may mean that it is possible that drinking water wells that are being used to supply the city do not get affected, at least the ones located at the south of the city, being JAPAY 1 and 2, while the plume reaches JAPAY 3 and 4 (east and west of the city). Nevertheless, is JAPAY 4 the one that seems more impacted by the plume, which also indicates a small gradient towards the west of the platform. JAPAY 3 is affected just in a small portion of the pumping wells, while JAPAY 4 seems to be susceptible to pollution as the whole field.

Nevertheless, there are many small communities that can be found scattered between Mérida and Progreso, which seems to be one of the major pollution paths. Those communities have shallow and artisanal pumping wells to supply drinking water This community settled in the path of the pollution, could be susceptible to drinking pollutant water in a nearby future, assuming NO_3 concentration have not increased already. There are elements to suggest that pollution has spread, and more sampling point data need to assess the current situation.

Results show that mostly pollution extension is driven by recharge in the vertical direction (affecting layers 1 and 2 more than the rest of the aquifer) and, while the hydraulic gradient towards the coast and from east to west also shapes the plume. Even though the hydraulic gradient is quite low, the plume moves exclusively up north, towards the sea in a preferential path that does not necessarily follow the preferential layer. Some concentration values seem to support the idea mainly 2 and 3 are where the most concentrate plume can be found, but the plume mostly follows the particle path.

It seems, nevertheless, that the path would only add to an already high vulnerability area according to most studies methods. If we look at the past vulnerability studies of the area, the pollution path overlaps with very high and high vulnerability areas considered like that by the mentioned methodologies (like DRISTPi or KRSTI) but also with other indexes that do not consider the area beyond moderately vulnerable (such PI). For instance, figure 52 shows that along the suggested concentrated plume given by the model, there are a wide number of both urban settlements and agricultural fields that can be affected by pollution but also contribute to increasing the NO_3 input, which then would imply an increase in the pollution traveling towards Progreso.

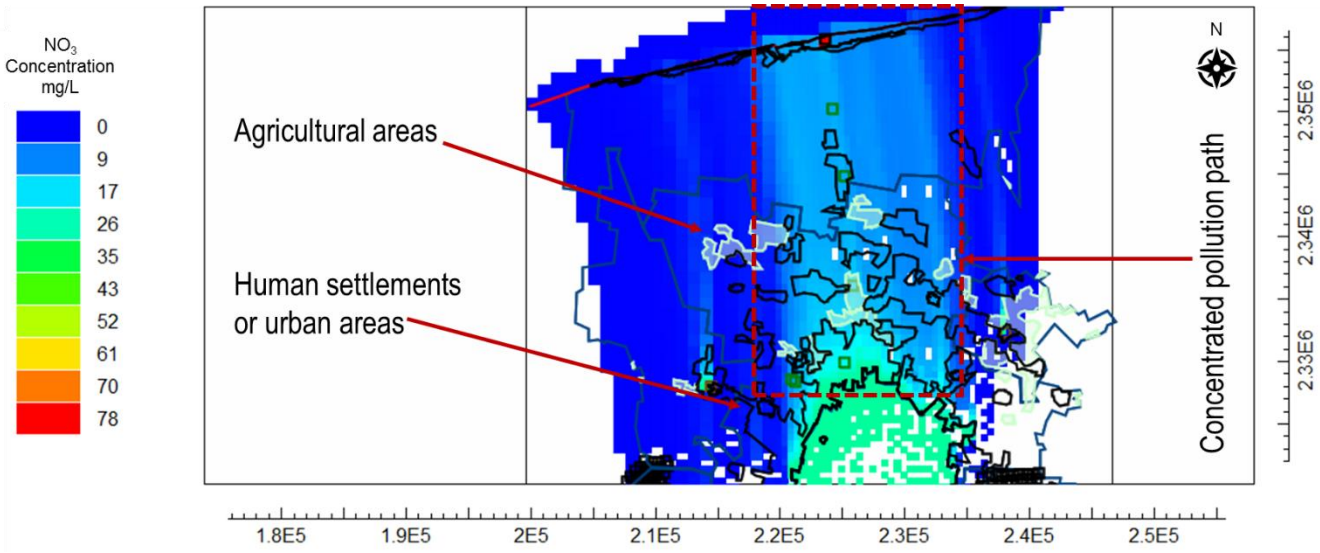

Figure 52: Concentrated pollution path after 60 years simulation

This also adds up to the pollution that is already being registered in the area, possible already registering pollution traveling from inland, from growing development of the coastal city and nearby agricultural areas. The synergetic effect of cumulative pollution is not accounted in the model, but figure 53 shows a stacked graph that aims to note pollution coming from both sides, Mérida an Progreso itself.

This means that pollution being carried out towards the coast would certainly be at some point discharge to the sea, causing not only pollution of drinking water sources in the way, but also unbalancing marine ecosystems as well. Although not many point trough the model goes beyond permissible NO_3 concentrations in national drinking guidelines (10 mg/L in México), some areas do show higher concentrations. Given that we used moderate values to simulate our transport model, the current NO_3 concentrations may be even higher than simulated.

The complexity of karst implies that more computational and conceptualization efforts need to be invested in any numerical modeling design. This project, for instance, can be improved by any of the model considerations in section 6.

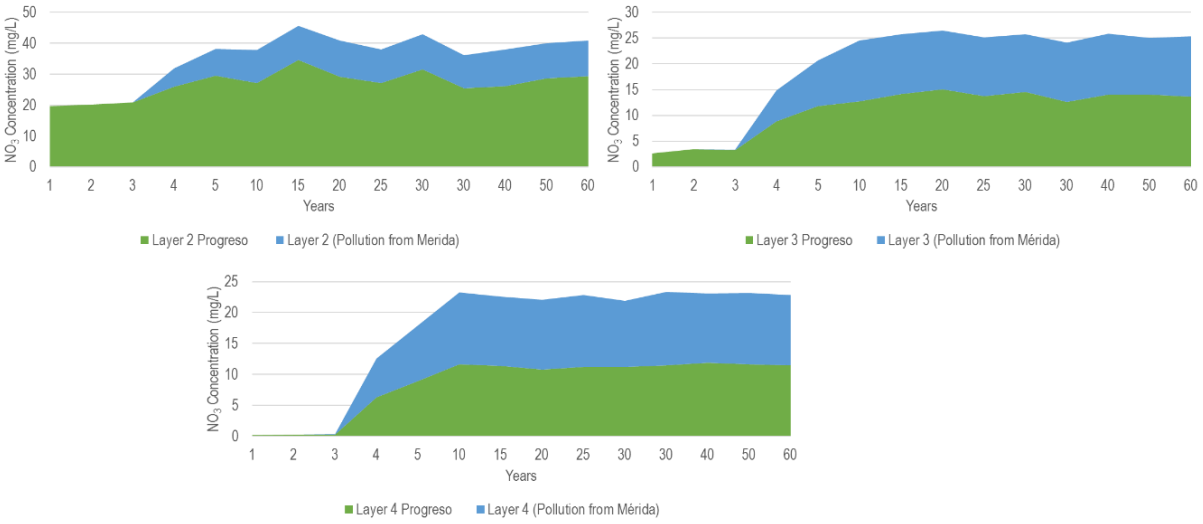

Figure 53: Concentration of NO_3 per layer. Comparison between concentration at the Progreso, final time of simulation, with and without Pollution from Progreso City.

A clear initial conceptual model is key to design a good numerical model and for coastal karst aquifers, especially along the coastal hydrological zones and especially the relationship between the saline interface, tides, and heads at the coast. We believe, thou, that this model is a good first approximation when it comes to implemented specific karstic numerical modeling tools (CFP) and integrate available data for the area in MODFLOW. We have established the absolute necessity of 1) running UZF package to more accurately model epikarst effects and 2) to couple a saline model with CFP to properly assess tides effects and saline interactions along the coast.

Maybe the main contribution is to stress that vulnerability indexes need to consider, in any possible way, the human activities along with some areas using any available parameter. Residence times points out to more than transport modelling and let us know that systems are interdepend and activities in a given area (such as Mérida City) are bound to impact others (Progreso city) and the acknowledge of those different levels of affectation can help us to manage resources, especially in countries on developing tracks that deal with scarce public and private resources, even more, when environmental matters are at hand.

Wells. Particle tracking suggests that there is already a cone in this area and the particles get delay due to pumping and the flow itself gets a delay because particles were captured by the wells in JAPAY 4. Based on particle tracking results, Wells located at west and east of Mérida city may be at risk of pumping polluted water. The good fields are vulnerable to pollution. If the pollution is generated at the south of the MMA, around the cenote ring, and according to the results, would capture particles coming from that source while if the pollution is generated at Mérida city, both JAPAY 3 and 4 would probably capture some degree of polluted water. So, if the pollution plume is generated at the south, near the

cenote ring drain system, JAPAY 4 field is vulnerable to pump that pollution, while if the plume comes from within the city, both good fields, JAPAY 3 and 4 are.

Integrating the results with vulnerability approach. How can adapt vulnerability methodologies with the residence time results show in this project? We can start by identifying major areas that contribute to pollution spread, such as town center and Mérida City, as we did in the model. Then, knowing the behavior of the plume, it was clear that not all of the study area stands to be affected at the same level. By prioritizing those targets of pollution, we can then move on to the next steps of vulnerability methodologies and rate which areas are considered the most vulnerable one, based on the fact of how long it takes for a pollutant to reach.

As results suggest, we have a wide brand of residence times than would obey different purposes of vulnerability classifications, be protection urban settlements from consuming polluted water, assure the best groundwater quality for agricultural purpose or just protection sensible areas to human pollution, that assessment will depend on our management goals.

We would suggest rate vulnerability one of the most important criteria to use would be all the areas that are within the pollution plume path and, within it, the ones that reached higher concentrations.

6 Model considerations and final remarks

Many step backs have been found through the process of building the model. To the best of our knowledge, no other groundwater model with a CFP approach has been done for the region, except Xu and Hu (2016). This meant many challenges, including preliminary steps towards the model, such as creating all the input files that a numerical model requires. As we know, any model is as good as its input data. Available information is considerable for some regional characteristics, but data needs to be processed, selected and clean to have good results. This model is then limited by the quality of the data and by the choices along the way we took to simplify, interpolate and build the necessary input files.

Limitations in this work arise by the incompatibility of CFP 2 (preferential flow paths), with MT3DMS. We believe the results in EPM approach would not completely reflecting the karst features but, by assigning high conductivity values, we aim to compensate for the lack of transport model in CFP 2. The fact that the ICR is a sedimentary basin and that most terrain is highly dense in fissures, but the karstic development is not as high as in other areas, such as the Chixchulub ring or the North-east part of the peninsula suggested that the behavior of the groundwater flow might generally resemble an EPM model. Nevertheless, we believe the model can be used for diffuse pollution that occurs mainly because of the lack of sewage. One of the main advantages of the package is that the main differences in the solutions just reflect themselves in the horizontal direction. This fact has been compensated by using high hydraulic conductivities. So, even if the transport package was not run with CFP, results may be good as the first attempt to build a regional model.

About calibration. Manual calibration is still one of the preferred calibration processes, although is time-consuming. Calibrating the model manually means a trial and error approach. The advantage of this method is the congruence between the calibrated values and the real conditions, meaning that sometimes automatically calibration can lead to good numerical fit values that are too high or not coherent with the data we have. Nevertheless, manual calibration has a major disadvantage besides the time-consuming process and is the fact that the number of possible combinations tried may not be comprehensive enough of the all possible optimal solutions. Usage of PEST or UCODE is a distinct possibility, given some changes in the model are made, like use the Manage Parameters tool.

About conceptual model and modeling: Among other limitations, we found the conceptual model itself – although conceptualization is a dynamic task though any modeling path-, the conceptual model oversimplifies the dynamics in the unsaturated area assuming an immediate infiltration and not accounting for the many delay process occurring within the unsaturated area. The current model assumes that the recharge in the top active cells occurs immediately, which is not depicting the reality, even considering that soils are thin or non-existence in some areas (see Figure 6, section 2.2, page 16) and infiltration happens quickly given the fissured terrain.

Finally, not all the original objectives were completely and resolve. While residence time was estimated, traveling time in the unsaturated zone was not. Many more input data are required to run UZF package such evapotranspiration, data set that is widely incomplete and need to be estimated with alternatives

tools, such as LANDSAT and the suggested method by Kilic and Tarboton (2012). We were able to suggest the existence of epikarst regions that, given groundwater level, would not be saturated through the year but may play an important role in pollution attenuation for surface input. Wetting capacity is activated in model muse thus allowing the model to go dry in some cells. When looking at layer one, some areas go dry at any simulated time and maybe some sort of developed epikarst that, although may keep pollution, does not release it continuously up until water level rises to wash out the pollutants. This area is pointed out in the following Figure and, mainly concentrated along the south-east part of the MMA, where heads are close to 4 meters above sea level. Build the model using GHB package to account for tides effects. If the model does not comply with head observations, couple a saline intrusion simulation along the coast to account for the head differences in the coast. The saline model would be a good addition to understand how injection wells that pump into the aquifer slightly polluted rainwater are moving the saline lenses toward the freshwater lens. Moreover, an extent of the transport model can also be made by the nonlinear flow package recently explained and release by Mayaud (2015).

About saline model: The original project aimed to combine, with the karst features, a saline intrusion model but, given the time framework and the learning curve that modeling entitled; it was not possible to assess its influence on the pollution behavior of the residence time. Nevertheless, some comments regarding saline interface were made in section 4.3.1 related to tiles influence in the coastal area. The saline interface seems to have a greater influence towards the coast, where water tables are shallower, and this specific area needs to be asses, apart from a regional groundwater model. Another limitation is that we neglected the tides effects on the coast. Nonetheless, given this lack of saline coupling, we may have underestimated head values towards the coast which also may have affected the calibration process.

Finally, not all the original objectives were completely and resolve. While residence time was estimated, traveling time in the unsaturated zone was not. Many more input data are required to run UZF package such evapotranspiration, data set that is widely incomplete and need to be estimated with alternatives tools, such as LANDSAT and the suggested method by Kilic and Tarboton (2012). We were able to suggest the existence of epikarst regions that, given groundwater level, would not be saturated through the year but may play an important role in pollution attenuation for surface input. Wetting capacity is activated in model muse thus allowing the model to go dry in some cells. When looking at layer one, some areas go dry at any simulated time and maybe some sort of developed epikarst that, although may keep pollution, does not release it continuously up until water level rises to wash out the pollutants. This area is pointed out in the following Figure and, mainly concentrated along the south-east part of the MMA, where heads are close to 4 meters above sea level.

7 References

Aguilar, Y., Bautista, F., Mendoza, M., *et al.* (2016) 'Density of karst depressions in YucatÁn state, Mexico', *Journal of cave and karst studies the National Speleological Society Bulletin*, 78, pp. 51–60.

Andreo, B., Barberá, J.A., Mudarra, M., Marín, A.I., García Orellana, J., Rodellas, V and Pérez, I. (2017) 'A multi-method approach for groundwater resource assessment in coastal carbonate (karst) aquifers: the case study of Sierra Almijara (southern Spain)', *Hydrogeology Journal*, pp. 41–56.

Arcega-Cabrera, F., Velázquez-Tavera, N., Fargher, L., Derrien, M. and Noreña-Barroso, E. (2014) 'Fecal sterols, seasonal variability, and probable sources along the ring of cenotes, Yucatan, Mexico', *Journal of contaminant hydrology*. Elsevier B.V., 168, pp. 41–49.

Batllori Sampedro, E., González-Piedra, J.I., Díaz Sosa, J. and Febles-Patrón, J.L. (2006) 'Caracterización hidrológica de la región costera noroccidental del estado de yucatán, MÉXICO', *Investigaciones Geograficas*, 59, pp. 74–92.

Bauer-Gottwein, P., Gondwe, B. R. N., *Charvet, G., Marín, L.E., Rebolledo-Vieyra, M. and Merediy-Alonso, G.* (2011) 'Review : The Yucatán Peninsula karst aquifer, Mexico', (130), pp. 507–524.

Botello, A. V (2015) *Golfo de México. Contaminación e Impacto Ambiental: Diagnostico y Tendencias*, *Statewide Agricultural Land Use Baseline 2015*.

Brikowski, T. (2013) 'GEOS 5311 Lecture Notes : Model Calibration Why Calibrate ?' Dallas, Texas: University of Texas, p. 24.

Brosig, K., Geyer, T., Subah, A. and sauter, M. (2008) *Travel time based approach for the assessment of vulnerability of karst groundwater: The Transit Time Method*, *Environmental Geology*.

Buckley, D. K.*, Macdonald, D.M.J., Villasuso P, M., Graniel C., E., Vasquez M., J. and Jimenez, M.V.* (1994) *Technical Report WD/94/4C Geophysical logging of a karstic limestone aquifer for hydrogeological purposes at Merida, Yucatan, Mexico*. Keyworth, Nottinghamshire.

CONABIO (2001) *Edafología- Suelos de Yucatán*. Comisión Nacional para el Conocimiento y Uso de la Biodiversidad. Available at: http://www.conabio.gob.mx/informacion/metadata/gis/eda251mgw.xml?_httpcache=yes&_xsl=/db/metadata/xsl/fgdc_html.xsl&_indent=no (Accessed: 21 August 2018).

CONAGUA (2015) 'Actualización de la disponibilidad media anual de agua en el acuífero Península de Yucatán (3105), Estado de Yucatán', *Diario Oficial de la Federación*.

CONAGUA (2002) 'Medición Piezométrica en el Acuífero Costero (Litoral Poniente) de la Península de Yucatán , Estado de Yucatán', p. 70.

CONAGUA (2012) *Análisis de las temporadas de huracanes de los años 2009, 2010 y 2011 en México*. Mexico City. Available at: http://www.conagua.gob.mx/conagua07/publicaciones/publicaciones/cgsmn-2-12.pdf.

CONAGUA and Betsco Consultants (2011) *Estudio de Instrumentación de la Red de Monitoreo Piezométrico del acuífero de la Península de Yucatán en la zona costera del estado de Yucatán*.

CONAGUA and C.V., I. H. y de S. S. A. de (2004) *Informe final: instrumentación y mediciüon de la red piezométrica de la zona costera del estado de Yucatán. 2da parte*.

CONAGUA and Costera-IC, C. en A. P.-A.-G. & H. (2009) *Implementación de red piezométrica en la zona poniente del estado de Yucatán, Noviembre de 2009*.

CONAGUA and Costera-IC, C. en A. P.-A.-G. & H. (2010) *Segunda parte de la implementación de red piezométrica en la zona poniente del estado de Yucatán*.

Dedewanou, M. *et al.* (2015) 'Groundwater Vulnerability and Risk Mapping Based on Residence Time Distributions: Spatial Analysis for the Estimation of Lumped Parameters', 29(15), pp. 5489–5504.

Delgado, C., Pacheco, J., Cabrera, A., Batllori, E., Orellana, R. and Bautista, F. (2010) 'Quality of groundwater for irrigation in tropical karst environment: The case of Yucatán, Mexico', *Agricultural Water Management*. Elsevier B.V., 97(10), pp. 1423–1433.

Escolero, O., Marín, L.E., Domínguez-Mariani, E. and Torres-Onofre, S. (2007) 'Dynamic of the freshwater-saltwater interface in a karstic aquifer under extraordinary recharge action: The Merida Yucatan case study', *Environmental Geology*, 51(5), pp. 719–723.

FAO. (2002) *Agricultura mundial : hacia los años 2015/2030 : informe resumido*. Organización de las Naciones Unidas para la Agricultura y la Alimentación. Available at: http://www.fao.org/docrep/004/y3557s/y3557s00.htm#TopOfPage (Accessed: 20 August 2018).

FAO- Food and Agriculture Organization of the UN (2018) *Soil classification | FAO SOILS PORTAL | Food and Agriculture Organization of the United Nations*. Available at: http://www.fao.org/soils-portal/soil-survey/soil-classification/en/ (Accessed: 22 August 2018).

Filippis, G., Borsi, I., Ghetta, M. and Rossetto, R. (2017) *FREE and Open Source Software Tools for Water Resource Management FREEWAT User Manual - Volume 1 (EU Horizon 2020 Project)*.

Ford, D. and Williams, P. (2007) *Karst Hydrogeology and Geomorphology*. Second, *Karst Hydrogeology and Geomorphology*. Second. Edited by L. John Wiley & Sons.

Fransson, A. (2015) 'Journal of Geophysical Research : Oceans', *J. Geophys. Res. Ocean.*, pp. 1–17.

Gallegos, J. J. (2011) 'Florida State University Libraries Modeling Groundwater Flow in Karst Aquifers : An Evaluation of MODFLOW- CFP at the Laboratory and Sub-Regional'.

Gómez, M. M., Pacheco A., J., Stefan, C. and Liedl, R. (2018) 'Evaluation and congruence of European karst vulnerability methods from their applicability on the Yucatán Karst, México', in *International Scientific meeting "Man and Karst 2017*. Zadar, Croatia.

Gondwe, B. R. N., Lerer, S., Stisen, S., Marín, L., Rebolledo-Vierya, M., Merediz-Alonso, G. and Bauer-Gottwein, P. (2010) 'Hydrogeology of the south-eastern Yucatan Peninsula: New insights from water level measurements, geochemistry, geophysics and remote sensing', *Journal of Hydrology*. Elsevier B.V., 389(1–2), pp. 1–17.

Gonzalez-Herrera, R., Martíney-Santibañey, E., Pacheco-Ávila, J. and Cabrera-sansores, A. (2014) 'Leaching and dilution of fertilizers in the Yucatan karstic aquifer', *Environmental Earth Sciences*, 72(8), pp. 2879–2886.

González Herrera, R., Sánchez y Pinto, I. and Gamboa Vargas, J. (2002) 'Groundwater-flow

modeling in the Yucatan karstic aquifer, Mexico', *Hydrogeology Journal*, 10(5), pp. 539–552.

IGRAC, BGR, IAH, KIT, & UNESCO. (2017). World Karst Aquifer Map, 1 : 40 000 000. Berlin, Reading, Karlsruhe, and Paris.

INEGI (2015) *México en Cifras*. Available at: http://www.beta.inegi.org.mx/app/areasgeograficas/?ag=31#tabMCcollapse-Indicadores (Accessed: 29 March 2018).

INEGI, I. N. de E. y G. (2016) *Estudio de información integrada del acuífero cárstico Península de Yucatán*. Aguascalientes.

Instituto Nacional de Estadística y Geografía, (Inegi) (2004) 'Guía para la Interpretación de Cartografía Edafología', *Sierra*, pp. 11–24. Available at: http://www.inegi.org.mx/prod_serv/contenidos/espanol/bvinegi/productos/geografia/publicaciones/guias-carto/edafo/EdafIII.pdf.

Kralik, M. and Keimel, T. (2003) 'Time-input, an innovative groundwater-vulnerability assessment scheme: Application to an alpine test site', *Environmental Geology*, 44(6), pp. 679–686.

Kilic, A. and Tarboton, D. (2012) *Estimating Evapotranspiration using Landsat 5 TM and ArcGIS 10.1 (Tutorial)*.

Kunianski, E. L. (2016) 'Simulating Groundwater Flow in Karst Aquifers with Distributed Parameter Models—Comparison of Porous-Equivalent Media and Hybrid Flow Approaches', *U.S. Geological Survey*, (Scientific Investigations Report 2016-5116), p. 14.

Marín, A. I., and Andreo, B. (2015) 'Vulnerability to Contamination of Karst Aquifers', in *Karst Aquifers—Characterization and Engineering*. Springer, Cham (Professional Practice in Earth Sciences), pp. 251–266.

Marín, A. I., Andreo, B. and Mudarra, M. (2015) 'Vulnerability mapping and protection zoning of karst springs. Validation by more multitrace tests', *Science of the Total Environment*. Elsevier B.V., 532, pp. 435–446.

Marín, L. E., Steinich, B., Pacheco, J. and Escolero, O.A. (2000) 'Hydrogeology of a contaminated sole-source karst aquifer, Merida, Yucatan, Mexico', *Geofisica International*, 39(4), pp. 359–365. Available at: http://www.researchgate.net/publication/26493177_Hydrogeology_of_a_contaminated_sole-source_karst_aquifer_Mrida_Yucatn_Mexico/file/9fcfd5092b6aa5a8d3.pdf.

Marín, L. E. *et al.* (2001) 'Hydrogeological investigations and numerical simulation of groundwater flow in the karstic aquifer of northwestern Yucatan, Mexico', 4, p. 15. Available at: http://www.olemiss.edu/sciencenet/saltnet/swica1/Marin-Perry-Essaid-paper.pdf.

Mayaud, C., Walker, P., Hergarten, S. and Birk, S. (2015) 'Nonlinear Flow Process: A New Package to Compute Nonlinear Flow in MODFLOW', *Groundwater*, 53(4), pp. 645–650.

Moreno Gómez, M., Pacheco A., J., Stefan, C. abd Liedl, R. (2018) *Evaluation and congruence of European karst vulnerability methods from their applicability on the Yucatán Karst , México*.

Moreno, M. (2017) *IKAV – Development of an Integrated Strategy for Karst Aquifer Vulnerability Assessment — Junior Research Group INOWAS — TU Dresden*. Available at: https://tu-dresden.de/bu/umwelt/hydro/inowas/research/projects/ikav (Accessed: 20 August 2018).

Navarro, A. (2013) 'Groundwater recharge assessment in karst aquifers by APLIS method and

potential at European scale', in Centre of Hydrogeology, U. of M. (ed.) *International Workshop on Groundwater systems in Europe*. Berlin.

Pacheco A., J. and Cabrera S., A. (1997) 'Groundwater Contamination by Nitrates in the Yucatan Peninsula, Mexico', *Hydrogeology Journal*, 5(2), pp. 47–53.

Pacheco Ávila, J., Cabrera Sansores, A. and Pérez Ceballos, R. (2004) 'Diagnóstico de la calidad del agua subterránea en los sistemas municipales de abastecimiento en el Estado de Yucatán, México', *Ingeniería*, 8(2), pp. 165–179.

Pacheco, J., Cabrera, A., Steinich, B., Frías, J., Coronado, V. and Vázquez, J. (2002) 'Efecto de la aplicación agrícola de la excreta porcina en la calidad del agua subterránea', *Ingeniería*, 6(3), pp. 7–17.

Parra, S. M*., Valle-Levinson, A., Mariño-Tapia, I. and Enriquey, C.* (2015) 'Salt intrusion at a submarine spring in a fringing reef lagoon', *Journal of Geophysical Research: Oceans*, pp. 2676–2700.

Palmer, R. (1998). Assessment of Groundwater Vulnerability in England and Wales. In N. Robins, *Groundwater Pollution, Aquifer Recharge and Vulnerability* (p. 224). London: Geological Survey

Pérez Ceballos, R. Y. (2003) (Thesis MSc*.) Vulnerabilidad del agua subterránea a la contaminación de nitrates en el Estado de Yucatán*. Universidad Autónoma de Yucatán.

Perry, E., & Velazquez-Oliman, G. a. (2003). Hydrogeology of the Yucatán Peninsula. In A. Gómez-Pompa, M. Allen, & S. a. Fedick, *The Lowland Maya Area* (pp. 115-136). Food Products Press.

Petelet-Giraud, E., Dörfliger, N. and Crochet, P. (2000) 'RISKE: Méthode d'évaluation multicritère de la vulnérabilité des aquifères karstiques. Application aux systèmes des Fontanilles et Cent-Fonts (Hérault, Sud de la France)', *Hydrogéologie*, 4, pp. 71–88.

Reimann, T. (2012) (Thesis, Ph.D)*Adaptation of Numerical Modeling Approaches for Karst Aquifer Characterization*

Reimann, T. and Hill, M. E. (2009) 'MODFLOW-CFP: A new conduit flow process for MODFLOW-2005', *Ground Water*, 47(3), pp. 321–325.

Rojas Fabro, A. Y. *et al.* (2015) 'Spatial distribution of nitrate health risk associated with groundwater use as drinking water in Merida, Mexico', *Applied Geography*, 65, pp. 49–57.

Robins, N. S. (1998) 'Recharge: the key to groundwater pollution and aquifer vulnerability', *Geological Society, London, Special Publications*, 130(June 2007), pp. 1–5

Sanchez, I. (1999) *(*Thesis MSc*.) Modelo numérico del flujo subterráneo de la porción acuífera N-NW del estado de Yucatán: implicaciones hidrogeológicas, Universidad Autónoma de Chihuahua, Facultad de Ingeniería. México.*

Shoemaker, W. B., Kunianskz, E.L., Birk, S., Bauer, S. and Swain, E.D. (2005) 'Documentation of a Conduit Flow Process (CFP) for MODFLOW-2005', *U.S. Geological Survey Techniques and Methods, book 6, chapter A24*, p. 50.

Shoemaker, W. B., Cunningham, K.J., Kunianskz, E.L. and Dixon, J. (2008) 'Effects of turbulence on hydraulic heads and parameter sensitivities in preferential groundwater flow layers', *Water Resources Research*, 44(3), pp. 1–11.

Socki, R., Hughes, B., and Socki, R. (2015) 'Hydrogeology of the Yucatán Peninsula Hydrogeology of the Yucatán Peninsula', (January 2003), available at Research Gate.

Steinich, B., and Marin, L. E. (1997) 'Determination of flow characteristics in the aquifer of the Northwestern peninsula of Yucatan, Mexico', *Journal of Hydrology*, 191, pp. 315–331.

Stevanović, Z. (2015a) *Karst Aquifers – Characterization and Engineering*. Edited by Springer.

Stevanović, Z. (2015b) 'Karst Environment and Phenomena', in *Karst Aquifers—Characterization and Engineering*. Springer, Cham (Professional Practice in Earth Sciences), pp. 19–46.

Torres, M. C., Basulto S., Y.Y., Cortés E., J., García U., K., Koh S., A., Puerto R., F., Pacheco A., J.G., (2014) 'Evaluación de la vulnerabilidad y el riesgo de contaminación del agua subterránea en Yucatán', *Ecosistemas y Recursos Agropecuarios*, 1(3), pp. 189–203.

Villasuso, M. and Méndez, R. (2000) *Population, Development, and Environment on the Yucatán Peninsula: From Ancient Maya to 2030*, *Population, Development, and Environment on the Yucatan Peninsula*.

Vrba, J. and Zaporozec, A. (1994) 'Guidebook on Mapping Groundwater Vulnerability', 16, p. 131.

Wenninger, J. (2017). *Introduction to Tracer Hydrology.* Delft: UNESCO-IHE Institute for Water Education.

Xu, Z. and Hu, B. X. (2016) 'Development of a discrete-continuum VDFST-CFP numerical model for simulating seawater intrusion to a coastal karst aquifer with a conduit system', *Water Resources Research*, pp. 1–24.

Zheng, B. C., and Wang, P. P. (1999) *MT3DMS: A modular three-dimensional multispecies transport model for simulation of advection, dispersion and chemical reactions of contaminants in groundwater systems. User´s Guide.*

Zhou, Y. (2017). *Applied Groundwater Modeling.* Delft: UNESCO IHE, Institute for Water Education.

Zwahlen, F. (Ed.) (2003) *COST Action 620 Vulnerability and Risk Mapping for the Protection of Carbonate (Karst) Aquifers Final Report*, European Commission.

8 Appendixes

8.1 Modeling files

Data for the model in CFP 2 and EPM for transport model with MT3DMS is available on request at the following mail addresses. The model files are contained in the CD version of this work, available at TU Dresden.

- carolina.martinez_salvador@mailbox.tu-dresden.de
- miguel.moreno@mailbox.tu-dresden.de

Disclaimer: Even thou we try to be as strict as possible with our management data, some errors may still be in the input files and a continuous process of improving data input files and modeling assumption, conceptualization and data analysis is always being made.

8.2 Original sinkhole distribution map used for previous vulnerability methodologies

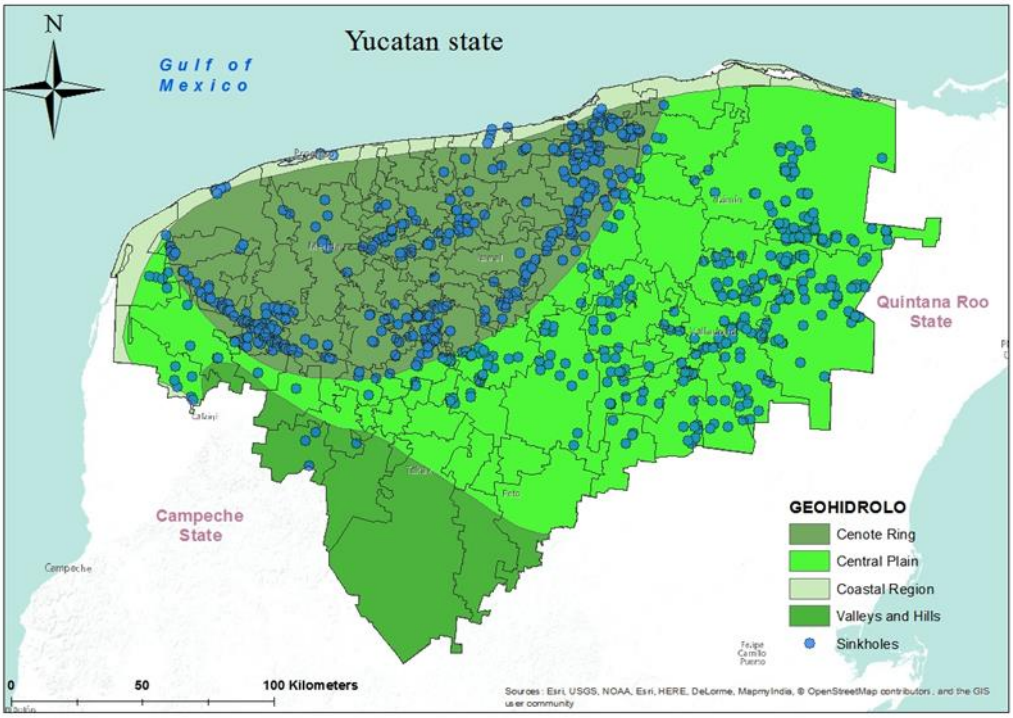

Figure 54: Original sinkhole distribution used to computer karstification degree used in most Vulnerability methods cited in this work. Source, Moreno, et.al. (2017)

8.3 Precipitation patterns used for APLIS, computed using climatoligica data from 66 stations and other maps used for APLIS.

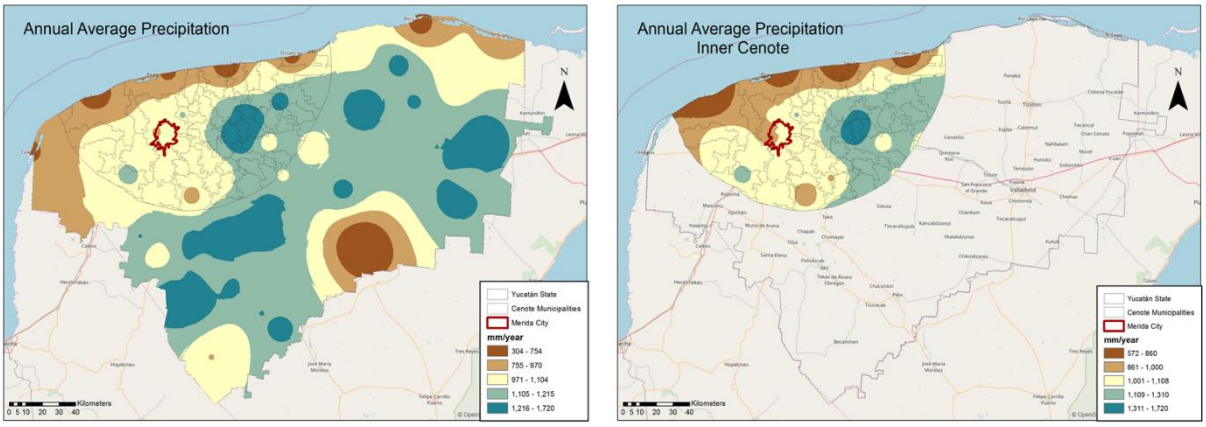

Figure 55: Precipitation patterns used for APLIS

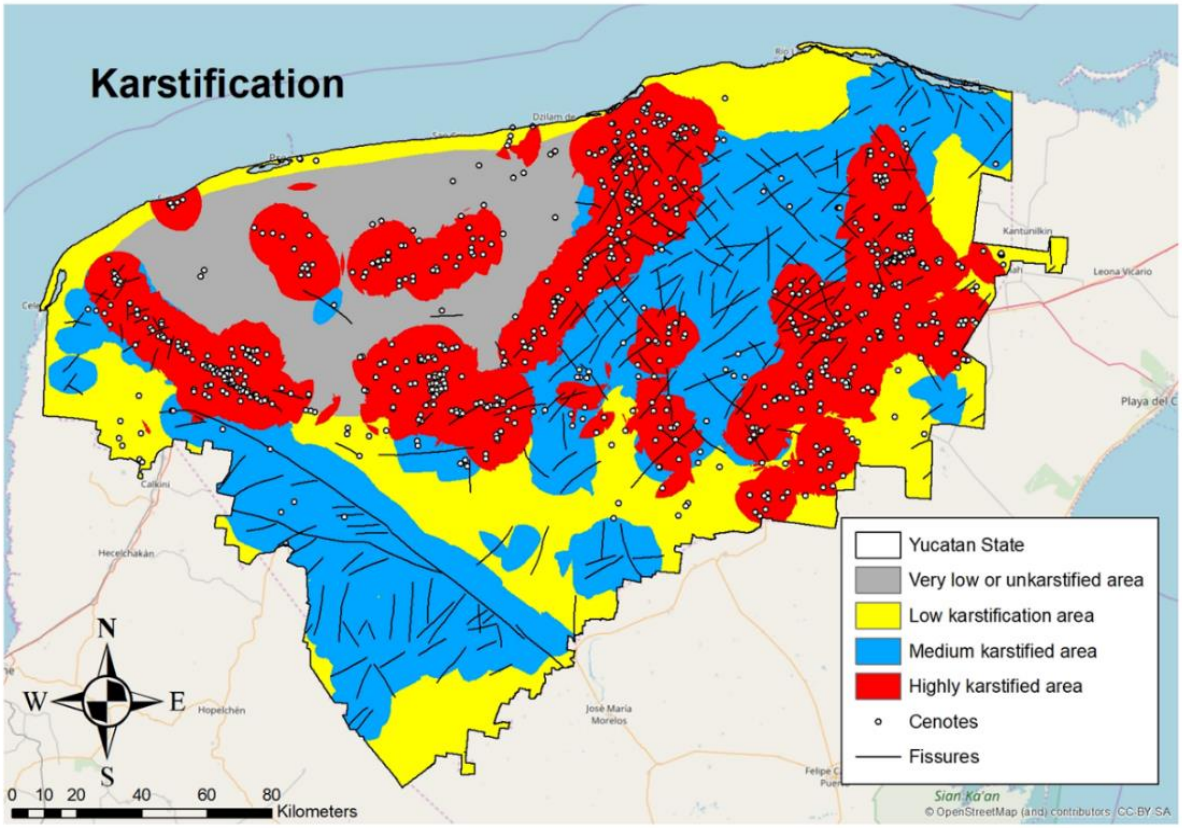

Figure 56: Karstification map used for APLIS purposes.

8.4 Nitrate spatial distribution reported by Pacheco, 2004

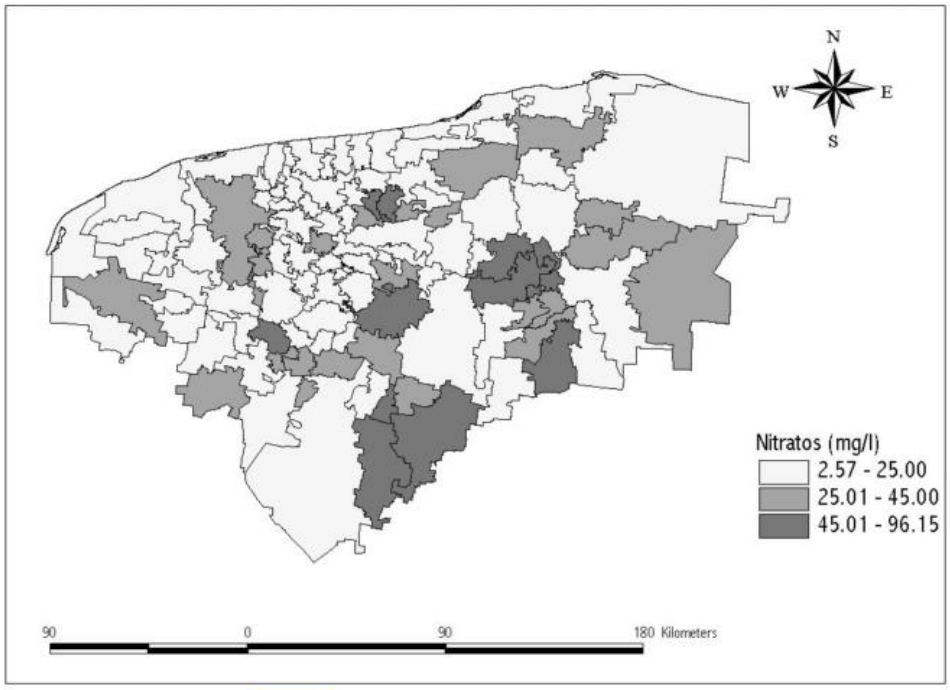

Figure 57: Average Nitrate concentration per municipality by Pacheco (2004)

8.5 General accepted groundwater flows paths in the study area

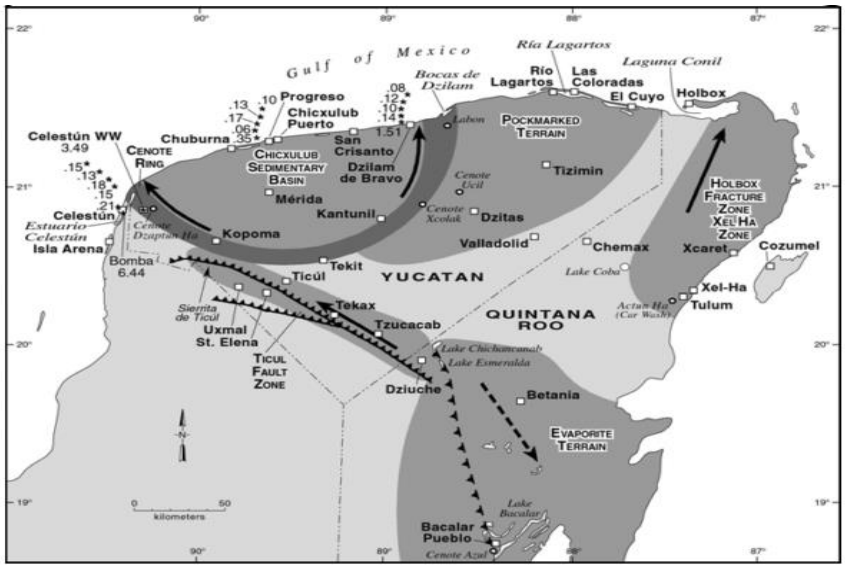

Figure 58: Current understanding of groundwater flows in Yucatán karst. Source: (Socki, Hughes and Socki, 2015)

8.6 Recharge behavior through calibration scenarios

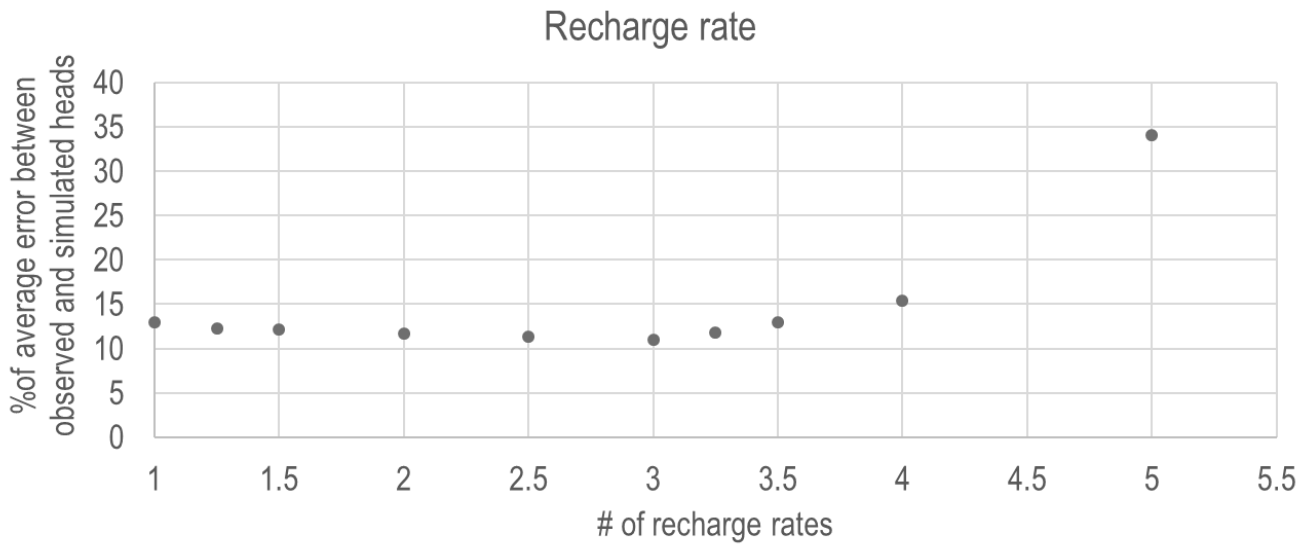

Figure 59: Recharge behavior when calibration recharge rates. After 3 times the input recharge rates, the model error increases again.

8.7 **Groundwater flow from** (Bauer-Gottwein, *et al.*, 2011)

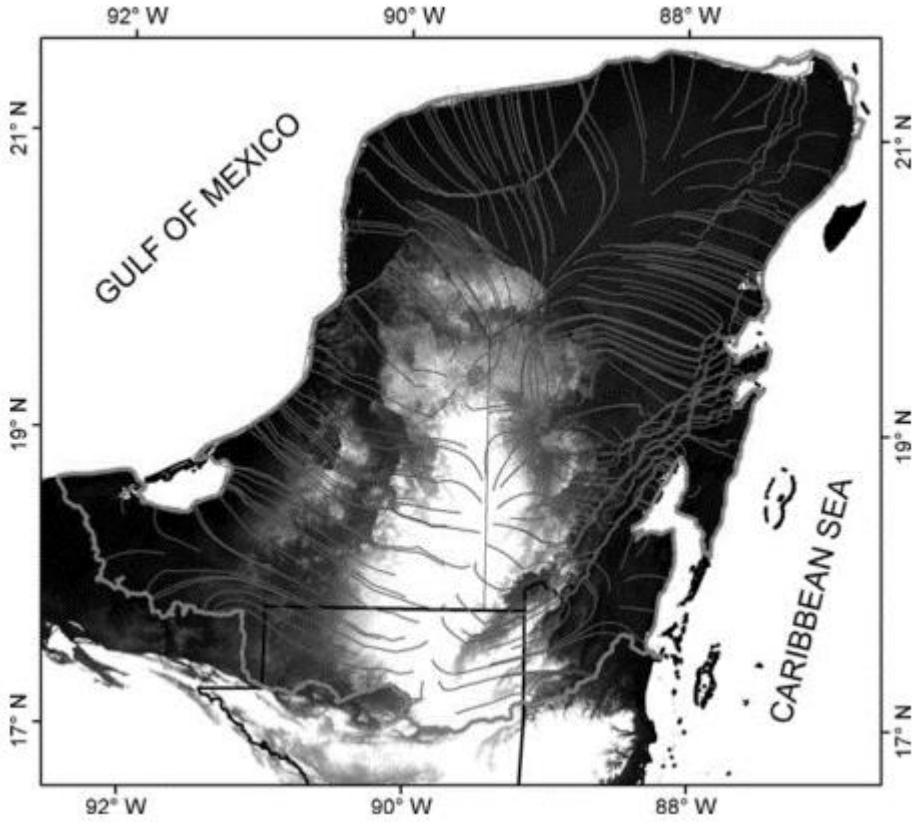

Figure 60: Model Flows reported by Bauer-Gottwein, et. al. (2011) that follow the same particle tracking that our model.

8.8 Concentration curves along transect Mérida Progreso at grid cells where HOB points are located. Values that supported traveling times for table 18, observation wells.

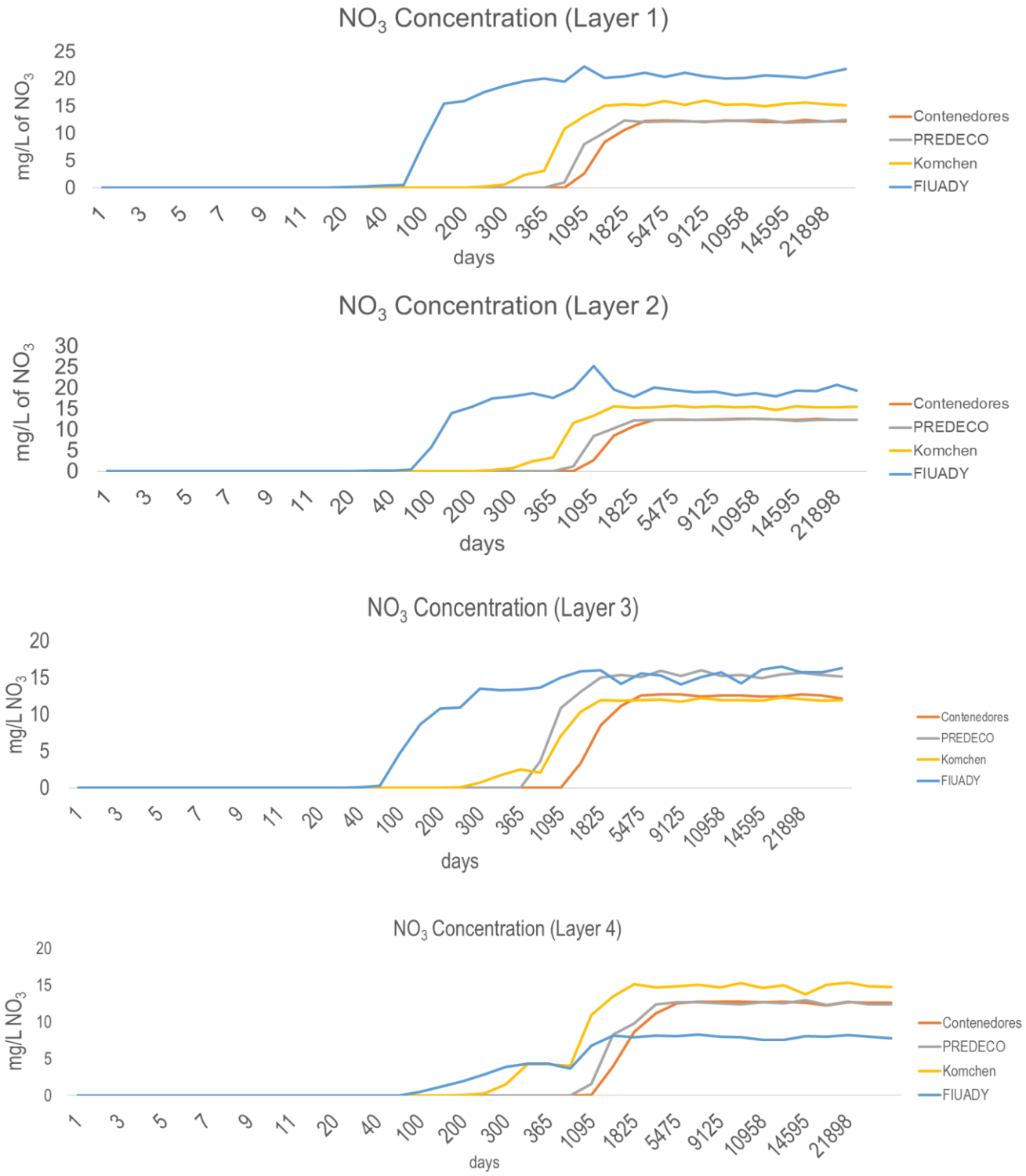

Figure 61: curves along transect Mérida Progreso at grid cells where HOB points are located. Values that supported travelling times for table 18, observation wells.